

Model-based control for active damping of crane structural vibrations

Dissertation

zur Erlangung des akademischen Grades

**Doktoringenieur
(Dr.-Ing.)**

von M. Sc. Ievgen Golovin
geboren am 22.09.1990 in Horliwka (Ukraine)

genehmigt durch die Fakultät für Elektrotechnik und Informationstechnik
der Otto-von-Guericke-Universität Magdeburg

Gutachter:

Prof. Dr.-Ing. habil. Achim Kienle

PD Dr.-Ing. Stefan Palis

Prof. Dr.-Ing. habil. Dipl.-Math. Klaus Röbenack

Promotionskolloquium am 05.07.2021

Zusammenfassung

Große Portalkräne werden häufig in Hafenterminals zum Be- und Entladen von Containern installiert. In den letzten Jahrzehnten war ein gängiger Trend im Kranbau die Verwendung von Leichtbauelementen. Dies führte einerseits zur Schonung von Ressourcen und erhöhte andererseits die Wirkung von elastischen Strukturschwingungen. Diese schwach gedämpften Schwingungen führen zu einem schnelleren Verschleiß der Konstruktion und verschlechtern die Gesamtleistung eines Kranbetriebs. Darüber hinaus ist die Vernachlässigung dieser Strukturschwingungen bei dem Entwurf des Regelungssystems nicht mehr zulässig, und ihre Dynamik muss berücksichtigt werden. Der Fokus dieser Arbeit liegt auf der Reduktion der unerwünschten niederfrequenten Schwingungen in Richtung der Katzfahrt durch den Katzantrieb. Dies kann durch eine zusätzliche Funktionalität des Motion-Control-Systems erreicht werden. Die Anwendung dieses Konzepts erfordert keine nennenswerten Investitionskosten, und es wird gezeigt, dass die erzielte Dämpfung mit anderen kosten-intensiveren bestehenden Ansätzen vergleichbar ist. In dieser Arbeit werden drei modellbasierte Regelungsmethoden vorgestellt und in den entsprechenden Simulations- und Experimentalstudien validiert.

In Kapitel 2 werden die mathematischen und physikalischen Modelle des Portalkrans mit Strukturodynamik vorgestellt. Zunächst wird die Herleitung des analytischen Modells des Portalkrans und dessen Vereinfachung gezeigt. Dann werden die physikalischen und mathematischen Modelle für zwei verschiedene Laborkonfigurationen vorgestellt. Schließlich werden die entsprechenden mathematischen Modelle experimentell validiert.

In Kapitel 3 wird die lineare robuste Regelung für Portalkrane vorgeschlagen. Dieser Ansatz erfordert keinen Neuentwurf des Motion-Control-Systems der Katze und kann daher leicht in die meisten Industriekrane integriert werden. Darüber hinaus erfüllt das auf der H_∞ - Loopshaping-Entwurfsmethode basierende Regelgesetz die robuste Stabilität und geforderten Leistungskriterien auch unter der Annahme, dass die Parameter des Portalkrans nicht genau bekannt sind. Zur Beschreibung der Unsicherheiten wurde die normalisierte koprime Faktor-Beschreibung in Kombination mit der Gap-Metrik verwendet.

In Kapitel 4 wird die lineare Regelung für Portalkrane auf der Basis eines parallelen Kompensators (PFC) vorgestellt. Diese Regelung erfordert keine zusätzliche Messung der Schwingungen und keinen Neuentwurf des Motion-Control-Systems der Katze. Dieser Ansatz ist jedoch nur für Portalkrankonfigurationen mit den starken Systemkopplungen zwischen Katze, Last und Struktur anwendbar, d.h. das betrachtende Ein-Ausgangssystem muss beobachtbar sein. Das Regelungssystem erreicht eine Positionierung der Last und Reduktion der Schwingungen über eine Kombination aus dem PFC und einem Regler. Der PFC ist für die Kompensation der Systemnullodynamik

entworfen und verleiht der erweiterten Strecke die Almost Strict Positive Real (ASPR) Eigenschaften. Das vorgeschlagene einfache lineare Entwurfsverfahren sorgt für eine gewünschte Platzierung der Nullstellen der erweiterten Strecke und reduziert den Bias-Beitrag der PFC. Das erweiterte System kann durch Anwendung eines ausgangsrückgekoppelten Reglers mit hoher Verstärkung stabilisiert werden.

In Kapitel 5 wird die nichtlineare Regelung für Portalkrane vorgeschlagen. Dieser Ansatz ermöglicht eine Ableitung des Regelgesetzes ohne Modellvereinfachung unter direkter Verwendung der Bewegungsgleichungen. Um die Dynamik des Portalkransystems zu stabilisieren, wird ein verallgemeinertes Fehlermaß, die sogenannte Diskrepanz, berücksichtigt. Unter Anwendung der Stabilitätstheorie in Bezug auf zwei Diskrepanzen wird das nichtlineare Regelgesetz für den unteraktuierten Portalkran basierend auf dem direkten Lyapunov-Entwurfsansatz abgeleitet.

Abstract

Large gantry cranes are often installed in port terminals for loading and unloading containers. In recent decades, a common trend in crane design was the use of lightweight structural elements. On the one hand, this led to a conservation of resources and, on the other hand, increased the impact of flexible structural vibrations. These weakly damped vibrations yield faster wear of construction and deteriorate the overall performance of crane operation. In addition, neglecting these structural vibrations in the design of control systems has become less valid, and their dynamics has to be taken into account. The focus of this thesis is to reduce the undesired low-frequency vibrations in a trolley travel direction using the trolley actuator. This can be accomplished by adding an additional functionality to the trolley motion control system, which requires its redesign. The application of this concept does not require significant investment costs, and it will be shown that the obtained damping is comparable with other higher-cost existing approaches. In this thesis, three model-based control approaches are presented and validated in the corresponding simulation and experimental studies.

In Chapter 2 the mathematical and physical models of gantry crane with structural dynamics are presented. Initially, the derivation of the analytical model of the gantry crane and its simplification are shown. Then the physical and mathematical models for two different laboratory configurations are presented. Finally, the corresponding mathematical models are experimentally validated.

In Chapter 3 the linear robust control for gantry crane is proposed. This approach does not require a full redesign of the trolley motion control system and, therefore, can be easily integrated into most industrial cranes. In addition, the controller based on the H_∞ - loop-shaping design procedure satisfies robust stability and required performance criteria under the assumption that gantry crane parameters are not exactly known. In order to introduce the parametric uncertainties, the normalized coprime factor description with the associated gap metric has been used and applied for the generation of a set of the gantry crane models.

In Chapter 4 the linear control for gantry crane based on a parallel feed-forward compensator (PFC) is presented. This control does not require the additional measurement of the oscillations and a full redesign of the trolley motion control system. However, the following approach is only applicable for gantry crane configuration with strong system couplings between the trolley, load, and structure, i.e., the input-output system plant is observable. The control system provides the positioning of the payload and reduction of the oscillations via a combination of the PFC and an output feedback controller. The PFC is designed to compensate the system zero dynamics and render an extended plant the almost strict positive real (ASPR) properties. The proposed simple linear

design procedure provides a zero placement of the augmented plant and reduces the bias contribution of the PFC. The augmented system can be stabilized by applying a high gain output feedback control.

In Chapter 5 the nonlinear control for a gantry crane is proposed. This approach allows a control law derivation without model simplification using the equations of motion directly. In order to stabilize the gantry crane system dynamics, a generalized error measure, called discrepancy, is taken into consideration. Applying the stability theory with respect to two discrepancies, the nonlinear control law for the underactuated gantry crane based on the Lyapunov direct design approach is derived.

Nomenclature

Gantry crane modeling

Symbols

T, U, E, W	kinetic, potential and total energies, and work
M, P, Q	mass, damping and stiffness matrices
R, S	normalized damping and stiffness matrices
A, B, C, D	system matrices of a state space model
$F(t)$	forces
L	length of crane legs
E	Young's modulus
\mathcal{I}	moment of inertia of a cross-sectional area
t	time
x	spatial coordinate
s	Laplace variable
$\delta(\cdot)$	variational operator
$q(t), \nu(x, t)$	vectors of generalized coordinates
$z(t)$	trolley position
$z_p(t)$	payload position
$\varphi(t)$	sway angle
$w(x, t)$	displacement of crane structure
$v(x, t)$	velocity of crane structure
$\tau(t)$	motor torque
$i(t)$	motor current
$x(t)$	state vector
$u(t)$	vector of inputs
$y(t)$	vector of outputs
m	mass
ρ	structure density
l	rope length

h	spatial step
c	structural damping
k, a, b	specific coefficients
λ	eigenvalues
f_i, ω_i, ξ_i	frequency, angular frequency and damping ratio of i -th mode
α, β	mass- and stiffness-proportional damping coefficients

Subscripts

a	armature (motor)
b	boundary
c	crane girder
co	Coulomb
d	discretized
e	end
fr	friction
g	gear
m	motor
o	overall
p	payload
r	reduced
ref	reference
s	sum
st	static
sb	Stribeck
t	trolley
Σ	total

Control design

Symbols

$\mathcal{L}_f h(x)$	Lee derivative of $h(x)$ along $f(x)$
V	Lyapunov functional
J	Quadratic cost functional
K	vector of feedback control gains
L	vector of observer gains
$P(s)$	transfer function of open loop system
$G(s)$	transfer function of closed loop system
$C(s)$	transfer function of controller
$F(s)$	transfer function of parallel feed-forward compensator
$N(s)$	transfer function numerator

$M(s)$	transfer function denominator
$L(s), W(s)$	auxiliary transfer function of interest

Δ	uncertainty
T	time constant
R	resistance

δ_b	gap metric
ϑ	relative degree
ρ	discrepancy

Subscripts

n	nominal
s	shaped

Abbreviations

DC	direct current
DPS	distributed parameter system
EC	electronically commutated
FDM	finite difference method
FEM	finite element method
HMI	human-machine interface
IMU	inertial measurement unit
IPC	industrial personal computer
LHP	left-half plane
LTI	linear time-invariant
ODE	ordinary differential equation
P	proportional (controller)
PD	proportional-derivative (controller)
PI	proportional-integral (controller)
PID	proportional-integral-derivative (controller)
PDE	partial differential equation
PFC	parallel feed-forward compensator
PLC	programmable logic controller
RHP	right-half plane
SISO	single-input single-output
STS	ship-to-shore

Contents

1. Introduction	1
1.1. Problem formulation	1
1.2. Motivation	4
1.3. Thesis overview	8
2. Crane modeling	10
2.1. Mathematical modeling	11
2.1.1. Hamilton's principle	11
2.1.2. Model derivation	12
2.1.3. Model linearization	15
2.1.4. Model discretization	16
2.1.5. Model order reduction	21
2.1.6. Friction model	22
2.2. Simplified configuration of laboratory crane model	23
2.2.1. Experimental setup	23
2.2.2. Drive mechanism	24
2.2.3. Drive control	25
2.3. Full configuration of laboratory crane model	27
2.3.1. Experimental setup	27
2.3.2. Drive configuration	28
2.3.3. Drive control	29
2.4. Model validation	30
2.4.1. Structural dynamics of laboratory gantry crane	30
2.4.2. Model of simplified crane configuration	30
2.4.3. Model of full crane configuration	33
3. Linear robust control	36
3.1. Uncertainty models	36
3.1.1. Coprime factor uncertainty	36
3.1.2. Gap metric	37
3.2. H_∞ - loop-shaping control design	38
3.3. Simulation study	39
3.3.1. Robust controller design	39
3.3.2. Gantry crane model uncertainties	41
3.3.3. Robust control of gantry crane	44
3.4. Experimental evaluation	46
4. PFC-based linear control	50
4.1. Relative degree and zero dynamics of the system	50

4.2.	Condition of almost strictly positive realness	57
4.3.	Parallel feed-forward compensation	58
4.3.1.	Control based on the parallel feed-forward compensation	58
4.3.2.	Design of parallel feed-forward compensator for unstable systems	59
4.3.3.	Design of parallel feed-forward compensator for stable systems	62
4.4.	Control design based on parallel feed-forward compensator	64
4.5.	Simulation study	65
4.5.1.	Gantry crane plant with undesired zeros	65
4.5.2.	PFC-based feedback control	66
4.6.	Experimental evaluation	70
5.	Discrepancy-based control	73
5.1.	Direct control of underactuated gantry cranes	73
5.2.	Stability with respect to two discrepancies	74
5.3.	Design of discrepancy-based control for gantry crane	75
5.3.1.	Extension of the control system	77
5.4.	Simulation study	78
5.4.1.	Evaluation of the state observer	78
5.4.2.	Evaluation of the discrepancy-based control	79
5.5.	Experimental evaluation	84
6.	Summary	92
6.1.	Conclusion	92
6.2.	Future perspectives	93
A.	Detailed derivation of gantry crane model	95
B.	Numerical-based model	99
C.	Model parameters	100
D.	Linear control approaches	101
E.	Energy-based control	105
	Bibliography	108

1. Introduction

1.1. Problem formulation

Nowadays, faster payloads transportation and well-thought-out logistics play an essential role in developing commerce and manufacturing industry. Time reduction of these operations requires the utilization of automated machines, including cranes. Gantry cranes are a broad class of cranes with load-carrying capacity from several to hundreds of tonnes, which can be found in many industrial places such as factories, building areas, marine ports, and railways. Large gantry cranes are regularly used for container handling at port terminals (Fig. 1.1). In order to reduce manufacture and operation costs, most of the crane structures have a lightweight design, e.g., using trusses. On the one hand, this reduction results in resource-saving, but, on the other hand, it commonly increases the sensitivity of the structure towards elastic vibrations.

During the last decades, the construction industry development aims to implement advanced automated technologies for productivity and safety improvements [106]. Consequentially, there has been strong research in the field of modeling and control of crane systems, which is summarized in overview works [1, 77]. One of the most important focal points is a reduction of load swinging during the positioning process. Here, a lot of feed-forward and feedback control strategies have been applied for solution of the problem: e.g. input shaping and model-reference command shaping approaches [47, 48, 58] and their combination with feedback control [60, 78, 82]; output-based input shaping techniques [2, 79]; error tracking control [120]; robust feedback control [37, 70, 105, 108]; adaptive tracking control [11, 13, 119]; model predictive control [4, 15, 98]; energy-based control [103, 104, 111, 122, 123]; sliding-mode control [57, 113, 109, 125, 121] etc. In most works mentioned above, the control law is designed under the assumption that the crane structure is of infinite stiffness and, therefore, its dynamics is negligible. Designed control laws are usually verified in simulation studies using the conventional mathematical models of the cranes or experimental studies using idealized small-scaled laboratory cranes of infinite stiffness. However, the application of lightweight structures for industrial cranes and their continuously increasing dimensions make this assumption for the control design less and less valid. Moreover, it is well known that the feedback control law designed for such an idealized system may suffer from uncertainties resulting in oscillatory or even unstable system dynamics [76]. Hence, for the control design, an accurate model including the coupling between the crane trolley, the hanging payload, and the crane structure has to be derived.

The problem of the structural dynamics has been stated in the literature for a variety of cranes ranging from slewing cranes [90, 81, 52] to overhead, gantry, and ship-to-



Figure 1.1.: The gantry crane from container port [55]

shore (STS) cranes [25, 112, 115, 116, 101, 59, 127, 126, 74, 100, 80]. During the operation of large gantry cranes, two critical problems of structural dynamics should be emphasized: vertical oscillations of the girder due to the travel of the crane trolley and large oscillations of the gantry frame in the direction of the trolley travel. Both problems result from a dynamic interaction between the crane structure and the moving trolley with the hanging payload [126]. Furthermore, there exist structural dynamics problems that are induced by external disturbances, e.g., higher modes excitation due to gusts of wind, waves, and seismic activity [19, 5, 114]. The problem of vertical vibrations is also called the moving load problem and it has been well covered with the modeling, analysis [69, 25, 115, 116] and solution approaches [54, 87].

In this work, the focus is on the elastic vibrations of the gantry frame structure in the direction of the trolley movement. In Fig. 1.2 the typical crane structure deflection of a large gantry crane is depicted. These vibrations have negative effect because of the high amplitudes of their excited first natural frequency and weakly damped behavior. On the one hand, they are responsible for faster construction wear due to the additional mechanical stresses, and, on the other hand, they deteriorate the operation performance. For precise payload positioning, e.g., in fully automated cranes, locations of all components should be known precisely, and such large deflections induced by the structure with limited stiffness make the task more difficult. In cranes operated via a human-machine interface (HMI) approximately 30% of time for each trolley travel is spent on load positioning and reducing the load swaying [127]. Therefore, the frequently observed associated excitation of low-frequency vibrations, being perceptible by the crane operator, are undesired. Moreover, in [74] it has been mentioned that crane operators complained about discomfort during the handling.

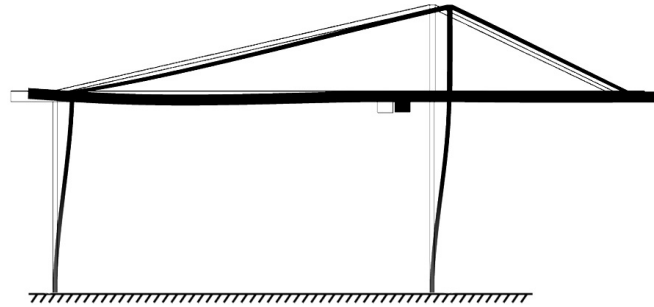


Figure 1.2.: Crane structure deflection in the direction of the trolley travel

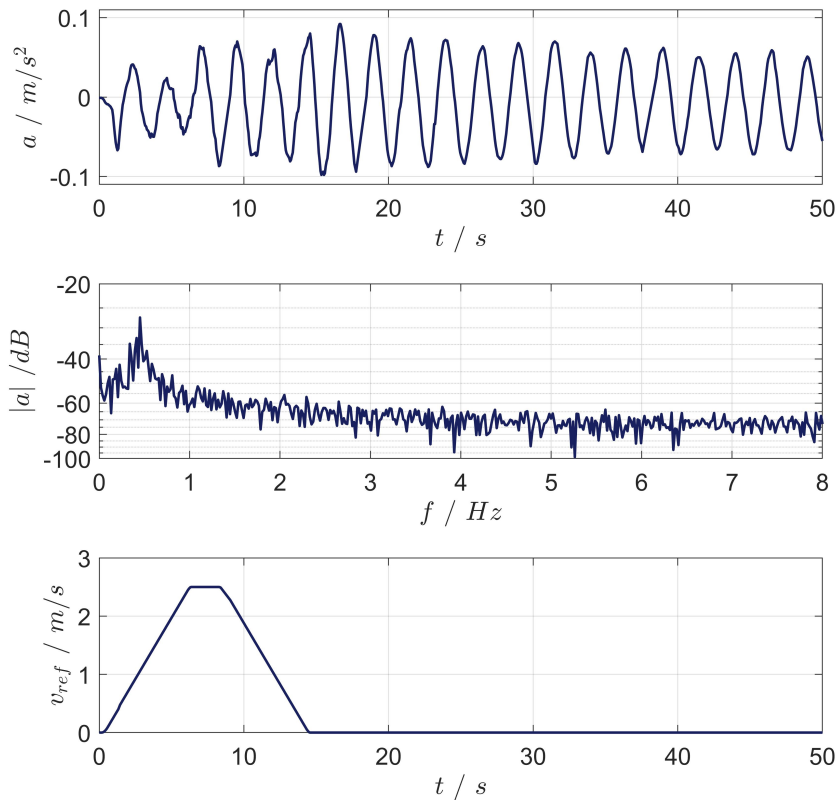


Figure 1.3.: Measurements of elastic vibrations of the large gantry crane: vibration acceleration (**top**), its fast Fourier transform (**center**) and reference velocity (**bottom**) [55]

In Fig. 1.3 and Fig. 1.4 the vibration measurements from two industrial gantry cranes are depicted. Here, in Fig. 1.3 the structure response of the large gantry crane (top) and its fast Fourier transform (center) on a single trolley travel are shown [55]. The crane has been manually operated in velocity control mode with the reference trajectory v_{ref}

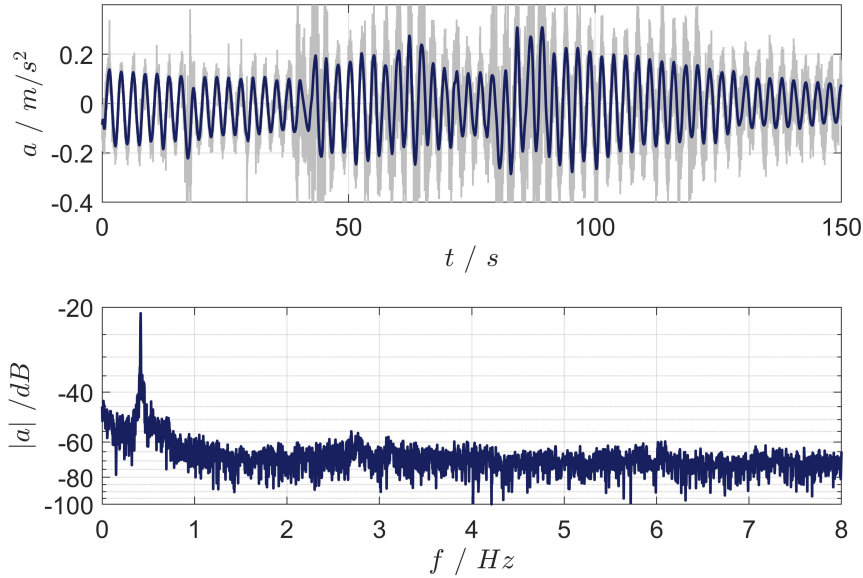


Figure 1.4.: Measurements of elastic vibrations of the STS gantry crane: vibration acceleration (**top**, gray), its filtered value (**top**, blue) and its fast Fourier transform (**bottom**, blue)

(bottom). The legs height of the crane is about 28 m and the outreach is about 37 m . The first natural frequency of the crane is $f_1 = 0.45\text{ Hz}$. In Fig. 1.4 the behavior of the STS container gantry crane on multiple trolley travels (top) and its fast Fourier transform (bottom) are represented. The legs height of this crane is about 50 m and the outreach is about 40 m . The first eigenfrequency of the crane is $f_1 = 0.41\text{ Hz}$. It can be seen that by multiple operational cycles, the amplitudes of vibrations may be boosted. Both figures show that the first natural frequencies have a dominant impact on the structural dynamics by normal operation. The typical frequency range for large gantry cranes can be $f_1 = 0.4 - 0.8\text{ Hz}$ [74, 106].

1.2. Motivation

At the present time, only a few approaches for the reduction of the gantry crane structural vibrations have been proposed in the literature. In [127] the authors propose the optimization of the gantry structure. This method relies on the stiffening of the crane structure by increasing supporting leg thickness or by stiffening of the portal frames. In [83] two solution concepts have been proposed. The first one is a passive damping approach via an additional counterweight acting in a couple with a classical mechanical damper. However, achieved system damping, in this case, is relatively small comparing to material and implementation costs. Typically, applying 30 t counterweight results in up to 10% of the system damping. The second concept is an application of an actuated counterweight, where the mass horizontal movement compensates the vibrations of the

structure. In this case, the resulting system damping can be up to 60 – 70 % using 5 t counterweight. However, its implementation demands high investment costs, e.g., an additional linear drive system and sensors.

Several studies have shown that the structural vibrations in different types of cranes can be taken into consideration as an additional control objective for the motion control system. In [100] the authors offer a combination of feedback and input shaping control for overhead cranes. Here, the payload positioning and disturbance rejection can be provided using classical PID-controllers, and motion-induced oscillatory dynamics can be reduced by applying the corresponding input shaping approach. In [81, 52] structural control concepts for active damping of flexible tower cranes are proposed. Here, the slewing motion feedback control provides the positioning and vibrations damping of the flexible tower and jib. In [81] the authors have presented a distributed parameter tower crane model based on the Euler-Bernoulli beam theory and an early-lumping control method. After spatial discretization with finite difference method and modal order reduction, a state feedback control law based on linear-quadratic regulation (LQR) or pole placement designs have been suggested for the active damping control. In [52] the optimal control problem for a flexible tower crane structural dynamics coupled with a trolley-payload subsystem has been presented.

In this work, for mitigating the gantry crane structural vibrations in the trolley travel direction, a concept of active vibration damping as additional functionality for the trolley motion control system is considered. In general, the main objective of the crane control system is to transfer the load to the desired position. This objective will be fulfilled entirely from a theoretical point of view if the following subtasks are fulfilled:

- positioning of the trolley,
- damping of the payload oscillations,
- damping of the crane oscillations.

Application of such a concept does not require additional actuators, materials, i.e., substantial investment costs. Moreover, it will be shown that the obtained system damping applying this less-cost concept is comparable to the concept with an additional active counterweight. In order to put this concept into practice, a redesign of the crane control system is needed. In the following, several practical and theoretical remarks are introduced.

Currently, most industrial gantry cranes are equipped with automated electric drive systems [106]. Manufacturers of those systems commonly provide a complex product with an individual software solution, e.g., a power converter with included fully-parameterizable cascade system providing the motion and additional anti-sway control as depicted in Fig. 1.5. Although such a design allows users to provide engineering solutions quickly for specific conventional objectives, adding new control specifications or implementing non-standard control laws may be technically more complicated, and, as usual, it requires additional equipment, e.g., programmable logic controllers (PLC) or industrial personal computers (IPC). From a practical point of view, two general

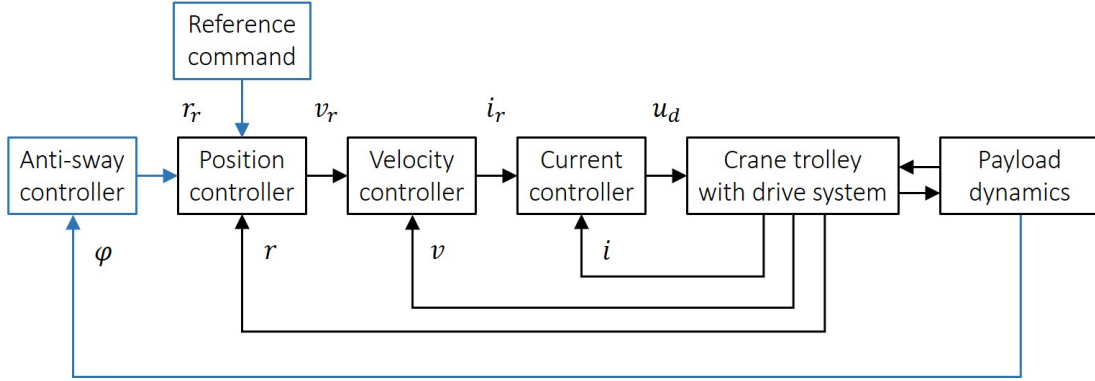


Figure 1.5.: Crane motion control scheme in fully automated cranes

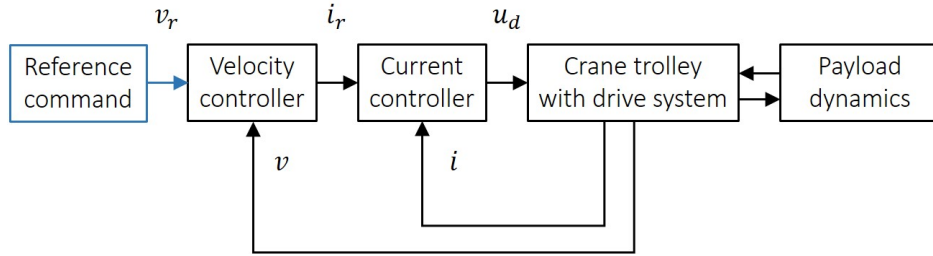


Figure 1.6.: Crane motion control scheme in cranes with operator

concepts for the control system redesign have to be emphasized:

- *Extension* of a given motion control system with the additional objective, i.e., the structural vibration damping,
- *Full redesign* of the control system by implementation of a new non-standard control law.

The payload transfer in cranes can be provided via HMI or by a fully automated control system. In the first case, the crane operator manually governs the load positioning producing the corresponding reference commands while the drive is typically operated in a velocity control mode as depicted in Fig. 1.6. Reduction of motion-induced load oscillations may be supported additionally by applying feed-forward control techniques, e.g., pre-filter, input shaping [48, 47]. Such a control scheme does not include any anti-sway feedback, i.e., no additional sensors are needed. Thus, in the presence of external disturbances and system parameter variations, the process performance depends mostly on the experience of the crane operator. In the second case, the crane is fully automated, and the control system provides the load positioning and anti-sway control (Fig. 1.5). For this task, additional information on the load oscillations can be provided directly via optical sensors (cameras), inertial measurement units (IMU) or indirectly via motor current sensor or encoder [77, 82]. Here, applying the motor measurements for the control is only valid when the coupling between the trolley connected to the drive system and the payload is sufficiently high, i.e., the system in this configuration is observable.

In general, flexible structures are infinite-dimensional systems or distributed parameter systems (DPS) described by partial differential equations. From a control theory point of view, three control design strategies for DPS can be distinguished:

- Early-lumping control design
- Late-lumping control design
- Direct finite-dimensional control design

Here, due to various finite-dimensional control approaches, the early-lumping procedure is the most commonly used. In this method, the DPS is reduced to a n -th order finite-dimensional system, and then a control law can be obtained on its basis. The late-lumping approach involves a derivation of an infinite-dimensional controller on the basis of the original DPS and its posterior lumping for realization. It can be seen that both of the procedures comprise approximation of the model or the control law. In contrast, a direct finite-dimensional control design based on DPS eliminates the need for any approximation. However, such a design is often applicable only for particular cases, e.g., problems with simple geometries [76, 14].

Taking into consideration the aforementioned practical and theoretical specificities, in the present thesis, three model-based control approaches will be proposed and evaluated in simulation studies as well as on two laboratory gantry cranes with a flexible support structure:

1. *Linear robust control* is an early-lumping control approach. It provides the extension of the conventional crane cascade control with an additional robust feedback controller. Here, the trolley drive system is considered to be in the position control mode such that the trolley position is a new control input. In order to attenuate the flexible structural vibrations, the H_∞ - loop-shaping procedure will be applied for a controller design, and robustness margins will be evaluated in terms of the gap metric.
2. *PFC-based linear control* is an early-lumping linear control approach. This approach is based on a parallel feed-forward compensator (PFC), and it can be applied in combination with a standard position control system. It provides the attenuation of crane structural vibrations and payload oscillations without additional sensors or estimations applying only a PFC. This approach is restricted for applications on the gantry cranes with sufficiently high couplings between the trolley, load, and structure.
3. *Discrepancy-based control* is a direct nonlinear control approach. This method requires the motion control system to be in the torque (current) control mode such that the trolley force can be considered as a control input. Here, to stabilize the overall system dynamics, a generalized error measure, called discrepancy, will be introduced. The control law will be derived applying the associated Lyapunov stability theory.

It has to be noticed, that parts of the results introduced in this thesis have been

published in advance as listed in the following:

- Ievgen Golovin, Stefan Palis. Design of parallel feed-forward compensator and its application to electromechanical system with friction load. *IFAC-PapersOnLine*, 50 (1) (2017), pp. 15524–15529.
- Ievgen Golovin, Stefan Palis. Control-based damping of elastic gantry crane vibrations. *IEEE-Proceedings of the 22nd International Conference on Methods and Models in Automation and Robotics*, MMAR 2017 8046896, pp. 599–604.
- Ievgen Golovin, Stefan Palis. Robust control for active damping of elastic gantry crane vibrations. *Mechanical Systems and Signal Processing*, 121 (2019), pp. 264–278.
- Ievgen Golovin, Stefan Palis. Modeling and discrepancy based control of under-actuated large gantry cranes. *21st IFAC World Congress (Berlin)*, (2020).
- Ievgen Golovin, Stefan Palis, Anton Maksakov. Gantry Crane Position Control via Parallel Feed-forward Compensator. *IEEE-Proceedings to 21th Mediterranean Conference on Control and Automation*, MED 2020 9182930, pp. 1045–1050.
- Ievgen Golovin, Anton Maksakov, Myroslav Shysh, Stefan Palis. Discrepancy-based control for positioning of large gantry crane. *Mechanical Systems and Signal Processing*, 163 (2022), 108199.

1.3. Thesis overview

This thesis consists of six Chapters that cover the concepts and ideas presented in the introduction. Chapter 2 presents mathematical and physical models of large gantry cranes. It begins with the mathematical modeling of the cranes with the corresponding structural dynamics in the trolley travel direction. Subsequently, the two configurations of the laboratory gantry crane with the associated mathematical models are introduced. Finally, the mathematical models of the corresponding configurations are validated and compared in the experimental study.

In Chapter 3 the linear robust feedback control for a gantry crane is presented. For designing a control law that fulfills the performance specifications and guarantees robust stability with respect to uncertain parameters, the H_∞ -loop-shaping synthesis is applied. To account for the parametric uncertainties, the normalized coprime factor description with the associated gap metric is utilized and applied to generate a set of the gantry crane models. The Chapter closes with the corresponding simulation and experimental studies.

Chapter 4 introduces linear control for a gantry crane based on PFC. Here, the PFC is designed to achieve desired zero dynamics for the augmented input-output plant. Thereafter, the closed loop system is stabilized, applying high-gain output feedback.

At the beginning of the Chapter, a theoretical background about the relative degree and the zero dynamics is provided. After this, several design procedures for PFC are shown, and one of them is applied for the gantry crane. Finally, corresponding simulation and experimental results are presented.

In Chapter 5 the direct nonlinear control for a gantry crane is presented. For stabilization of the gantry crane system dynamics, a generalized error measure, called discrepancy, is introduced. Applying the associated stability theory with respect to two discrepancies, derivation of the nonlinear control law based on the Lyapunov direct method is shown. To obtain lacking system states, an additional state observer is presented and validated. The Chapter closes with the corresponding simulation and experimental studies.

Chapter 6 summarizes the results presented in the thesis and gives an outlook to future perspectives.

2. Crane modeling

Application of model-based design techniques for a specific control task demands establishing a relatively accurate plant model, e.g., a mathematical model based on first principles or a model identified from experimental data. Cranes are a typical example of electromechanical systems where well-known physical laws and methods can be utilized to derive an appropriate mathematical model.

An operational cycle of gantry cranes comprises three main phases: the hoisting of the load, horizontal movement, and lowering. During the horizontal movement phase, the payload should be delivered as fast as possible to the desired position without swaying. Thus, from a control point of view, the horizontal movement stage is the most challenging task. As stated in the previously mentioned publications [74, 83, 55], for large cranes, such movements typically excite the natural frequencies of the crane structure in the trolley travel direction. Therefore, these important effects should be reflected in the dynamic model of the plant.

In this work, it is considered that the mass and stiffness of the flexible crane structure are distributed continuously along the spatial coordinate. Subsystems of trolley, rope, and payload contain rigid bodies within their particular parts. The analytical gantry crane model can be derived applying the extended Hamilton's principle, resulting in a system with hybrid coordinates described by a set of partial differential equations (PDE) and ordinary differential equations (ODE).

In order to apply the early-lumping control approaches, the infinite-dimensional model subsystem has to be approximated as a finite-dimensional model of n -th order, e.g., using the finite difference method (FDM) or finite element method (FEM). The resulting approximated models are usually of high order and application of control approaches for such systems yields the high-order controllers. To overcome this, an additional application of model order reduction approaches for the model or the controller is needed. Here, the modal truncation approach is applied for the order reduction of the plant model, resulting in a low-order crane model.

In this thesis, two configurations of laboratory gantry cranes are investigated.

1. *Simplified* gantry crane configuration (Fig. 2.1, left).
 - The trolley is assumed to be in the position control mode, such that the reference position is a control input for outer damping control loops.
 - The trolley motor is equipped with a high-ratio reduction gear resulting in non-back-drivability of the trolley mechanism [24]. Therefore, the cor-

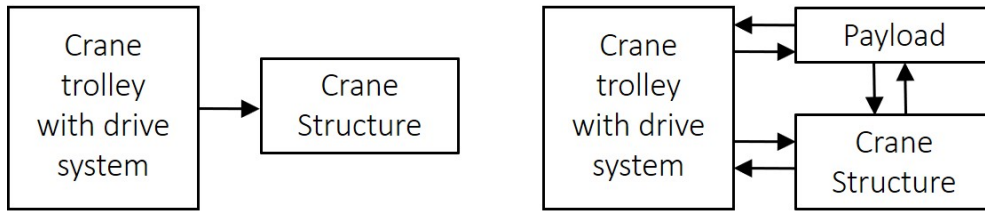


Figure 2.1.: Interaction schemes of the simplified (left) and the full (right) configurations of laboratory cranes

responding influence of the payload and structure on the trolley can be neglected.

- As the frequencies range of the payload and structural oscillations are different, the couplings between them can also be neglected. Assuming that the payload dynamics can be stabilized by an optimized reference trajectory or a competent operator, it is neglected for this configuration, and the focus is on the crane structural dynamics.

2. Full gantry crane configuration (Fig. 2.1, right).

- The trolley is assumed to be in the current control mode, such that the trolley linear force can be considered as a control input.
- Internal couplings of the system are sufficiently strong and all system parts have to be taken into account.

In the following, mathematical and physical models of gantry cranes with structural dynamics are presented. At first, analytical model derivation and simplifications for a gantry crane are shown [38]. Then, the simplified and the full configurations of gantry laboratory crane with corresponding mathematical models are introduced. After this, the associated mathematical models are validated in the experimental study.

2.1. Mathematical modeling

2.1.1. Hamilton's principle

Hamilton's principle is one of the most famous variational principles of analytical mechanics that can be utilized to derive the governing equations of motion for finite and infinite-dimensional systems. This integral principle can be directly derived from the more general Lagrange-d'Alembert's variational principle [51, 18]. The advantages of using this method to derive equations of motion are:

- operation with scalar energy quantities of the system,
- natural boundary conditions for resulting PDEs are obtained automatically.

Hamilton's principle states that under the arbitrary variations $\delta(\cdot)$ that vanish at points of time t_1 and t_2 , i.e., $\delta(t_1) = \delta(t_2) = 0$, the actual motion of the system is determined by the following integral equation

$$\int_{t_1}^{t_2} (\delta T - \delta U + \delta W) dt = 0, \quad (2.1)$$

where $T(t)$ is the kinetic energy, $U(t)$ is the potential energy, $W(t)$ is the virtual work done by non-conservative forces, δ represents the variational operator, t_1 and t_2 are initial and final points of time.

In the following, 1-dimensional flexible problem for a system with hybrid coordinates is considered. Here, Θ is a spatial domain filling a place of undeformed flexible bodies, the vector of generalized coordinates $q = [q_1(t) \ q_2(t) \ \dots \ q_m(t)]^T$ is related to motion of rigid bodies and the vector of distributed coordinates $\nu = [\nu_1(x, t) \ \nu_2(x, t) \ \dots \ \nu_n(x, t)]^T$ is related to the motion of elastic bodies that depend on position x of undeformed bodies. The kinetic and potential energies in this hybrid coordinates can be written as follows:

$$T = T_{disc} \left(\frac{\partial q}{\partial t}, \frac{\partial \nu(x_{bc})}{\partial t} \right) + \int_{\Theta} T_{dist} \left(\frac{\partial \nu}{\partial t} \right) dx, \quad (2.2)$$

$$U = U_{disc}(q, \nu(x_{bc})) + \int_{\Theta} U_{dist} \left(\nu, \frac{\partial \nu}{\partial x}, \frac{\partial^2 \nu}{\partial x^2} \right) dx, \quad (2.3)$$

where U_{disc} and T_{disc} are energies terms that are functions of the discrete and boundary coordinates or their derivatives with respect to time, U_{dist} and T_{dist} are energies integrands related to distributed coordinates, x_{bc} represents spatial positions on the domain boundaries.

The virtual work done by non-conservative forces can be expressed as

$$\delta W = F_{disc}^T \delta q + \int_{\Theta} F_{dist}^T \delta \nu dx, \quad (2.4)$$

where F_{disc} is the vector of generalized non-conservative forces associated with q , F_{dist} is the density vector of generalized non-conservative forces associated with ν , and δq and $\delta \nu$ are the corresponding virtual displacements.

Applying the principle (2.1) for such a system will result in a set of n PDEs of motion, a set of m ODEs of motion, and a set of the natural boundary conditions.

2.1.2. Model derivation

As discussed previously, the focus of this work is elastic vibrations of a large gantry crane in the travel direction of the trolley. Hence, for convenience, it is assumed that the crane frame structure comprises two supported columns that have limited lateral stiffness and a rigid in flexure upper horizontal beam. Applying the symmetry property for the frame structure, the problem can be reduced, and only one half of the structure is taken into consideration.

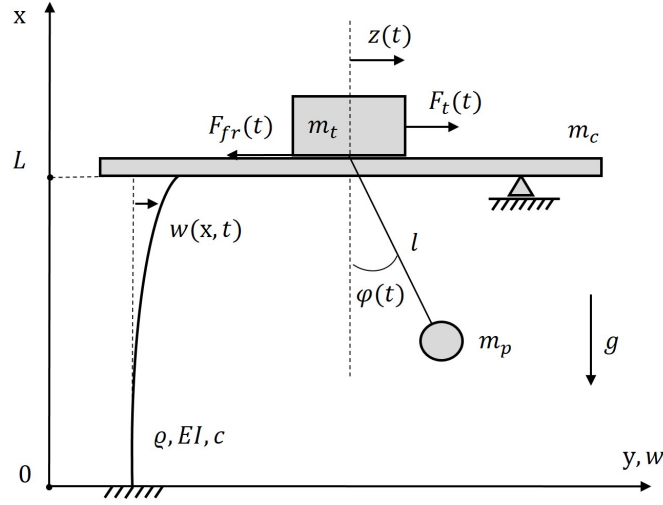


Figure 2.2.: Gantry crane motion scheme

In Fig. 2.2 the schematic motion diagram of the gantry crane with flexible structural dynamics is depicted. Here, $z(t)$ is the trolley displacement, $\varphi(t)$ is the sway angle which is defined in the range $(-\pi/2, \pi/2)$, $w(x, t)$ is the displacement of the crane structure in horizontal direction depending on both position x and time t , $F_t(t)$ is the external force applied to the trolley, F_{fr} is the friction force of the trolley with a drive system, m_t is the mass of the crane trolley, m_p is the mass of the payload, m_c is the mass of the crane girder, l is the rope length, L is the length of the crane legs. The mass density ρ and bending stiffness $E\mathcal{I}$ are homogeneously distributed along the spatial coordinate of column x , where E is Young's modulus and \mathcal{I} is the moment of inertia of a cross-sectional area. Buckling effects, shear deformation, and rotary inertia of the structure can be neglected. The trolley and the payload are assumed to be connected by a massless rigid rope with constant length, i.e., the hoisting process is neglected. The moment of inertia of the payload can also be neglected.

The gantry crane is considered as a hybrid coordinate system where the vector of generalized coordinates expressing motions of rigid bodies can be chosen as follows:

$$q = [z(t) \ \varphi(t)]^T, \quad (2.5)$$

while the distributed coordinate expressing the elastic motion of the column is defined as

$$\nu = w(x, t). \quad (2.6)$$

For shorter notation, the partial derivatives with respect to time will be further denoted as

$$\frac{\partial w(x, t)}{\partial t} = \dot{w}(x, t), \quad (2.7)$$

and the partial derivative with respect to spatial coordinate as

$$\frac{\partial w(x, t)}{\partial x} = w'(x, t). \quad (2.8)$$

The position vectors of discrete rigid bodies of the crane girder r_c , trolley r_t and payload r_p can be defined as follows:

$$r_c = \begin{bmatrix} w(L) \\ 0 \end{bmatrix}, \quad (2.9)$$

$$r_t = \begin{bmatrix} w(L) + z \\ 0 \end{bmatrix}, \quad (2.10)$$

$$r_p = \begin{bmatrix} w(L) + z + l \sin \varphi \\ -l \cos \varphi \end{bmatrix}, \quad (2.11)$$

where $w(L)$ is a compact representation for $w(L, t)$.

Then, the velocity vectors can be calculated as

$$\dot{r}_c = \begin{bmatrix} \dot{w}(L) \\ 0 \end{bmatrix}, \quad (2.12)$$

$$\dot{r}_t = \begin{bmatrix} \dot{w}(L) + \dot{z} \\ 0 \end{bmatrix}, \quad (2.13)$$

$$\dot{r}_p = \begin{bmatrix} \dot{w}(L) + \dot{z} + \dot{\varphi} l \cos \varphi \\ \dot{\varphi} l \sin \varphi \end{bmatrix}. \quad (2.14)$$

According to (2.2) the kinetic energy of the gantry crane can be represented as follows:

$$\begin{aligned} T &= \frac{1}{2} m_c \dot{r}_c^T \dot{r}_c + \frac{1}{2} m_t \dot{r}_t^T \dot{r}_t + \frac{1}{2} m_p \dot{r}_p^T \dot{r}_p + \frac{1}{2} \int_0^L \rho \dot{w}^2 dx, \\ &= \frac{1}{2} m_p [(\dot{w}(L) + \dot{z} + \dot{\varphi} l \cos \varphi)^2 + (\dot{\varphi} l \sin \varphi)^2] \\ &\quad + \frac{1}{2} m_t (\dot{w}(L) + \dot{z})^2 + \frac{1}{2} m_c \dot{w}^2(L) + \frac{1}{2} \int_0^L \rho \dot{w}^2 dx, \end{aligned} \quad (2.15)$$

where the last summand represents the kinetic energy of the distributed coordinate.

The potential energy of the gantry crane with accordance to (2.3) can be formulated as follows:

$$U = -m_p g l \cos \varphi + \frac{1}{2} \int_0^L EI (w'')^2 dx. \quad (2.16)$$

The virtual work done by non-conservative forces can be written as

$$\delta W = (F_t - F_{fr}) \delta z - \int_0^L c \dot{w} \delta w dx, \quad (2.17)$$

where the last term represents the energy dissipation in the flexible column with c as the linear structural damping coefficient.

Substituting the system kinetic (2.15), potential (2.16) energies and the virtual work (2.17) into the extended Hamilton's principle (2.1), performing corresponding variations, applying integration by parts with respect to t and x , and taking into consideration the geometrical boundary conditions $w(0, t) = w'(0, t) = 0$, the following equation

is obtained

$$\begin{aligned}
0 = & - \int_{t_1}^{t_2} \int_0^L \left[\rho \ddot{w} + E\mathcal{I}w'''' + c\dot{w} \right] \delta w \, dx \, dt - \int_{t_1}^{t_2} \left[E\mathcal{I}w''(L) \right] \delta w'(L) \, dt \\
& - \int_{t_1}^{t_2} \left[m_\Sigma \ddot{w}(L) + m_s \ddot{z} + m_p l \ddot{\varphi} \cos \varphi - m_p l \dot{\varphi}^2 \sin \varphi - E\mathcal{I}w''''(L) \right] \delta w(L) \, dt \\
& - \int_{t_1}^{t_2} \left[m_s \ddot{w}(L) + m_s \ddot{z} + m_p l \ddot{\varphi} \cos \varphi - m_p l \dot{\varphi}^2 \sin \varphi - F_t + F_{fr} \right] \delta z \, dt \\
& - m_p l \int_{t_1}^{t_2} \left[l \ddot{\varphi} + \ddot{w}(L) \cos \varphi + \ddot{z} \cos \varphi + g \sin \varphi \right] \delta \varphi \, dt, \tag{2.18}
\end{aligned}$$

where $m_\Sigma = m_p + m_t + m_c$, $m_s = m_p + m_t$, and time dependence has been omitted, i.e., $w(0, t) = w(0)$. Calculation of variations for gantry crane model derivation is represented in Appendix A in more details.

From (2.18) can be seen that for arbitrary variations, the equation holds only if the integrands vanish. Therefore, the governing equations of motion of the gantry crane with the structural dynamics yield

$$\rho \ddot{w} + E\mathcal{I}w'''' + c\dot{w} = 0, \tag{2.19}$$

$$w(0) = w'(0) = w''(L) = 0, \tag{2.20}$$

$$m_\Sigma \ddot{w}(L) + m_s \ddot{z} + m_p l \ddot{\varphi} \cos \varphi - m_p l \dot{\varphi}^2 \sin \varphi - E\mathcal{I}w''''(L) = 0, \tag{2.21}$$

$$m_s \ddot{w}(L) + m_s \ddot{z} + m_p l \ddot{\varphi} \cos \varphi - m_p l \dot{\varphi}^2 \sin \varphi - F_t + F_{fr} = 0, \tag{2.22}$$

$$l \ddot{\varphi} + \ddot{w}(L) \cos \varphi + \ddot{z} \cos \varphi + g \sin \varphi = 0, \tag{2.23}$$

where PDE (2.19) corresponds to the flexible structural dynamics with energy dissipation, (2.20) represents two geometrical boundary conditions for $w(0)$ and one natural boundary condition for $w(L)$, (2.21) corresponds to the motion of girder and loading condition for the structure in $w(L)$, (2.22) represents the motion of the trolley under applied external actuator force F_t and friction force F_{fr} , (2.23) is associated with the payload motion. It should be mentioned that the resulting model is fully coupled.

From this Section and Appendix A it can be seen that the application of this analytical approach, even for a simple geometry problem, requires lengthy mathematical developments and manipulations. Therefore, for more complex problems, the utilization of numerical-based methods is reasonable as presented in Appendix B.

The above derived gantry crane model will be used for the direct control design. In order to apply the early-lumping linear control approaches, this model should be simplified, as will be discussed in the following.

2.1.3. Model linearization

The gantry crane model comprises the linear PDE (2.19) with its boundary conditions (2.20) and the system of ODEs (2.21), (2.22) and (2.23) that contain trigonometric

nonlinearities due to payload motion. Furthermore, (2.22) includes the friction force F_{fr} as an additional input (Section 2.1.6).

For a gantry crane, the equilibrium state of interest is $\varphi = 0$. Taking into consideration that the angles φ during the crane operation are small, the model can be linearized as follows:

$$\rho \ddot{w} + EI w'''' + c \dot{w} = 0, \quad (2.24)$$

$$w(0) = w'(0) = w''(L) = 0, \quad (2.25)$$

$$m_\Sigma \ddot{w}(L) + m_s \ddot{z} + m_p l \ddot{\varphi} - EI w''''(L) = 0, \quad (2.26)$$

$$m_s \ddot{w}(L) + m_s \ddot{z} + m_p l \ddot{\varphi} - F_t + F_{fr} = 0, \quad (2.27)$$

$$l \ddot{\varphi} + \ddot{w}(L) + \ddot{z} + g \varphi = 0. \quad (2.28)$$

2.1.4. Model discretization

In this work, to approximate the infinite-dimensional crane model, the method of lines is applied [89]. It provides a discretization of spatial derivatives only, yielding a set of high dimensional ODEs.

The spatial coordinate x of the continuous function $w(x, t)$ is discretized with an equidistant grid of n nodes. Here, x_i is a grid point, where $i \in [1, \dots, n]$. The spatial derivatives can be approximated point-wise via finite FDM applying the following central difference schemes

$$\left. \frac{\partial w(x, t)}{\partial x} \right|_{x=x_i} \approx \frac{-w_{i-1} + w_{i+1}}{2h}, \quad (2.29)$$

$$\left. \frac{\partial^2 w(x, t)}{\partial x^2} \right|_{x=x_i} \approx \frac{w_{i-1} - 2w_i + w_{i+1}}{h^2}, \quad (2.30)$$

$$\left. \frac{\partial^3 w(x, t)}{\partial x^3} \right|_{x=x_i} \approx \frac{-w_{i-2} + 2w_{i-1} - 2w_{i+1} + w_{i+2}}{2h^3}, \quad (2.31)$$

$$\left. \frac{\partial^4 w(x, t)}{\partial x^4} \right|_{x=x_i} \approx \frac{w_{i-2} - 4w_{i-1} + 6w_i - 4w_{i+1} + w_{i+2}}{h^4}, \quad (2.32)$$

where $h = x_{i+1} - x_i$ is the distance between two grid points, $w_i = w(x_i, t)$ is the value of w at grid node i . The truncation error of the scheme is of the second order.

Applying the FDM to PDE (2.24) yields

$$\ddot{w}_i = \frac{EI}{\rho h^4} [w_{i-2} - 4w_{i-1} + 6w_i - 4w_{i+1} + w_{i+2}] - \frac{c}{\rho} \dot{w}_i. \quad (2.33)$$

In Fig. 2.3 the FDM discretization scheme of the crane flexible structure is depicted. Here, it can be seen that for approximation of spatial derivative w_i'''' at point x_i the displacements from w_{i-2} to w_{i+2} have to be known. Approximation of the derivatives at

points close to the boundaries, e.g., x_1 , x_{L-1} and x_L , is usually derived using so-called displacements in virtual points (Fig. 2.3, red points), i.e., w_{-1} , w_{L+1} , and w_{L+2} , that can be obtained from the given boundary conditions.

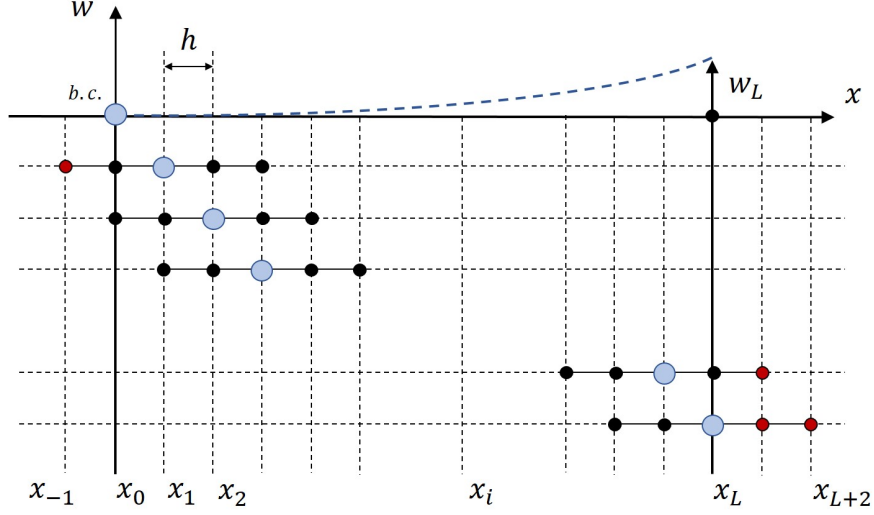


Figure 2.3.: Discretization scheme via FDM

The geometrical boundary conditions that restrict the displacement at point x_0 yield

$$w_0 = 0, \quad (2.34)$$

$$w'_0 = \frac{w_{-1} - w_1}{2h} = 0. \quad (2.35)$$

From (2.35) the displacement in the virtual point x_{-1} follows

$$w_{-1} = w_1. \quad (2.36)$$

Applying these geometrical boundary conditions results in the following approximation of PDE at points x_1 and x_2

$$\ddot{w}_1 = \frac{EI}{\rho h^4} [7w_1 - 4w_2 + w_3] - \frac{c}{\rho} \dot{w}_1, \quad (2.37)$$

$$\ddot{w}_2 = \frac{EI}{\rho h^4} [-4w_1 + 6w_2 - 4w_3 + w_4] - \frac{c}{\rho} \dot{w}_2. \quad (2.38)$$

The boundary condition $w''_L = 0$ can be discretized as follows:

$$w''_L = \frac{w_{L-1} - 2w_L + w_{L+1}}{h^2} = 0, \quad (2.39)$$

and, hence, the displacement for the virtual point x_{L+1} can be derived as

$$w_{L+1} = 2w_L - w_{L-1}. \quad (2.40)$$

Then, substituting (2.40) in the discretized PDE results in an approximation at the point x_{L-1}

$$\ddot{w}_{L-1} = \frac{EI}{\rho h^4} \left[w_{L-3} - 4w_{L-2} + 5w_{L-1} - 2w_L \right] - \frac{c}{\rho} \dot{w}_{L-1}. \quad (2.41)$$

The crane flexible structure subsystem is coupled with trolley and payload subsystems via loading condition (2.26) at point x_L which can be discretized as follows:

$$m_\Sigma \ddot{w}_L + m_s \ddot{z} + m_p l \ddot{\varphi} - EI \frac{-w_{L-2} + 2w_{L-1} - 2w_{L+1} + w_{L+2}}{2h^3} = 0. \quad (2.42)$$

From this condition the displacement value at the virtual point x_{L+2} follows

$$\begin{aligned} w_{L+2} &= \frac{2h^3}{EI} \left[m_\Sigma \ddot{w}_L + m_s \ddot{z} + m_p l \ddot{\varphi} \right] + w_{L-2} - 2w_{L-1} + 2w_{L+1} \\ &= \frac{2h^3}{EI} \left[m_\Sigma \ddot{w}_L + m_s \ddot{z} + m_p l \ddot{\varphi} \right] + w_{L-2} - 4w_{L-1} + 4w_L. \end{aligned} \quad (2.43)$$

Here, taking into account displacements at the virtual points x_{L+1} (2.40) and x_{L+2} (2.43), the crane acceleration at point x_L according to PDE (2.33) yields

$$\begin{aligned} \ddot{w}_L &= \frac{\rho h}{\rho h + 2m_\Sigma} \left(-\frac{EI}{\rho h^4} \left[2w_{L-2} - 4w_{L-1} + 2w_L \right] \right. \\ &\quad \left. - \frac{2}{\rho h} \left[m_s \ddot{z} + m_p l \ddot{\varphi} \right] - \frac{c}{\rho} \dot{w}_L \right). \end{aligned} \quad (2.44)$$

High-dimensional state-space model

Equations (2.27) and (2.28) show that the trolley and payload subsystems are coupled with the structure subsystem via acceleration of the girder \ddot{w}_L described by (2.44). These equations are an implicit system of ODEs. Solving this system with respect to the highest derivatives, the following system of ODEs is obtained

$$\begin{aligned} \ddot{z} &= b_b \frac{EI}{\rho h^4} \left[2w_{L-2} - 4w_{L-1} + 2w_L \right] + b_b \frac{c}{\rho} \dot{w}_L + \frac{gm_p}{m_t} \varphi \\ &\quad + \left(\frac{1}{m_t} + \frac{2}{2m_c + \rho h} \right) (F_t - F_{fr}), \end{aligned} \quad (2.45)$$

$$\ddot{\varphi} = -\frac{gm_s}{lm_t} \varphi - \frac{1}{lm_t} (F_t - F_{fr}), \quad (2.46)$$

$$\begin{aligned} \ddot{w}_L &= -b_b \frac{EI}{\rho h^4} \left[2w_{L-2} - 4w_{L-1} + 2w_L \right] - b_b \frac{c}{\rho} \dot{w}_L \\ &\quad - b_b \frac{2}{\rho h} (F_t - F_{fr}), \end{aligned} \quad (2.47)$$

where

$$b_b = \frac{\rho h}{\rho h + 2m_c}. \quad (2.48)$$

Then, taking into account the approximations (2.33), (2.37), (2.38), (2.41), (2.47), and introducing the vector of displacements $w = [w_1, \dots, w_L]^T \in \mathbb{R}^n$ and vector of inputs $u = [F_t, F_{fr}]^T \in \mathbb{R}^2$, the discretized PDE (2.33) can be represented in matrix form as follows:

$$\ddot{w} = -Sw - R\dot{w} - B_1u, \quad (2.49)$$

where stiffness matrix $S \in \mathbb{R}^{n \times n}$, damping matrix $R \in \mathbb{R}^{n \times n}$, and input matrix $B_1 \in \mathbb{R}^{n \times 2}$ are obtained as

$$S = \frac{EI}{\rho h^4} \begin{bmatrix} 7 & -4 & 1 & 0 & 0 & \cdots & 0 & 0 & 0 & 0 & 0 \\ -4 & 6 & -4 & 1 & 0 & \cdots & 0 & 0 & 0 & 0 & 0 \\ 1 & -4 & 6 & -4 & 1 & \cdots & 0 & 0 & 0 & 0 & 0 \\ 0 & 1 & -4 & 6 & -4 & \cdots & 0 & 0 & 0 & 0 & 0 \\ 0 & 0 & 1 & -4 & 6 & \cdots & 0 & 0 & 0 & 0 & 0 \\ \vdots & \vdots & \vdots & \vdots & \vdots & \ddots & \vdots & \vdots & \vdots & \vdots & \vdots \\ 0 & 0 & 0 & 0 & 0 & \cdots & 1 & -4 & 6 & -4 & 1 \\ 0 & 0 & 0 & 0 & 0 & \cdots & 0 & 1 & -4 & 5 & -2 \\ 0 & 0 & 0 & 0 & 0 & \cdots & 0 & 0 & 2b_b & -4b_b & 2b_b \end{bmatrix}, \quad (2.50)$$

$$R = \frac{c}{\rho} \begin{bmatrix} 1 & 0 & 0 & \cdots & 0 & 0 \\ 0 & 1 & 0 & \cdots & 0 & 0 \\ 0 & 0 & 1 & \cdots & 0 & 0 \\ \vdots & \vdots & \vdots & \ddots & \vdots & \vdots \\ 0 & 0 & 0 & \cdots & 1 & 0 \\ 0 & 0 & 0 & \cdots & 0 & b_b \end{bmatrix}, \quad (2.51)$$

$$B_1 = \frac{2}{\rho h} \begin{bmatrix} 0 & 0 & \cdots & 0 & 0 & b_b \\ 0 & 0 & \cdots & 0 & 0 & -b_b \end{bmatrix}^T. \quad (2.52)$$

Defining the additional velocity vector $v = \dot{w} = [v_1, \dots, v_L]^T \in \mathbb{R}^n$ and the state vector $x = [w_1, \dots, w_L, v_1, \dots, v_L]^T \in \mathbb{R}^{2n}$, the subsystem of crane flexible structure can be represented in state-space form as:

$$\begin{aligned} \dot{x} &= A_d x + B_d u \\ &= \begin{bmatrix} 0 & I \\ -S & -R \end{bmatrix} x + \begin{bmatrix} 0 \\ -B_1 \end{bmatrix} u, \end{aligned} \quad (2.53)$$

where $A_d \in \mathbb{R}^{2n \times 2n}$ is the system matrix and $B_d \in \mathbb{R}^{2n \times 2}$ is the input matrix of the flexible structure subsystem.

From (2.45) it can be seen that the acceleration of trolley \ddot{z} comprises the acceleration of girder \ddot{w}_L with the opposite sign. Thus, the output equation of the flexible structure subsystem with the output of interest $y = -\ddot{w}_L$ that acts on the trolley plant subsystem can be formulated as follows:

$$\begin{aligned} y &= C_d x + D_d u \\ &= [S_e \quad R_e] x + B_{1,e} u, \end{aligned} \quad (2.54)$$

where $C_d \in \mathbb{R}^{1 \times 2n}$ is the output matrix, $D_d \in \mathbb{R}^{1 \times 2}$ is the feedthrough matrix, $S_e \in \mathbb{R}^n$, $R_e \in \mathbb{R}^n$, and $B_{1,e} \in \mathbb{R}^2$ are last rows of the matrices S , R , and B_1 respectively.

Thereafter, taking into account the state-space subsystem of the crane structural dynamics (2.53), (2.54), the system of ODEs (2.45), (2.46), (2.47) and introducing the state vector of the overall system $x_o = [w_1, \dots, w_L, v_1, \dots, v_L, z, \dot{z}, \varphi, \dot{\varphi}]^T \in \mathbb{R}^{(2n+4)}$ yields

$$\begin{aligned} \dot{x}_o &= A_o x_o + B_o u_o \\ &= \begin{bmatrix} A_d & 0 & 0 & 0 & 0 \\ 0 & 0 & 1 & 0 & 0 \\ C_d & 0 & 0 & k_{\varphi 1} & 0 \\ 0 & 0 & 0 & 0 & 1 \\ 0 & 0 & 0 & k_{\varphi 2} & 0 \end{bmatrix} x_o + \begin{bmatrix} B_d \\ 0 \\ k_{F1} + D_d \\ 0 \\ k_{F2} \end{bmatrix} u, \end{aligned} \quad (2.55)$$

where $A_o \in \mathbb{R}^{(2n+4) \times (2n+4)}$ is the corresponding system matrix, $B_o \in \mathbb{R}^{(2n+4) \times 2}$ is the input matrix, $k_{\varphi 1} = gm_p/m_t$, $k_{\varphi 2} = gm_s/lm_t$, $k_{F1} = [1/m_t, 1/m_t]$, and $k_{F2} = [1/lm_t, 1/lm_t]$.

From (2.55) it can be seen that $2n + 4$ -th order of the flexible structure subsystem depends directly on the number of grid elements chosen for the approximation. From a numerical point of view, the accuracy of such approximation depends on the discretization scheme and the number of nodes n . Consequently, for a large number of nodes, this results in high-dimensional models with higher accuracy. However, for early-lumping control approaches lower order models are preferable.

Rayleigh damping model

Equation (2.51) shows that material and air induced dissipation is performed only by the density (mass) proportional component c . Such a dependency typically results in under-damping effects for high-frequency modes. In order to overcome these issues, the structural dissipation can be represented by Rayleigh damping model [99]. Here, the damping matrix is expressed as the following linear combination

$$R = \alpha I + \beta S, \quad (2.56)$$

where α and β are the mass-proportional and stiffness-proportional coefficients respectively, and I is identity matrix. These damping parameters can be calculated using the following equation

$$\begin{bmatrix} \alpha \\ \beta \end{bmatrix} = \frac{2\omega_i\omega_j}{\omega_j^2 - \omega_i^2} \begin{bmatrix} \omega_j & -\omega_i \\ -\frac{1}{\omega_j} & \frac{1}{\omega_i} \end{bmatrix} \begin{bmatrix} \xi_i \\ \xi_j \end{bmatrix}, \quad (2.57)$$

where ω_i and ω_j , ξ_i and ξ_j are the frequencies and damping ratios of two system modes of interest.

In this work, the proposed damping model has been utilized for the structural subsystem (2.53), (2.54) replacing the damping matrix R (2.51) with (2.56). The corresponding damping coefficients α and β have been obtained from experimental data.

2.1.5. Model order reduction

The approximation of infinite-dimensional systems using a numerical discretization procedure usually leads to very high-order finite-dimensional systems. Most control design procedures for such systems generate controllers of at least the same order, resulting in problems during practical implementation. From a control theory point of view, the plant model or the designed controller should be, thus, reduced to some appropriate order. There are a number of methods for order reduction that can be applied to finite-dimensional systems. Many of them are based on a truncation procedure of state-space models in some specific forms, e.g., modal or balanced [96, 10, 65]. In this work, the modal truncation approach is applied to approximate a flexible structure subsystem of the crane.

The modal truncation approach is based on a modal representation form of a state-space model. Consider a linear time-invariant system of high-order n , which is described by the model

$$\dot{x} = Ax + Bu, \quad (2.58)$$

$$y = Cx + Du, \quad (2.59)$$

where system matrix A has only complex conjugate eigenvalues. Then, using the similarity transformation, this matrix can be represented in a block diagonal form as follows:

$$\hat{A} = \hat{T}^{-1}A\hat{T} = \begin{bmatrix} \lambda_1 & 0 & \cdots & 0 \\ 0 & \lambda_2 & \cdots & 0 \\ \vdots & \vdots & \ddots & \vdots \\ 0 & 0 & 0 & \lambda_n \end{bmatrix}, \quad (2.60)$$

where

$$\lambda_i = \begin{bmatrix} \sigma_i & -\omega_{d,i} \\ \omega_{d,i} & \sigma_i \end{bmatrix}, \quad |\omega_{d,1}| < |\omega_{d,2}| < \cdots < |\omega_{d,n}|. \quad (2.61)$$

Here, the matrix \hat{T} comprises the eigenvectors of matrix A and $\lambda_i = \sigma_i \pm j\omega_{d,i}$ are the eigenvalues of matrix A .

Transforming the state-space model into its modal form results in

$$\dot{\hat{x}} = \hat{A}\hat{x} + \hat{B}u, \quad (2.62)$$

$$y = \hat{C}\hat{x} + \hat{D}u, \quad (2.63)$$

where

$$\hat{A} = \hat{T}^{-1}A\hat{T}, \quad \hat{B} = \hat{T}^{-1}B, \quad \hat{C} = C\hat{T}, \quad \hat{D} = D.$$

Here, the state vector \hat{x} can be divided into two parts $[\hat{x}_1, \hat{x}_2]^T$ such that the vector \hat{x}_1 the eigenmodes that should be retained and \hat{x}_2 the modes that can be neglected. Therefore, model (2.62), (2.63) can be rewritten as follows:

$$\begin{bmatrix} \dot{\hat{x}}_1 \\ \dot{\hat{x}}_2 \end{bmatrix} = \begin{bmatrix} \hat{A}_1 & 0 \\ 0 & \hat{A}_2 \end{bmatrix} \begin{bmatrix} \hat{x}_1 \\ \hat{x}_2 \end{bmatrix} + \begin{bmatrix} \hat{B}_1 \\ \hat{B}_2 \end{bmatrix} u, \quad (2.64)$$

$$y = \begin{bmatrix} \hat{C}_1 & \hat{C}_2 \end{bmatrix} \begin{bmatrix} \hat{x}_1 \\ \hat{x}_2 \end{bmatrix} + \hat{D}u. \quad (2.65)$$

Applying the truncation procedure to the system part corresponding to \hat{x}_2 yields an approximation of (2.58), (2.59) as

$$\hat{\dot{x}}_1 = \hat{A}_1 \hat{x}_1 + \hat{B}_1 u, \quad (2.66)$$

$$y = \hat{C}_1 \hat{x}_1 + \hat{D} u, \quad (2.67)$$

with the following equivalent transfer function

$$P_1(s) = \hat{C}_1 (sI - \hat{A}_1)^{-1} \hat{B}_1 + \hat{D}, \quad (2.68)$$

and corresponding additive H_∞ error norm

$$\|P(s) - P_1(s)\|_\infty = \left\| \hat{C}_2 (sI - \hat{A}_2)^{-1} \hat{B}_2 \right\|_\infty. \quad (2.69)$$

It can be seen that the residual in (2.69) depends on the input-output relation of the neglected modes, i.e., \hat{B}_2 and \hat{C}_2 , as well as on their damping. The main advantage of modal truncation is that the eigenvalues of the low-order model are a subset of the eigenvalues of the high-order model and, thus, physical interpretation is preserved [96].

An essential difficulty of the application of this method is the choice of dominant and non-dominant modes. The number of eigenmodes that should be retained in the model after truncation depends always on the specific case of application. Typically, it can be motivated analyzing the system in the frequency domain.

Low-order crane model

In order to obtain a low-order gantry crane model, which can be used for the control design, the discussed modal truncation procedure can be applied. Choosing the number of retained modes n_r , the crane structural subsystem (2.53), (2.54) with redesigned Rayleigh damping matrix R can be represented in block diagonal form and truncated to order $2n_r$. Thus, the reduced crane model with the state vector $x_r = [\hat{x}_1, z, \dot{z}, \varphi, \dot{\varphi}]^T \in \mathbb{R}^{(2n_r+4)}$ can be represented as follows:

$$\begin{aligned} \dot{x}_r &= A_r x_r + B_r u_r \\ &= \begin{bmatrix} \hat{A}_1 & 0 & 0 & 0 & 0 \\ 0 & 0 & 1 & 0 & 0 \\ \hat{C}_1 & 0 & 0 & k_{\varphi 1} & 0 \\ 0 & 0 & 0 & 0 & 1 \\ 0 & 0 & 0 & k_{\varphi 2} & 0 \end{bmatrix} x_r + \begin{bmatrix} \hat{B}_1 \\ 0 \\ k_{F1} + \hat{D} \\ 0 \\ k_{F2} \end{bmatrix} u_r, \end{aligned} \quad (2.70)$$

where $A_r \in \mathbb{R}^{(2n_r+4) \times (2n_r+4)}$ is the system matrix and $B_r \in \mathbb{R}^{(2n_r+4) \times 2}$ is the input matrix of reduced order model.

2.1.6. Friction model

Modeling friction forces for a concrete system is generally a non-trivial task because of the limited understanding of the friction phenomenon. It often results in the high

uncertainties of a plant model. From a control perspective, the friction may cause some undesirable effects in closed loop system dynamics, e.g., poor control performance, limit cycles, and steady-state errors [67]. Many works are dedicated to studying this natural phenomenon in mechanical systems with a focus on control purposes. Here, many static models, e.g., Coulomb, Karnopp, Armstrong models, etc., as well as dynamic models, e.g., Dahl, LuGre, elastoplastic models, etc., have been proposed for modeling, identification, and control of systems with friction [3, 68, 85, 73, 88, 49]. If a friction model of some specific system is known, it can be used for a corresponding model-based friction force compensation. The more accurate the model, the better the friction can be eliminated from the system dynamics.

For most electromechanical systems the static friction models can be applied. Here, a number of friction effects may appear, e.g., static, kinetic (Coulomb), viscous, and Stribeck effects. There exist many different models that combine these friction effects [3]. A frequently used model [67] is:

$$F_{fr} = (F_{st} - F_{co}) e^{-|\dot{z}/b_{sb}|} \operatorname{sgn}(\dot{z}) + F_{co} \operatorname{sgn}(\dot{z}) + F_{vi} \dot{z}, \quad (2.71)$$

where F_{st} is the static friction force, which should be overcome by the motor in order to set the trolley in motion, b_{sb} is the empirical parameter characterizing Stribeck effect, F_{co} is the Coulomb friction force, and F_{vi} is the viscous dissipation force.

In order to overcome numerical issues, the discontinuous function $\operatorname{sgn}(\dot{z})$ is replaced by continuous function $\tanh(k_{fr}\dot{z})$, where k_{fr} is a tuning parameter for slope changing of the trigonometric function in the region of zero. Then, the friction force of the trolley with electric drive is:

$$F_{fr} = (F_{st} - F_{co}) e^{-|\dot{z}/b_{sb}|} \tanh(k_{fr}\dot{z}) + F_{co} \tanh(k_{fr}\dot{z}) + F_{vi} \dot{z}. \quad (2.72)$$

2.2. Simplified configuration of laboratory crane model

2.2.1. Experimental setup

In this work, the proposed control systems are validated on a self-built scaled model of a gantry crane (Fig. 2.4). In order to reflect the flexible system properties of large gantry cranes, the supporting legs of thin plate material have been selected. This yields a limit stiffness and, therefore, the oscillating dynamic behavior of the structure in the trolley direction. As has been mentioned, two experimental configurations of gantry crane with structural dynamics are considered: *simplified* and *full* laboratory gantry crane configurations. The main difference between them is that in the *simplified* configuration the focus is only on the dynamics of the crane structure, while the payload dynamics is neglected. In order to reflect the loading effects an additional mass has been rigidly mounted on the top of the trolley.

The structural scheme of the *simplified* experimental configuration is represented in Fig. 2.5. The crane model comprises a trolley that travels over a girder and flexible

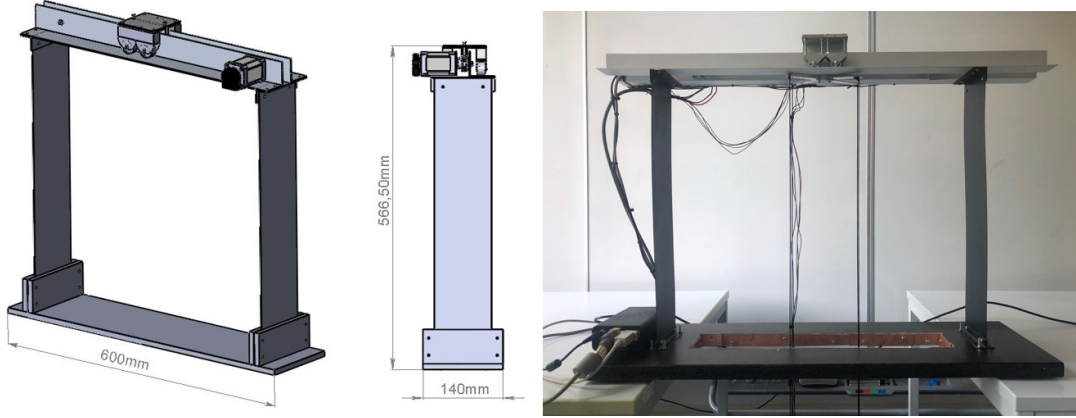


Figure 2.4.: CAD Model and photo of the laboratory gantry crane model

supporting legs that are locked from the bottom. The crane trolley is actuated utilizing a direct current (DC) motor with an epicyclic reduction gear connected with a tooth-belt drive that is assembled on the girder. In order to perform the angular velocity and position measurements, an incremental encoder with 64 counts per revolution is mounted on the opposite side of the shaft. The drive is equipped with a current sensor *INA219*. For the girder oscillations measurements, an additional IMU, *MinIMU-9*, is installed on the top of the crane girder. It provides the direct measurement of the girder acceleration \ddot{w}_L . The DC motor is controlled by the motor driver *VNH5019*, which is supplied with 12V DC voltage. All control algorithms with corresponding signal processing are implemented on *Arduino Mega 2560* micro-controller. In order to avoid bias effects and measurement noise in the measured acceleration \ddot{w}_L , an additional Butterworth band-pass filter is used.

2.2.2. Drive mechanism

In Fig. 2.6 a mechanical scheme of the presented crane drive configuration is depicted. Here, the crane trolley is connected with the motor via the tooth-belt and reduction gear. The gear ratio can be calculated as follows:

$$k_g = \frac{\tau_g}{\tau_m} = \frac{\omega_m}{\omega_g}, \quad (2.73)$$

where τ_m and ω_m are torque and velocity on the motor shaft, τ_g and ω_g are torque and velocity on the gear shaft.

According to Fig. 2.6, the linear forces and the trolley mass augmented by the motor inertia are obtained as follows:

$$F_t = k_g r_r \tau_m, \quad (2.74)$$

$$F_{fr} = k_g r_r \tau_{fr,m} + F_{fr,t}, \quad (2.75)$$

$$m_t = m_{t,t} + \frac{2}{r_r^2} k_g^2 J_m. \quad (2.76)$$

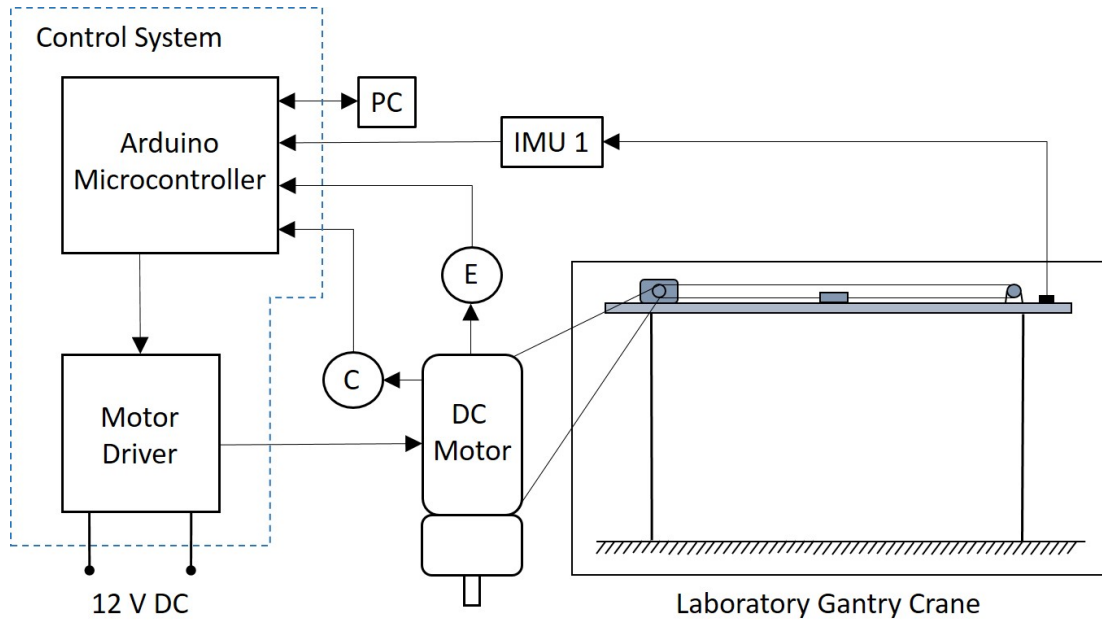


Figure 2.5.: *Simplified* experimental configuration of laboratory gantry crane

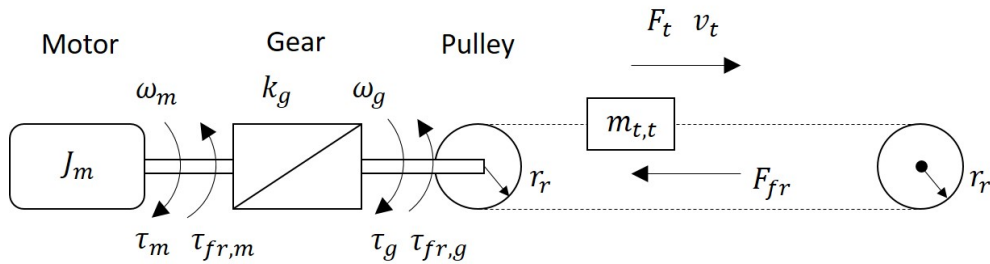


Figure 2.6.: Crane drive scheme for the *simplified* experimental configuration

2.2.3. Drive control

In this configuration, the gear ratio amounts to $k_g = 19$ making it non-back-drivable from the trolley side. Here, it is assumed that the position-controlled DC drive accomplishes the trolley movement along the linear girder axis so that the trolley position can be considered as a control effort for further damping control. In the following, the conventional drive control system is presented.

Conventional cascade control of trolley drive system

Cascade control with PI controllers for drive control is a quasi-standard because of its simplicity and good disturbance rejection [91, 92]. Moreover, due to cascade control it can be assumed that the electromotive and friction effects are compensated in inner control loops so that they can be neglected. In Fig. 2.7 a typical cascade control scheme

is depicted. It comprises the following control loops: inner current (torque) control loop $G_i(s)$, velocity control loop $G_v(s)$, and outer position control loop $G_r(s)$. Here, the transfer function of the electrical subsystem from the voltage input of the rectifier to the motor current $P_i(s)$ is given as follows:

$$P_i(s) = \frac{i(s)}{u_d(s)} = \frac{1}{T_\mu s + 1} \cdot \frac{1/R_a}{T_a s + 1}, \quad (2.77)$$

where T_μ is the time constant of the rectifier, R_a is the resistance of the electrical part of the motor, T_a is the time constant of the electrical part of the motor ($T_a \gg T_\mu$).

The transfer functions of the mechanical subsystems from the motor current to the trolley velocity $P_v(s)$ and from the trolley velocity to the trolley position $P_r(s)$ follow

$$P_v(s) = \frac{v(s)}{i(s)} = \frac{k_m}{m_t s}, \quad (2.78)$$

$$P_r(s) = \frac{r(s)}{v(s)} = \frac{1}{s}, \quad (2.79)$$

where k_m is the coefficient which transfers the motor current to a linear force applied to the trolley mass m_t .

For the current and velocity control loops PI controllers $C_i(s)$ and $C_v(s)$ are used. The outer position loop is more often controlled by a P controller $C_r(s)$. The controller parameter tuning is obtained step by step. At first, the parameters of the fastest inner PI controller $C_i(s)$ for the subsystem plant $P_i(s)$ are tuned. Here, to adjust the parameters the magnitude (modulus) optimum is typically applied [91]. The idea of this procedure is to compensate the biggest time constant in the loop T_a by choosing the appropriate integral time constant and to tune the gain for fast reference tracking. Then, the parameters of the velocity PI controller $C_v(s)$ for the augmented velocity plant $G_i(s)P_v(s)$ are tuned. For the tuning of this loop the magnitude (modulus) or symmetric optimum can be used. At last, the gain of the position P controller $C_r(s)$ for the augmented $G_v(s)P_r(s)$ is optimized.

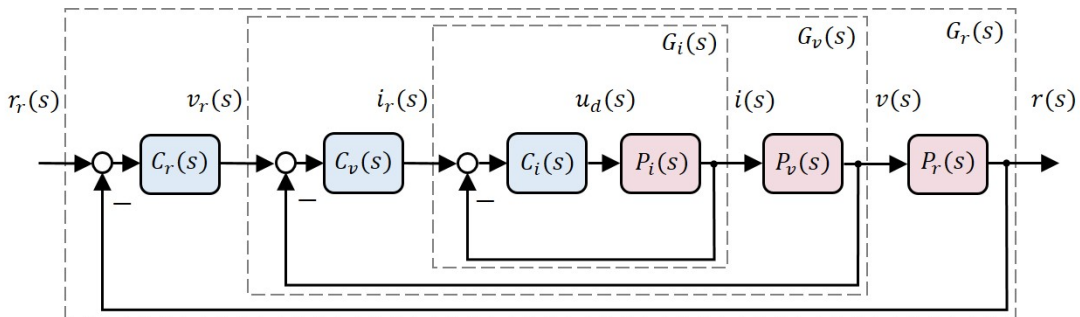


Figure 2.7.: Gantry crane position control scheme

Trolley position control

In this work, the coefficients of the current and velocity control loops are adjusted according to the magnitude optimum. The position controller gain has been tuned in order to get transients of the position responses without overshoots.

In Fig. 2.8 transients of the crane trolley in the position control mode are presented. Here, the trolley reaches the reference position $z_{ref} = 200 \text{ mm}$ (red) after about 2 seconds. A small undershoot of about 1 % in position transient can be seen, which is caused by the Coulomb friction effects. The peak of the current value is 1.5 A, which is 50 % of the limitation current value $i_{max} = 3 \text{ A}$.

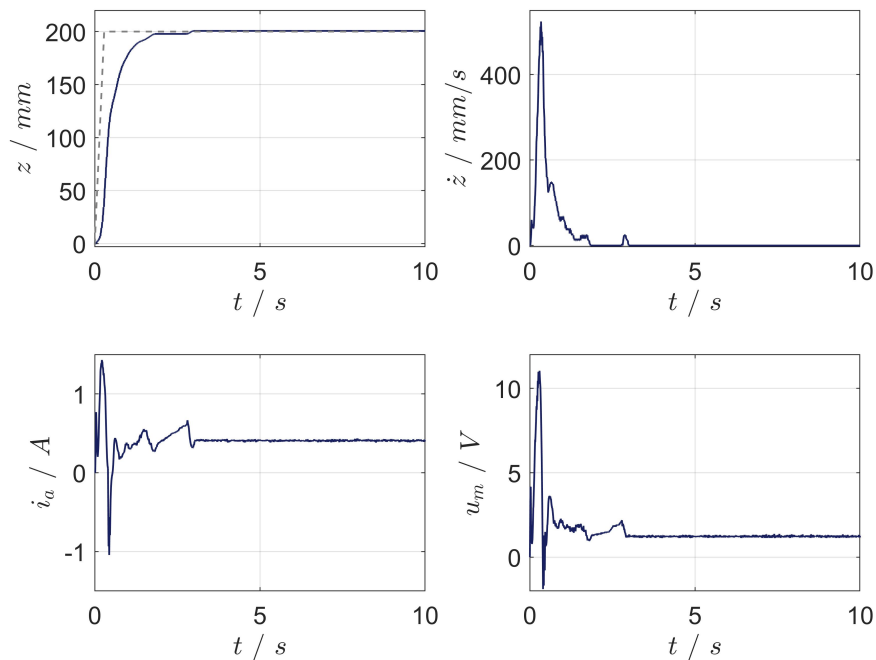


Figure 2.8.: Experimental time responses of drive system in the position control mode (blue) applying a position reference signal (gray)

2.3. Full configuration of laboratory crane model

2.3.1. Experimental setup

The structural scheme of the *full* experimental configuration is represented in Fig. 2.9. Here, the gantry crane model consists of the crane construction with a limited stiffness (Fig. 2.4), the trolley that moves along the linear axis, and a hanging payload.

The crane trolley is driven via a tooth-belt drive by the *Maxon* 118888 electronically

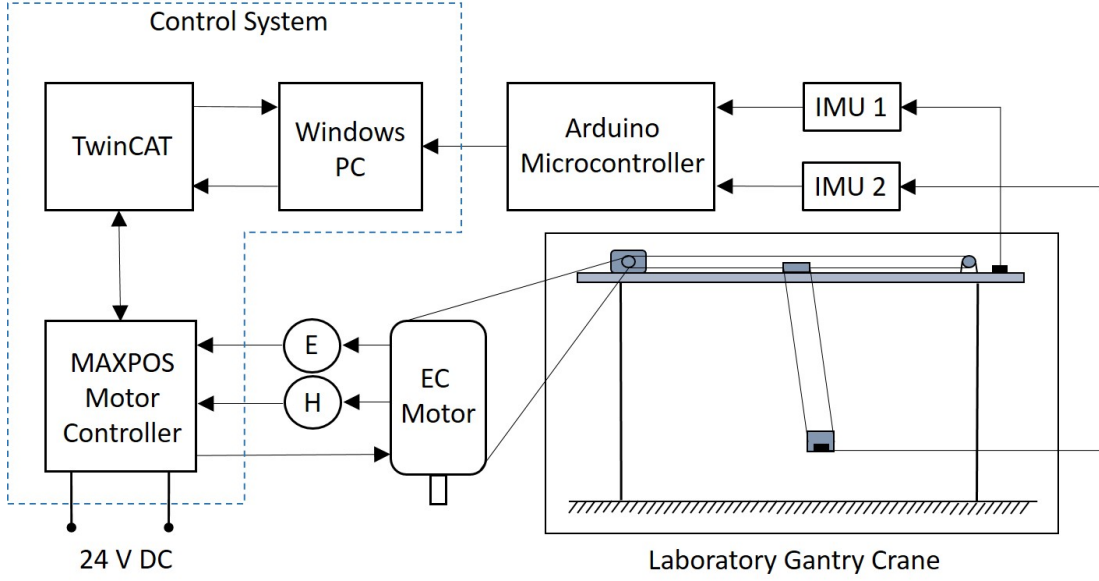


Figure 2.9.: *Full* experimental configuration of laboratory gantry crane

commutated (EC) motor without additional reduction gear. The motor is equipped with a current sensor, Hall-sensor, and incremental encoder with 2000 counts per revolution to measure the current, the rotation angle, and the angular velocity. The oscillations measurements of crane girder and payload are provided by accelerometers from additional IMUs, i.e., IMU 1 - *MinIMU-9* and IMU 2 - *MPU-9250/6500* as depicted in Fig. 2.9. The IMUs are connected via I^2C -interface with an *Arduino Mega 2560* microcontroller, where these signals are processed and filtered. The motor is controlled by the *MAXPOS 50/5* control device. This device can be flexibly parametrized via *EtherCAT* network using a *Beckhoff TwinCAT* real-time PC-based controller. Here, all control algorithms can be implemented in *MATLAB Simulink* environment and can be exported in *TwinCAT* via *Simulink Coder*. *MAXPOS* controller provides the field-oriented current control of the EC motor.

2.3.2. Drive configuration

In Fig. 2.10 the mechanical scheme of the crane drive for the *full* configuration is presented. In this case, the crane trolley is connected with the motor directly via the tooth-belt mechanism. For this configuration, the resulting forces and the trolley mass augmented by the motor inertia are given as

$$F_t = r_r \tau_m, \quad (2.80)$$

$$F_{fr} = r_r \tau_{fr,m} + F_{fr,t}, \quad (2.81)$$

$$m_t = m_{t,t} + \frac{2}{r_r^2} J_m, \quad (2.82)$$

where r_r is a pulley radius, $\tau_{fr,m}$ is a motor friction torque component, $F_{fr,t}$ is a trolley friction force component, $m_{t,t}$ is a trolley mass and J_m is a motor inertia.

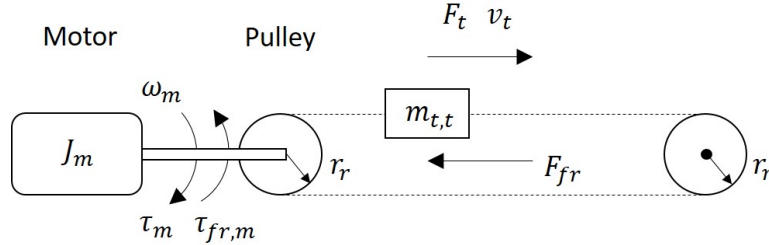


Figure 2.10.: Crane drive scheme for the *full* configuration

2.3.3. Drive control

Motor current control

The combination of *MAXON* EC motor with its native *MAXPOS* controller provides an embedded parameterizable drive control system. Depending on the application case, the drive can be operated in different modes, e.g., field-oriented current control, velocity, or position control. In this configuration, the motor is assumed to be operated in the current control mode. Here, as the controlled current is proportional to the motor torque and, hence, the linear force of the trolley, the latter can be considered as a control effort.

In Fig. 2.11 the reference tracking of the current control loop (blue) using different reference signals are presented. Here, dynamics of the current control loop is typically much faster compared to the mechanical processes. Therefore, it can be neglected for a further active damping control design.

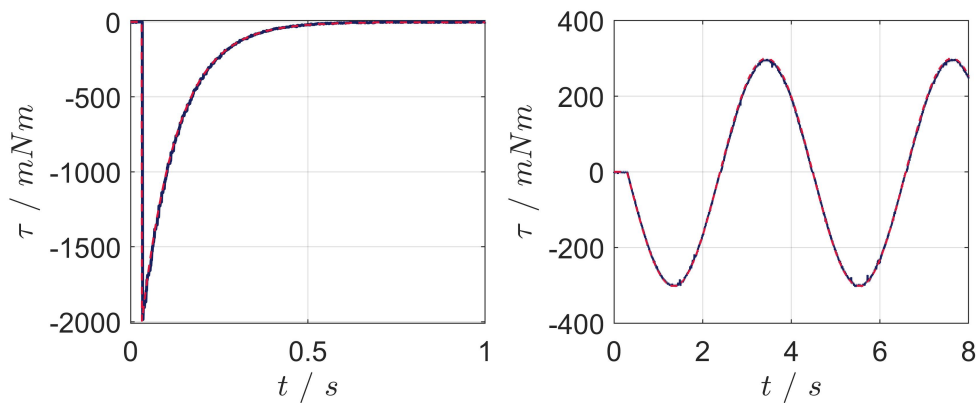


Figure 2.11.: Experimental time responses of motor torque in torque control mode (blue) applying reference signal (red)

2.4. Model validation

2.4.1. Structural dynamics of laboratory gantry crane

The essential challenge for the early-lumping linear control design is the choice of the reduced model order. In order to motivate an appropriate order reduction, the flexible structural dynamics should be analyzed in the frequency domain. For this reason, an additional simulation and experimental study are considered. Here, a sinusoidal sweep signal of small amplitude and frequency range $0.5 \text{ Hz} - 50 \text{ Hz}$ ($3.14 \text{ rad/s} - 314 \text{ rad/s}$) has been applied as the input signal on the laboratory crane without a payload. In this study, the configuration with the EC Motor in current control mode is considered. From the obtained input-output signals, i.e., motor torque τ_m and girder acceleration \ddot{w}_L respectively, a transfer function of 16-th order has been estimated and compared with the analytically derived model from Section 2.1.

In Fig. 2.12 the Bode magnitude plots of the identified transfer function and mathematical model are presented. In the considered frequency range two pole pairs that correspond to the eigenfrequencies of the mechanical structure can be observed, i.e., the first eigenfrequency $f_1 = 1.6 \text{ Hz}$ ($\omega_1 = 10.24 \text{ rad/s}$) and the second eigenfrequency $f_2 = 21 \text{ Hz}$ ($\omega_2 = 130.3 \text{ rad/s}$). From the results, a good match between both models can be seen. The present differences are a result of nonlinearities and measurement noise. In Fig. 2.13 the corresponding eigenforms for the two frequencies obtained from additional FEM study are depicted.

This study shows that these two eigenfrequencies have a significant contribution to the structural dynamics in the frequency range of $0.5 \text{ Hz} - 50 \text{ Hz}$. However, it should be mentioned that the second eigenfrequency $f_2 = 21 \text{ Hz}$ is relatively high compared to the gantry crane dynamics with the payload. In addition, experimental data, e.g., real gantry crane vibrations presented in Fig. 1.3 and Fig. 1.4 as well as laboratory gantry crane experiments, shows that during regular crane operation, this frequency is not excited. Therefore, for the early-lumping linear control design, it is assumed that only the first system eigenmode with eigenfrequency $f_1 = 1.6 \text{ rad/s}$ can be influenced, and, thus, a second-order model approximation $n_r = 2$ is reasonable.

It should also be mentioned that during the work, various system parameters for different experimental configurations, e.g., L crane legs length, E Young's modulus, and m_p payload mass, were different, resulting in corresponding variation of the eigenfrequencies. However, the motivation for the model simplification mentioned above remains the same.

2.4.2. Model of simplified crane configuration

In this Section, the mathematical model of the *simplified* crane configuration is compared and validated against the experimental data. In the first step, the position control loop of the trolley with electric drive, which has been described in Section 2.2, is vali-

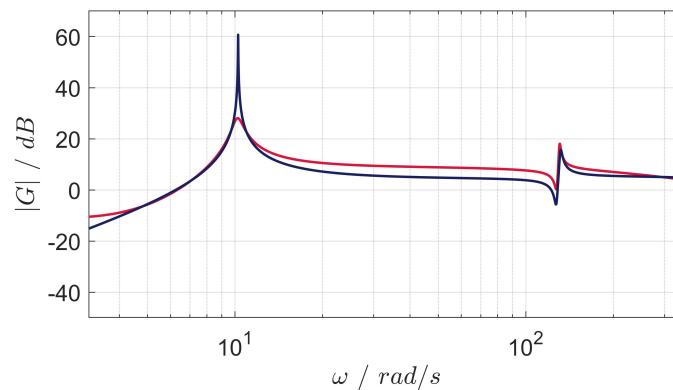


Figure 2.12.: The Bode magnitude plots of the identified transfer function from experiment (red) and model (blue)

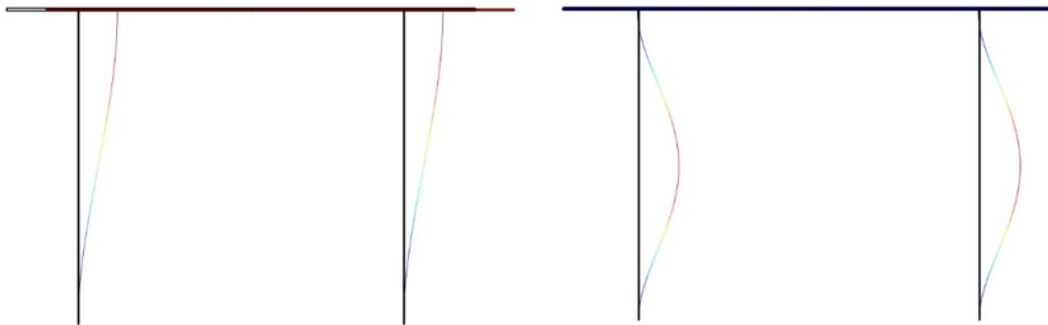


Figure 2.13.: Eigenforms of the 1-st frequency $f_1 = 1.6 \text{ Hz}$ (left) and 2-nd frequency $f_2 = 21 \text{ Hz}$ (right)

dated and simplified. Then, the overall crane model of the experimental configuration is validated. The model parameters are summarized in Tab. C.1 of Appendix C.

Controlled electric drive

In order to validate the mathematical model of the electric drive against the data from the laboratory crane, tracking of the position in the corresponding control mode has been studied. For this reason, a step change of the reference position to $z_{ref} = 200 \text{ mm}$ is considered. Simulation and experimental results are depicted in Fig. 2.14. Here, the trolley reaches the desired position after about 2 sec without any overshoot. It can be seen that the linear model of the trolley drive in position control mode reflects the dynamics of the experimental data, and the position time response resembles the dynamics of a linear first-order system. The mismatches of the control voltage and the motor current are caused by neglected friction forces. However, as aforementioned, these

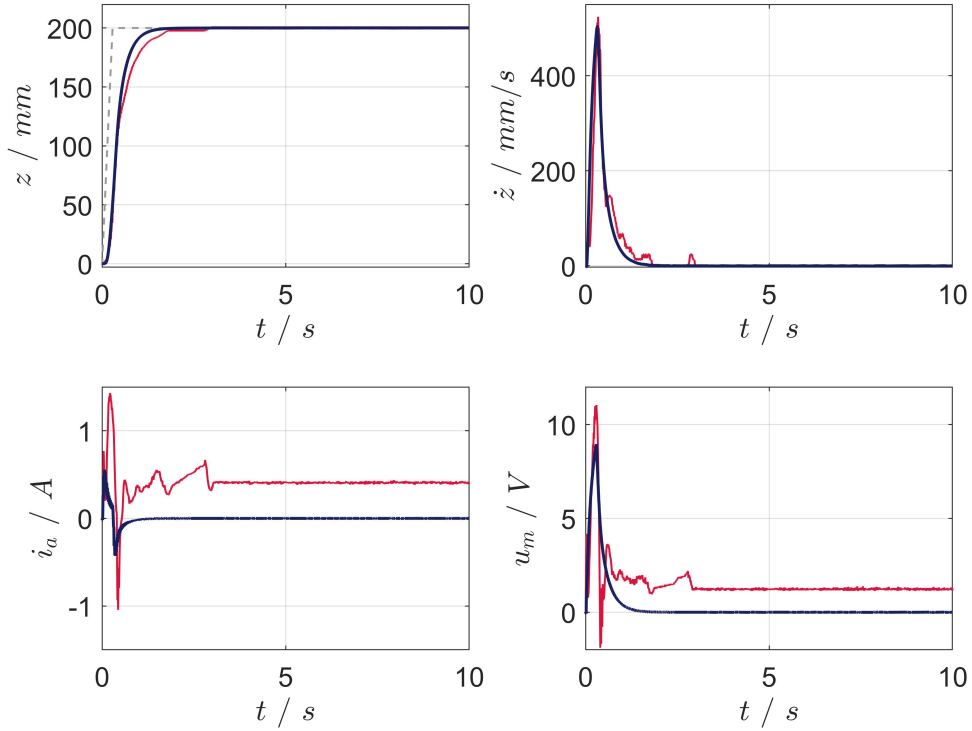


Figure 2.14.: Simulated (blue) and experimental (red) time responses of the trolley positioning applying a reference trajectory (gray)

effects are compensated in the inner current loop and have no impact on the position steady-state. As the peak of the current is around 50 % of the limitation current value of $i_{max} = 3 \text{ A}$, it can be considered that the system is operated in the linear region. Hence, for convenience, for the further control design, it is assumed that the closed loop system $G_z(s)$ can be approximated as a simple first-order system

$$G_z(s) = \frac{z(s)}{z_{ref}(s)} = \frac{1}{T_z s + 1}, \quad (2.83)$$

where T_z is the time constant which can be directly identified from the time responses.

Overall plant model

The structural dynamics of this *simplified* crane configuration can be obtained according to the system of equations (2.19), (2.20), (2.21), (2.22) and (2.23) as follows:

$$q\ddot{w} + E\mathcal{I}w'''' + c\dot{w} = 0, \quad (2.84)$$

$$w(0) = w'(0) = w''(L) = 0, \quad (2.85)$$

$$m_\Sigma\ddot{w}(L) + F_t - E\mathcal{I}w'''(L) = 0. \quad (2.86)$$

The low order transfer function from the trolley force to the girder acceleration $P_1(s)$ can be obtained according to Section 2.1.

Then, the overall plant model $P_o(s)$, which represents the gantry crane motion with structural dynamics for the *simplified* system configuration, is represented in Fig. 2.15. Here, the trolley drive system is in position control mode, and the trolley acceleration force F_t excite the elastic crane vibrations. This force is derived using the approximated second derivative with the low pass filter, where T_{d1} is the associated filter constant. The output of interest for the control design is the acceleration of girder point \ddot{w}_L and the control input is the reference position z_{ref} .

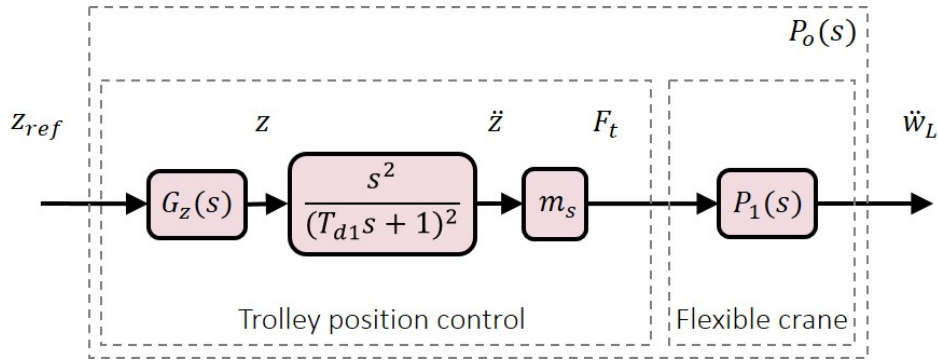


Figure 2.15.: Crane plant augmented by the trolley position control

Simulation and experimental results of trolley positioning and flexible crane dynamics are presented in Fig. 2.16. As can be seen, the crane model reflects the dynamics of the laboratory model with small mismatches due to nonlinearities of real flexible legs. The trolley motion during this experiment excites the first system eigenmode with eigenfrequency $f_1 = 0.93Hz$ ($\omega_1 = 5.87 rad/s$).

2.4.3. Model of full crane configuration

In this Section, the mathematical model of the *full* crane configuration is compared and validated against the experimental data. For this experimental configuration, the system couplings between the trolley, payload, and structure have to be taken into account. The fully coupled gantry model is presented in Section 2.1. There, it has been assumed that the payload is coupled with the trolley via a massless rigid rope. However, in the laboratory crane configuration, a soft rope has been utilized. Due to the fact that the crane structural vibrations are damped in the rope and are not transmitted to the load, this results in weak coupling of payload and crane structure. Therefore, this coupling can be neglected, i.e., the acceleration angle of the payload $\ddot{\varphi}$ in (2.23) does not directly depend on the acceleration of structure girder \ddot{w}_L .

Considering this additional assumption, equations of motion of this *full* experimental configuration can be obtained according to (2.19), (2.20), (2.21), (2.22) and (2.23) as

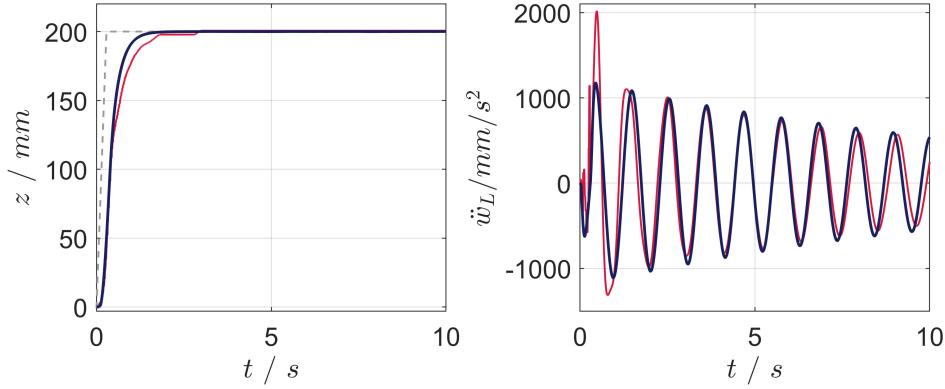


Figure 2.16.: Simulated (blue) and experimental (red) time responses of the elastic gantry crane with the trolley position control

follows:

$$\rho \ddot{w} + EI w'''' + c \dot{w} = 0, \quad (2.87)$$

$$w(0) = w'(0) = w''(L) = 0, \quad (2.88)$$

$$m_{\Sigma} \ddot{w}(L) + m_s \ddot{z} + m_p l \ddot{\varphi} \cos \varphi - m_p l \dot{\varphi}^2 \sin \varphi - EI w''''(L) = 0, \quad (2.89)$$

$$m_s \ddot{w}(L) + m_s \ddot{z} + m_p l \ddot{\varphi} \cos \varphi - m_p l \dot{\varphi}^2 \sin \varphi - F_t + F_{fr} = 0, \quad (2.90)$$

$$l \ddot{\varphi} + \ddot{z} \cos \varphi + g \sin \varphi = 0. \quad (2.91)$$

The simulation model for this configuration can be obtained applying the same model simplification procedures according to Section 2.1, whereas the model parameters are summarized in Tab. C.2 of Appendix C.

In this case, the trolley drive is considered to be in the current control mode. As mentioned in Section 2.3.3, the resulting control loop is relatively fast compared to the mechanical subsystems, such that it can be neglected, and the trolley force F_t can be considered as the plant input. Depending on the control system, the following outputs of interest of the plant model can be considered as measured:

- trolley position z ,
- trolley velocity \dot{z} ,
- acceleration of crane girder $\ddot{w}(L)$,
- acceleration of payload \ddot{z}_p .

Here, it should be mentioned that the horizontal acceleration of the payload is measured, i.e.,

$$\ddot{z}_p = \ddot{z} + l \ddot{\varphi} \cos \varphi - l \dot{\varphi}^2 \sin \varphi. \quad (2.92)$$

Linearizing the horizontal payload acceleration \ddot{z}_p in the equilibrium point $\varphi = 0$ yields

$$\ddot{z}_p = \ddot{z} + l \ddot{\varphi}. \quad (2.93)$$

Simulation and experimental results of the open-loop crane operation are presented in Fig. 2.17. Here, the plant output measurements are compared to the model outputs, whereas the system dynamics is excited by the trolley force impulse input F_t with peak value 1.72 N and width 0.15 s . From the experimental data, a relatively good matching between the model and measured signals can be seen. Small differences are caused mostly by the model uncertainties due to the friction effects. It can be seen that the trolley motion excites the load oscillations with eigenfrequency $f_p = 0.6 \text{ Hz}$ ($\omega_1 = 3.82 \text{ rad/s}$) and the first structure eigenfrequency $f_1 = 1.6 \text{ Hz}$ ($\omega_1 = 10.24 \text{ rad/s}$).

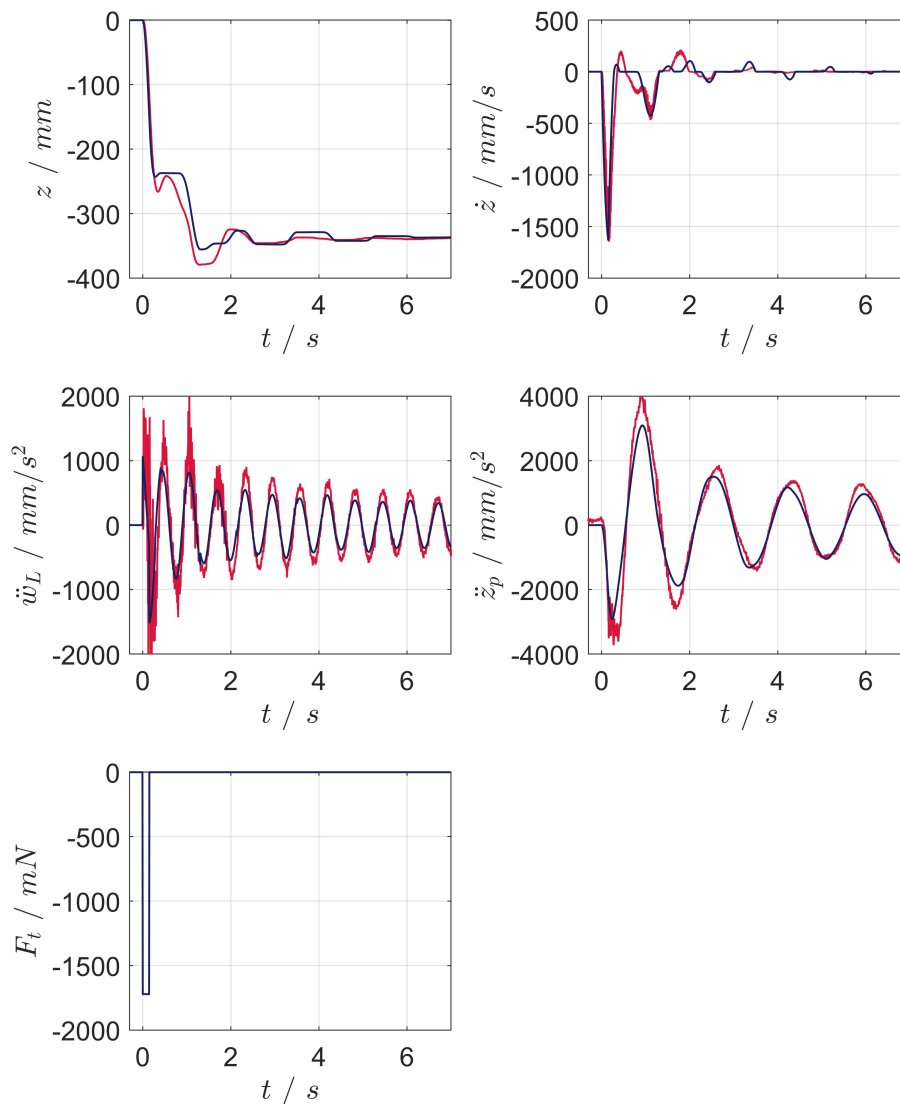


Figure 2.17.: Simulated (blue) and experimental (red) time responses of the elastic gantry crane applying a trolley force impulse input (**bottom**, left)

3. Linear robust control

In this Chapter, linear robust control design for the *simplified* configuration of laboratory gantry crane is proposed [35, 37]. This control design does not require a drive control system redesign and, therefore, can be easily implemented in most industrial cranes. The idea here is to design a robust control law applying H_∞ - loop-shaping design procedure. This control law has to satisfy robust stability and specific performance criteria under the assumption that gantry crane parameters are not exactly known. In the following, the uncertainty models and the control design procedure will be presented. After that, the proposed method will be verified in the simulation and experimental study.

3.1. Uncertainty models

The application of control is inherently concerned with the presence of uncertainties. There exist different ways how uncertainties can be described and included in a control system. In this Chapter, dynamic perturbation uncertainties based on the coprime factor description are introduced. It is considered that the parameters of the gantry crane for different loading are not constant, and the stiffness of the flexible part is not accurately known. Besides, uncertainties related to model order reduction can also be considered.

3.1.1. Coprime factor uncertainty

From a control design perspective, a set of models for various parameters can be embedded into a plant with nominal parameters $P_n(s)$ and a family of bounded uncertainties that, in general, should be stable and have a finite H_∞ -norm [96, 124]. In plants with weakly damped or undamped dynamics, utilization of the coprime factor description is well suited for including the model uncertainties. The normalized coprime factorization for the nominal system can be represented as follows:

$$P_n(s) = \frac{N_n(s)}{M_n(s)}, \quad (3.1)$$

where $M_n(s), N_n(s)$ are coprime transfer functions that fulfill the following Bezout identity

$$M_n(s)M_n(-s) + N_n(s)N_n(-s) = 1. \quad (3.2)$$

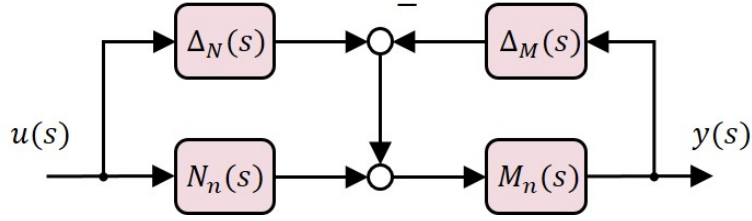


Figure 3.1.: Coprime factor uncertainty

In Fig. 3.1 the coprime factor uncertainty scheme is presented. Here, a plant model with uncertain parameters $P_\Delta(s)$ can be expressed by the nominal system $P_n(s)$ and coprime factor uncertainties $\Delta_M(s)$ and $\Delta_N(s)$ as follows:

$$P_\Delta(s) = \frac{N_n(s) + \Delta_N(s)}{M_n(s) + \Delta_M(s)}. \quad (3.3)$$

This representation does not provide a unique realization of the uncertainty transfer functions $\Delta_M(s)$ and $\Delta_N(s)$, resulting in a supplementary degree of freedom for their selection. A common choice is a coprime factor description with a minimal H_∞ -norm for $[\Delta_M(s), \Delta_N(s)]$ resulting in the gap metric.

3.1.2. Gap metric

According to [27, 107], the gap metric δ_g between the system with nominal parameters $P_n(s)$ and the system with uncertainty $P_\Delta(s)$ can be obtained as the maximum of the directed gaps

$$\delta_g(P_n, P_\Delta) = \max\{\vec{\delta}_g(P_n, P_\Delta), \overleftarrow{\delta}_g(P_\Delta, P_n)\}, \quad (3.4)$$

where

$$\vec{\delta}_g(P_n, P_\Delta) := \inf_{[\Delta_M \Delta_N]} \{\|\Delta_M \Delta_N\|_\infty : P_\Delta\}. \quad (3.5)$$

It should be mentioned that the gap metric values may be in the range from zero to one. Here, the systems $P_n(s)$ and $P_\Delta(s)$ are considered close in sense of the gap metric, i.e., can be stabilized by the same controller, if $\delta_g(P_n, P_\Delta)$ is close to zero and vice-versa. From a robust control design perspective, the corresponding value of the gap metric between the model with nominal parameters and set of models with uncertain parameters can be utilized to measure the necessary robustness margin.

In order to estimate several error sources, the triangular inequality property can be applied

$$\delta(P_1, P_3) \leq \delta(P_1, P_2) + \delta(P_2, P_3). \quad (3.6)$$

For example, the triangular inequality can be used to obtain the distance between the low-order model with uncertain parameters P_Δ and the original model with nominal parameters P in terms of the gap metric $\delta(P_\Delta, P)$. For this reason, according to the triangular inequality (3.6): $P_1 = P_\Delta$ is considered as a low-order approximation of the

system with uncertain parameters, $P_2 = P_n$ as a low-order approximation of the original system with nominal parameter and $P_3 = P$ as a high-order realization of the original system with nominal parameters. Hence, the numerical discretization errors and model order reduction errors can be taken into consideration in a unified manner.

3.2. H_∞ - loop-shaping control design

The main idea of the H_∞ - loop-shaping design is to combine the classical loop shaping method with the H_∞ - based robust stabilization for the fulfillment of both - performance and robustness criteria [96, 124, 33]. Here, the design of the corresponding controller comprises two stages. A compensator is applied for an adjustment of the open-loop system eigenvalues such that the desired performance specifications for the closed loop system are satisfied. After that, a robust stabilizing controller can be obtained with regard to the normalized coprime factor uncertainty.

The desired closed loop performance specifications can be derived by shaping the open-loop system using a compensator $W_s(s)$ as illustrated in Fig. 3.2,

$$P_s(s) = P_n(s)W_s(s). \quad (3.7)$$

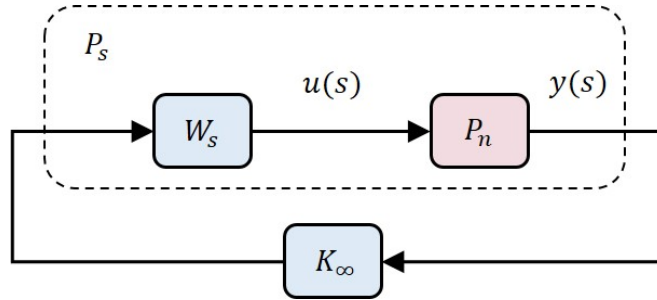


Figure 3.2.: Shaped plant of closed loop system

Taking into consideration the weighted open-loop plant in its normalized coprime factor representation $P_s(s) = N_n(s)/M_n(s)$ and the following H_∞ - control problem

$$\left\| \begin{bmatrix} K_\infty \\ 1 \end{bmatrix} \frac{1}{(1 + P_s K_\infty) M_n} \right\|_\infty \leq \epsilon^{-1}, \quad (3.8)$$

the controller K_∞ , which guarantees a robustness margin ϵ with regard to the normalized coprime factor uncertainties, can be derived.

The maximum robustness margin ϵ_{max} , which can be achieved is given as follows:

$$\epsilon_{max} = (1 + \rho_r(XZ))^{-1/2}. \quad (3.9)$$

Here, $\rho_r(\cdot)$ is the spectral norm (maximum eigenvalue), X and Z are the associated positive definite solutions of the algebraic Riccati equations

$$(A - BR^{-1}DC)^T X + X(A - BR^{-1}DC) - XB^T R^{-1}BX + CR^{-1}C^T = 0, \quad (3.10)$$

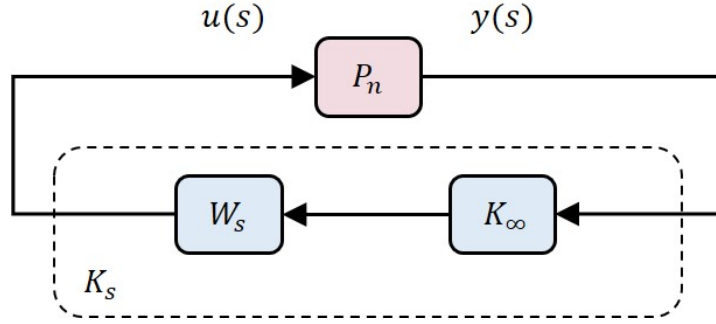


Figure 3.3.: Stabilizing controller

$$(A - BR^{-1}DC)Z + Z(A - BR^{-1}DC)^T - ZC^T R^{-1}CZ + BR^{-1}B^T = 0, \quad (3.11)$$

where $R = 1 + D^2$ and A, B, C, D are the state-space matrices of the shaped nominal plant $P_s(s)$.

The controller K_∞ that satisfies (3.8) can be calculated for predefined $\epsilon < \epsilon_{max}$ as follows:

$$K_\infty = \left[\begin{array}{c|c} A + BF + \epsilon^{-2}(L^T)^{-1}ZC^T(C + DF) & \epsilon^{-2}(L^T)^{-1}ZC^T \\ \hline B^T X & -D^T \end{array} \right], \quad (3.12)$$

with

$$F = -R^{-1}(D^T C + B^T X), \quad (3.13)$$

$$L = (1 - \epsilon^{-2})I + XZ. \quad (3.14)$$

Application of the presented control design for the shaped nominal plant $P_s(s)$ results in the controller K_∞ with the stability margin ϵ . Then, if $\delta_g(P_s, P_\Delta) < \epsilon$, the controller guarantees stability for the shaped uncertain plant $P_\Delta(s)$.

The overall controller K_s can be derived as depicted in Fig. 3.3 as follows:

$$K_s(s) = K_\infty(s)W_s(s). \quad (3.15)$$

3.3. Simulation study

3.3.1. Robust controller design

In this Section, the described robust control design procedure is applied for the nominal gantry crane of the *simplified* configuration. Here, from the Fig. 3.4 it can be seen that the nominal plant transfer function $P_n(s)$ (blue line) possesses a peak at the first eigenfrequency $\omega_1 = 5.87 \text{ rad/s}$ with magnitude $|G_s(j\omega_1)| = 47 \text{ dB}$, slopes $n_l =$

+80 dB/decade at the low frequency range and $n_h = -80$ dB/decade at the high frequency range, and the gain crossover frequency $\omega_c = 191$ rad/s. It can also be mentioned that the model has an unbiased output state and a relatively high gain crossover frequency ω_c , which can increase the influence of the measurement noise or high-frequency modes dynamics that has been neglected. The second eigenfrequency of the structural dynamics is $\omega_2 \approx 130$ rad/s. As this dynamics has been neglected for the controller design, shaping the open-loop singular values should primarily reduce this frequencies range. In addition, the trade-off between given robustness requirements and fast transients has been taken into account. Thus, the compensator $W_s(s)$, which weights the open-loop nominal plant $P_n(s)$, is chosen as follows:

$$W_s(s) = \frac{0.1}{0.05s + 1}. \quad (3.16)$$

In Fig. 3.4 the Bode magnitude plots of the nominal and shaped plant are presented. Solution of the problem (3.8) for the given precompensator $W_s(s)$ yields the robust controller K_∞ with the stability margin

$$\epsilon = 0.48. \quad (3.17)$$

The Bode plot of the overall controller K_s is depicted in Fig. 3.5.

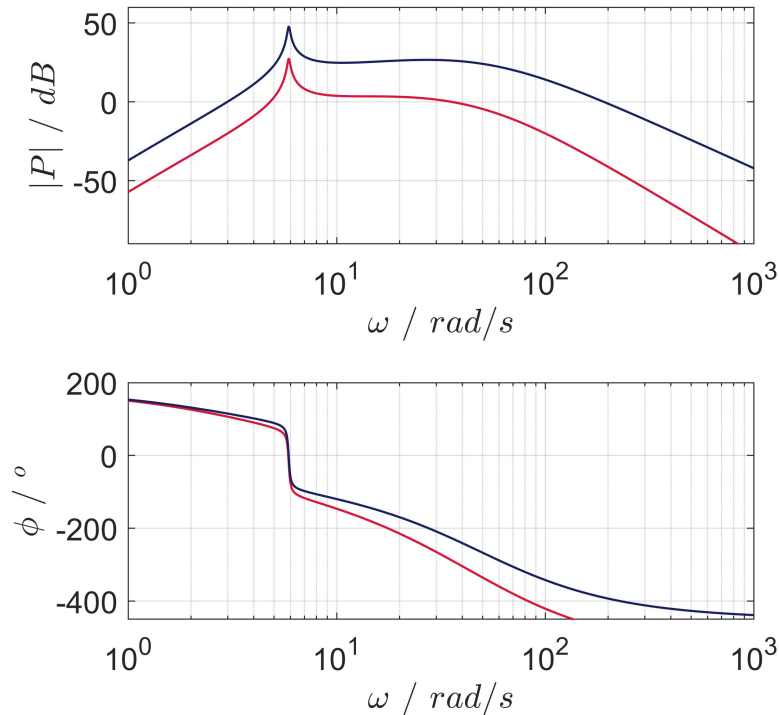
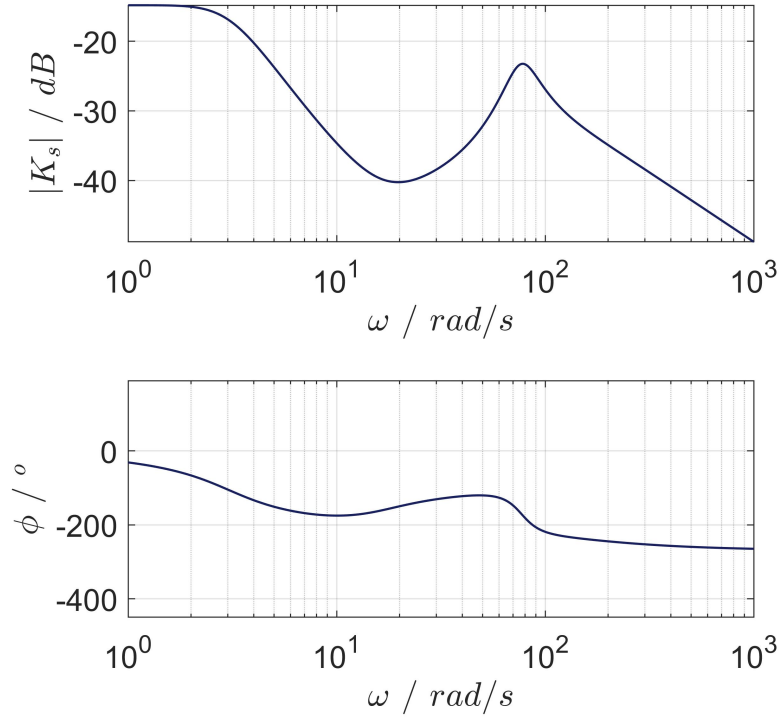


Figure 3.4.: Bode diagrams for the nominal system plant (blue) and the shaped system plant (red)

Figure 3.5.: The Bode diagram of controller $K_s(s)$

3.3.2. Gantry crane model uncertainties

In the following, the numerical uncertain crane models are presented, and the required robustness margin is evaluated. During the operation of gantry cranes, parameter variations and uncertainties are unavoidable, e.g., different masses of payload, different rope lengths, neglected high-frequency dynamics, etc. In this work, the system structural dynamics for unloaded and loaded cases and stiffness of the crane legs are assumed to be coarsely known. Thus, a set of crane models can be achieved applying the methodology, which has been presented in Section 2.1. Here, the set of models Π_C which includes 169 models, is generated from the nominal model by variations of the following parameters:

- additional mass on the girder $m_s = m_{t,t} + m_p$, where mass of the trolley is constant and mass of the payload m_p varies,
- elastic modulus E of the material of the gantry legs.

It is considered that these parameters for model variations are within certain intervals

$$m_s = \bar{m}_s(1 + k_m \Delta_m), \quad (3.18)$$

$$E = \bar{E}(1 + k_E \Delta_E), \quad (3.19)$$

where \bar{m}_s and \bar{E} are the values of the nominal model, k_m , k_E and Δ_m , Δ_E define possible variations.

Here, the following values for parameter variations are chosen:

- $k_m = 0.5$, $-1 \leq \Delta_m \leq 1$ yielding up to 50% variation in the crane loading,
- $k_E = 0.3$, $-1 \leq \Delta_E \leq 1$ representing up to 30% in crane legs stiffness.

Therefore, the nominal model $P_n(s) \in \Pi_C$ can be obtained by substituting $\Delta_m = \Delta_E = 0$ which corresponds to a half of the crane loading capacity. Here, the transfer function of the nominal crane model is obtained as:

$$P_n(s) = -3 \cdot 10^7 \cdot \frac{s^4}{(s+10)(s+50)^4(s^2+0.16s+34.62)}. \quad (3.20)$$

The domain of the considered parameters is visualized in Fig. 3.6.

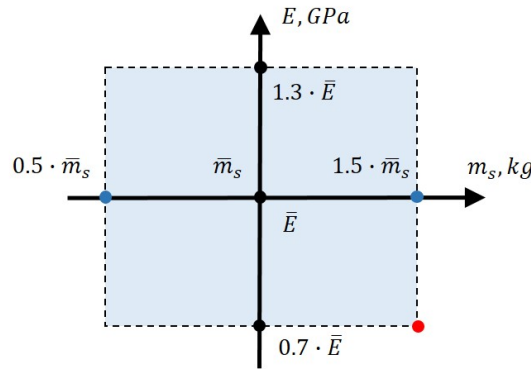


Figure 3.6.: Domain of parameter variations

In Fig. 3.7, Fig. 3.8 and Fig. 3.9 the obtained simulation results are depicted. Fig. 3.7 and Fig. 3.8 represent the Bode diagrams and step responses of the model with nominal parameter (blue) and models with uncertain parameters (gray). From the results can be seen how the system eigenfrequency for different uncertain parameters varies. Here, the first eigenfrequency of the mechanical structure for nominal parameters is approximately $f_1 = 0.93 Hz$ ($\omega_1 = 5.87 rad/s$) and the frequency variation for the uncertain parameter systems is in a range $0.72 - 1.16 Hz$ ($4.57 - 7.27 rad/s$).

In Fig. 3.9 the calculated gap metrics for a set of shaped crane models are depicted. Here, the maximum of the gap metric which corresponds to the case of maximum loading and minimal value of Young's modulus E (Fig. 3.6, red point) follows

$$\delta_g(P_\Delta, P_s) = 0.29 \quad (3.21)$$

and the order reduction error in sense of the gap metric can be calculated as

$$\delta_g(P_s, P) = 0.02. \quad (3.22)$$

Thus, according to [107], applying the triangular inequality (3.6) the required robustness margin for the stabilizing controller can be obtained as

$$\delta(P_\Delta, P) \leq \delta(P_\Delta, P_s) + \delta(P_s, P) = 0.31. \quad (3.23)$$

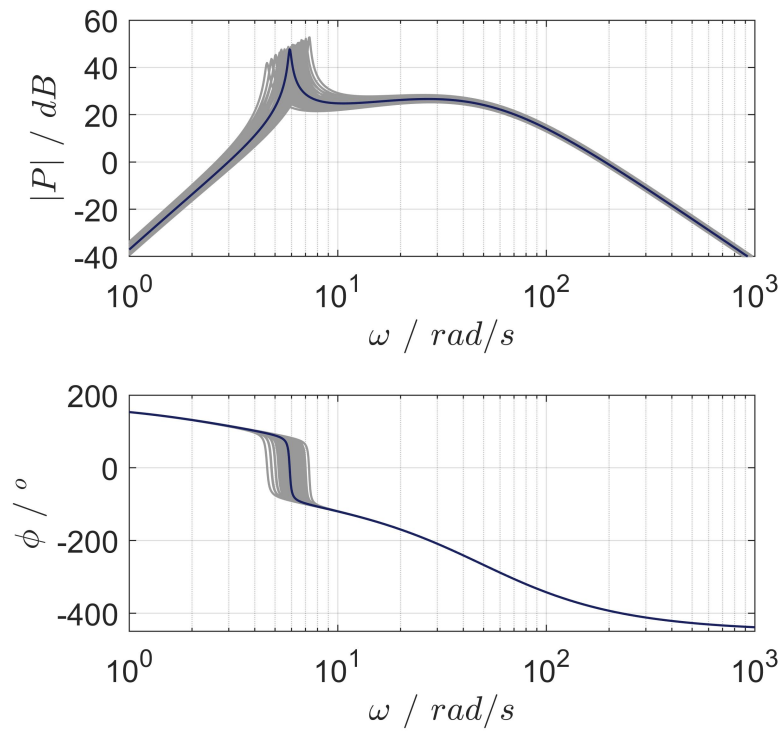


Figure 3.7.: The Bode diagram of the nominal system (blue) and the uncertain crane systems (gray)

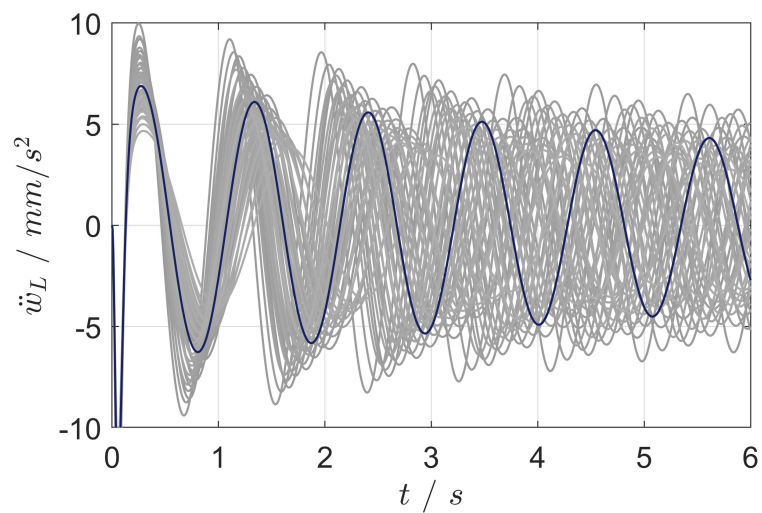


Figure 3.8.: Step responses for the uncertain crane systems

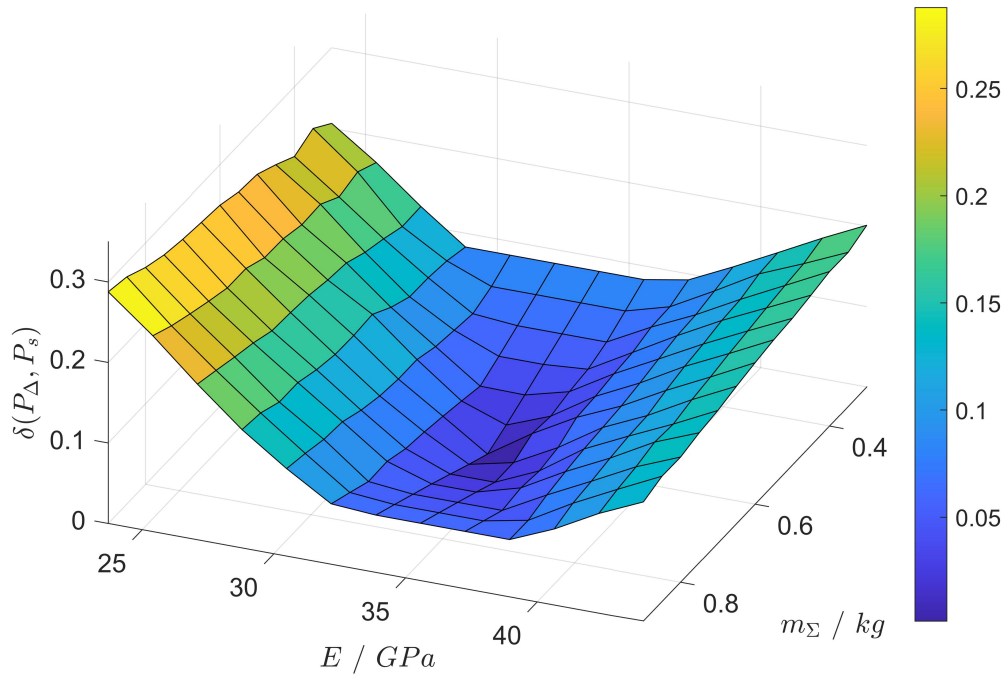


Figure 3.9.: Gap metric sequence

3.3.3. Robust control of gantry crane

In this Section, the resulting controller K_s validated in the simulation study. From (3.17) and (3.23) follows that the stability margin $\epsilon = 0.48$ is greater than the maximum of the gap metric $\delta_{g,max} = 0.31$, i.e., the obtained controller guarantees robust stability for the given set of uncertain gantry crane models.

In Fig. 3.10, Fig. 3.11 and Fig. 3.5 the obtained simulation results of the closed loop systems are represented. Fig. 3.7 and Fig. 3.8 show the Bode diagrams and step responses of the model with nominal parameter (blue) and models with uncertain parameters (gray). From the results a notable damping of the crane vibrations for different uncertain parameters can be seen.

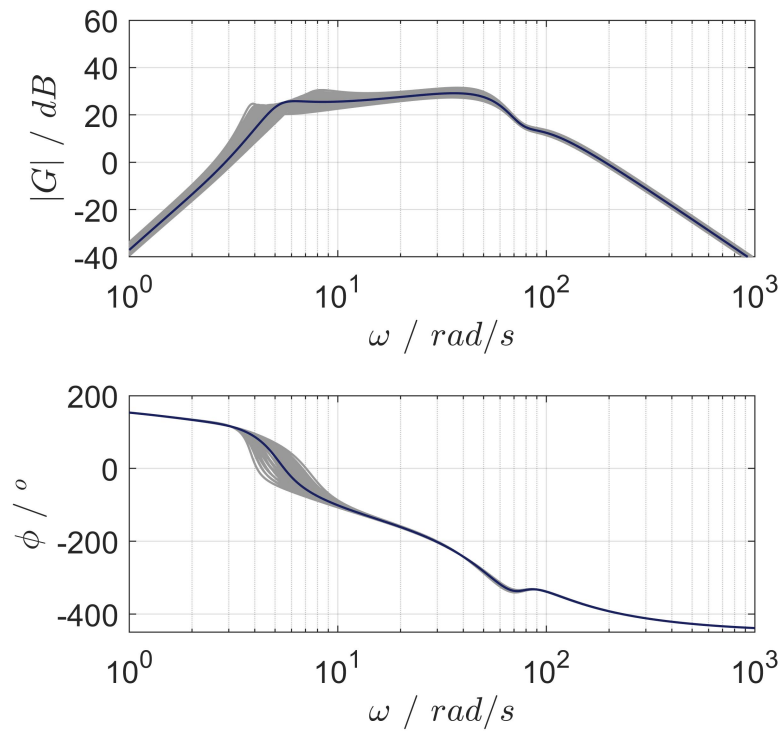


Figure 3.10.: The Bode diagrams of the closed loop nominal system (blue) and the closed loop uncertain crane systems (gray)

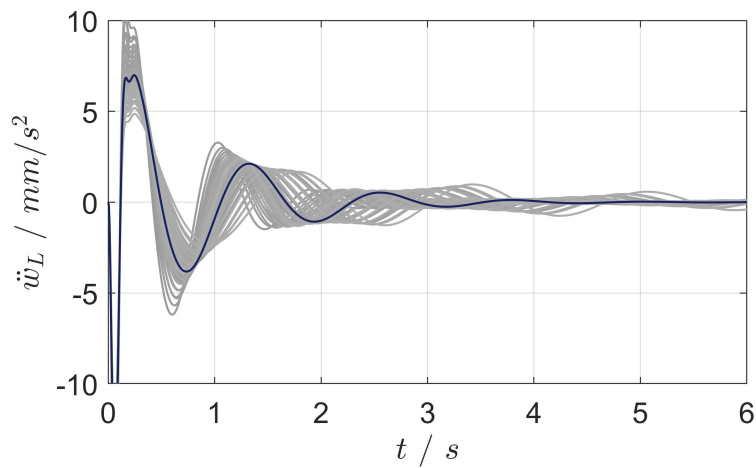


Figure 3.11.: Step responses of the closed loop nominal system (blue) and the closed loop uncertain crane systems (gray)

3.4. Experimental evaluation

In the following, the proposed control approach for active damping of structural vibrations is validated on a laboratory gantry crane of the *simplified* configuration. For this reason, tracking of the trolley position with a step change of the reference signal to $z_r = 200 \text{ mm}$ is studied.

The designed linear robust controller has been implemented on the *simplified* configuration of the laboratory crane setup. The obtained results are presented in Fig. 3.12, Fig. 3.13, Fig. 3.14, Fig. 3.15, and Fig. 3.16. Here, Fig. 3.12 shows the comparison of the simulation and experimental results. From simulation results of the nominal model can be seen that the trolley rises to the desired position (95 % of the z_{ref} is considered) after approximately 0.78 s and settles after 2.37 s with an overshoot 9 %. The vibrations of the structure are notably damped after 2.3 s. The experimental results show that the trolley position rises after 0.84 s and settled after 4 s with an overshoot 14 %. The structural vibrations are notably damped after 2.3 s with relatively small residual oscillations, i.e., the maximal magnitude of acceleration in the steady state $\ddot{w}(L) \approx 40 \text{ mm/s}^2$. The mismatches between the simulation and experimental results are caused mostly by friction effects in the gear.

For comparison, the experimental results for the trolley positioning with and without the proposed robust control approach are depicted in Fig. 3.13. The results show the importance of taking the structural dynamics of large gantry cranes into account for control purposes. The application of the proposed linear control leads to notable damping of the crane structural dynamics.

In Fig. 3.14 experimental results of disturbance rejection are shown. Here, an impulse disturbance is applied to the mechanical structure at time 15 s. It can be seen that the vibrations are notably damped after approximately 2.4 s with relatively small residual oscillations, i.e., the maximal magnitude of acceleration in the steady-state $\ddot{w}(L) \approx 100 \text{ mm/s}^2$.

For experimental evaluation of the robustness properties of the obtained control system, additional experimental responses for a varying mass m_s are presented in Fig. 3.15 and Fig. 3.16. Here, two cases are considered:

- overall mass $m_s = 0.3 \text{ kg}$ contains only the mass of the trolley (left blue point in Fig. 3.6),
- overall mass $m_s = 0.9 \text{ kg}$ relates to the maximum loading condition (right blue point in Fig. 3.6)

In both figures a notable vibrations damping for the described conditions of crane loading can be seen.

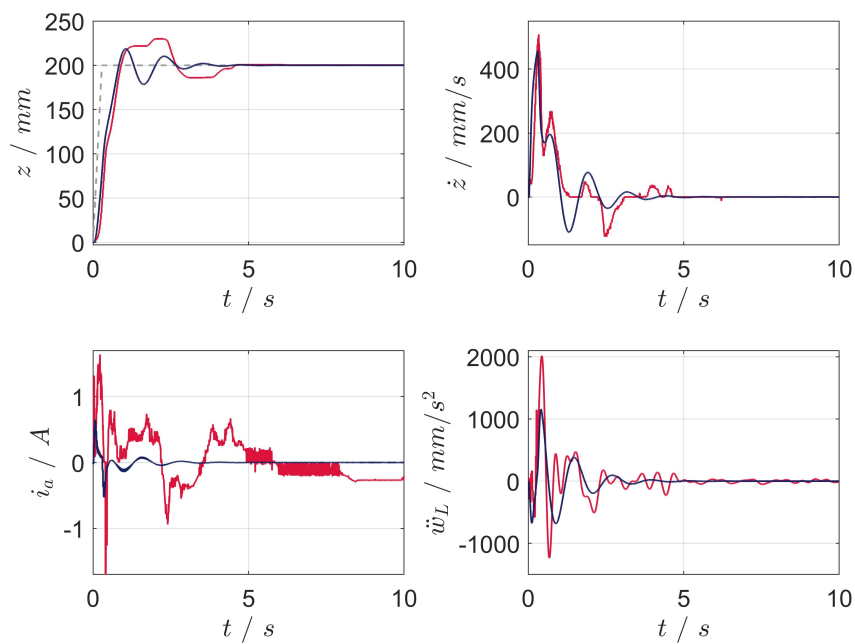


Figure 3.12.: Simulated (blue) and experimental (red) time responses of the elastic gantry crane by reference tracking applying linear robust control

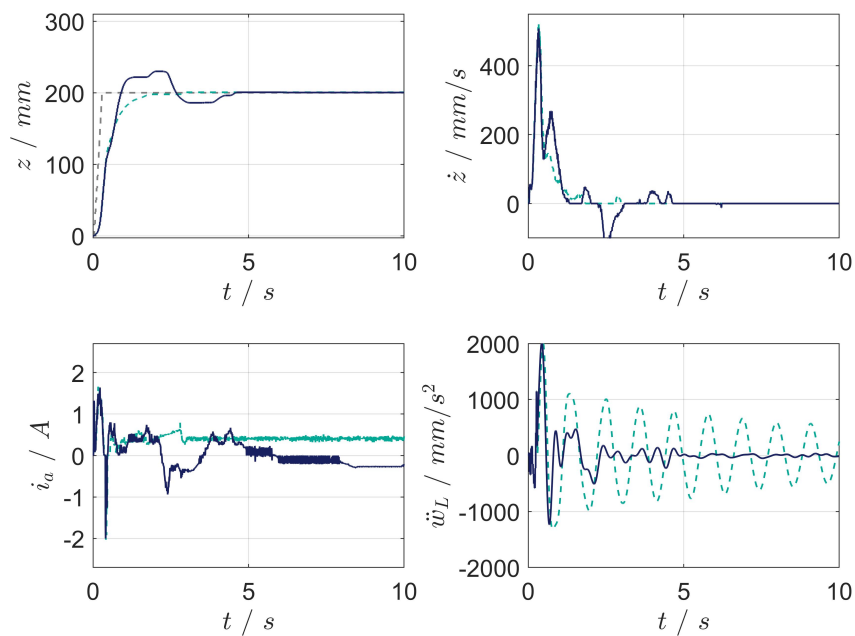


Figure 3.13.: Experimental time responses of the elastic gantry crane applying linear robust control (blue) and position control without damping (green)

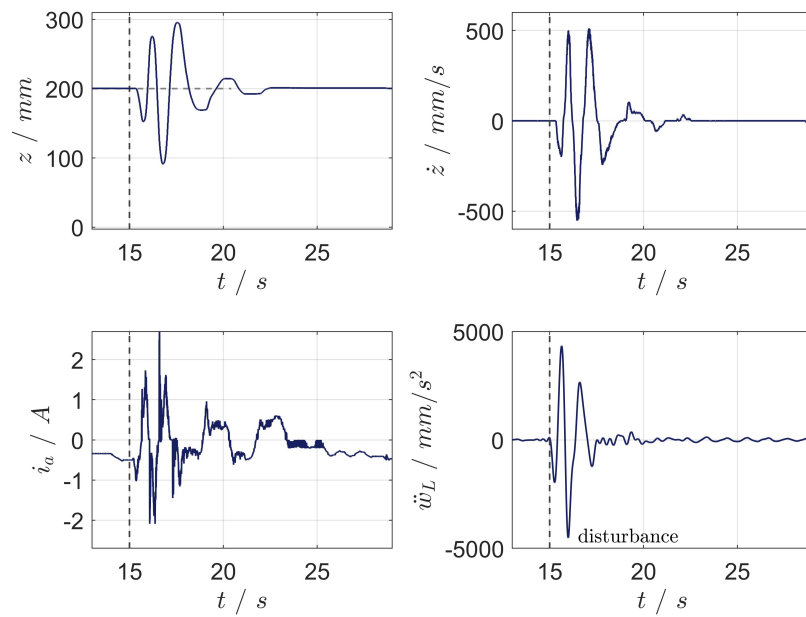


Figure 3.14.: Experimental time responses of the elastic gantry crane applying linear robust control with a disturbance on the mechanical structure at time 15 s

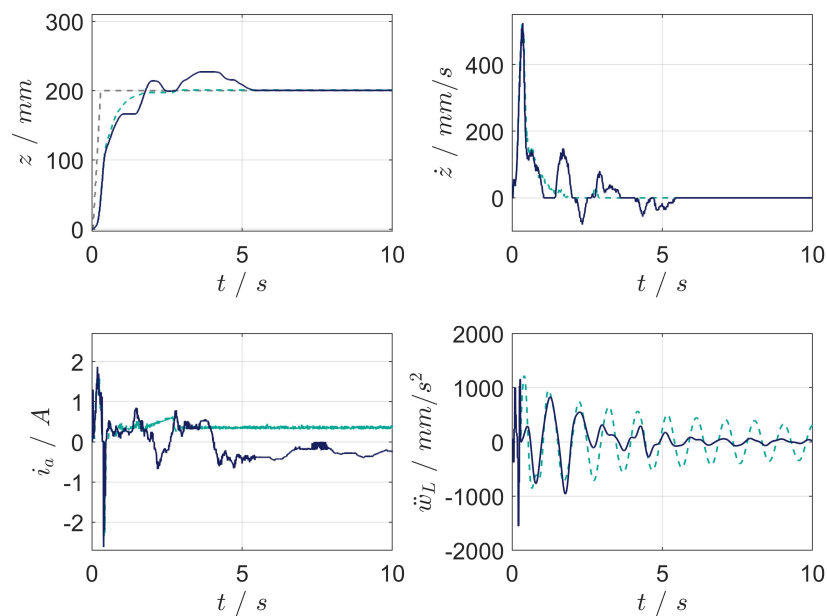


Figure 3.15.: Experimental time responses of the elastic gantry crane in the unloaded case applying linear robust control (blue) and position control without damping (green)

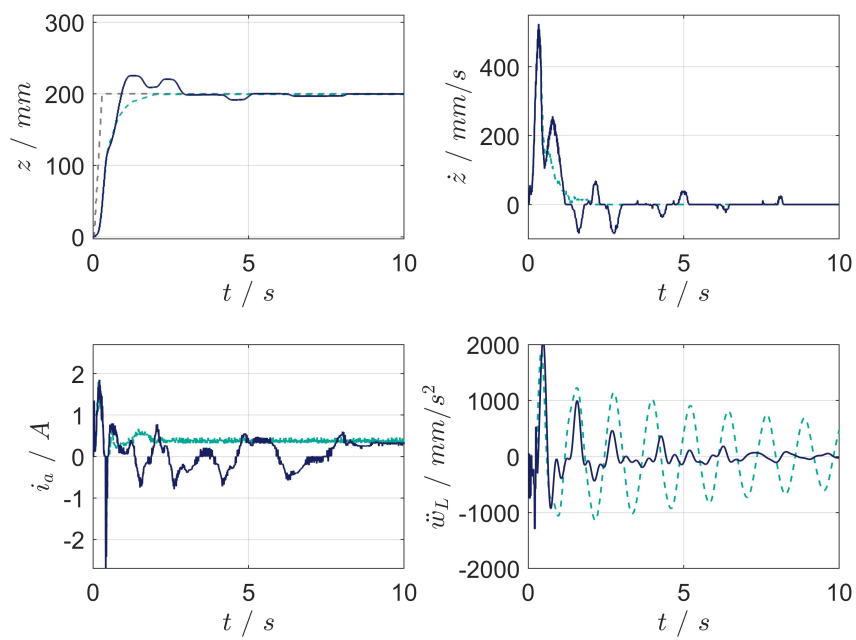


Figure 3.16.: Experimental time responses of the elastic gantry crane in the fully-loaded case applying linear robust control (blue) and position control without damping (green)

4. PFC-based linear control

In this Chapter, the PFC-based linear control design for the *full* configuration of the laboratory gantry crane is presented [36, 34]. This control provides the positioning of the payload and damping of the oscillating dynamics via a combination of a parallel feed-forward compensator (PFC) and an output feedback controller. Here, the PFC is designed for a compensation of the system zero dynamics and for rendering the extended plant almost strict positive real (ASPR). The proposed design provides a zero placement of the extended plant and reduces the bias contribution of the PFC. Thereafter, the augmented system can be stabilized by applying a high-gain output feedback control. The main advantages of the proposed control can be summarized as follows:

- no additional sensors for oscillations measurements are needed;
- simple linear design procedure for the considered single-input single-output (SISO) plant of the gantry crane;
- no redesign of the motion control system is needed, i.e., simple integration into a classical cascade control scheme.

The following approach is only applicable for gantry crane configurations with strong couplings between the trolley, load, and structure, i.e., the system plant is observable in this configuration. The presented approach is verified in the corresponding simulation study and on the *full* experimental crane configuration.

4.1. Relative degree and zero dynamics of the system

The relative degree of a system and its zero dynamics are essential properties for feedback control design. In the following, definitions of the relative degree and zero dynamics of a system are presented according to [43, 32, 61, 84].

Consider the following nonlinear SISO system with an affine input

$$\dot{x} = f(x) + g(x)u, \quad (4.1)$$

$$y = h(x), \quad (4.2)$$

where the functions $f(\cdot)$, $g(\cdot)$ and $h(\cdot)$ are infinitely differentiable, $x \in \mathbb{R}^n$ and consider the local behavior of the system in the neighborhood of $x = x_0$. The relative degree of the system can be obtained by sequential differentiation of the output equation (4.2) with respect to time.

For instance, if by taking the first derivative

$$\begin{aligned}\dot{y} &= \frac{\partial h}{\partial x} \dot{x} \\ &= \frac{\partial h}{\partial x} f(x) + \frac{\partial h}{\partial x} g(x)u,\end{aligned}\quad (4.3)$$

the term

$$\frac{\partial h}{\partial x} g(x) \neq 0, \quad (4.4)$$

then an explicit dependency of \dot{y} on the input u at the point x_0 and its neighborhood exists, and the relative degree is $\vartheta = 1$. Otherwise, assuming that

$$\dot{y} = h_2 = \frac{\partial h}{\partial x} f(x), \quad (4.5)$$

the second derivative of (4.2) is obtained and can be represented as follows:

$$\ddot{y} = \frac{\partial h_2}{\partial x} f(x) + \frac{\partial h_2}{\partial x} g(x)u. \quad (4.6)$$

Here, the same procedure is applied. If the term

$$\frac{\partial h_2}{\partial x} g(x) \neq 0, \quad (4.7)$$

the system possesses the relative degree $\vartheta = 2$. Otherwise, \ddot{y} does not depend on u directly and the procedure continues until an explicit dependency appears.

In general, consider the following set of functions that is defined as

$$h_i = \frac{\partial h_{i-1}}{\partial x} f(x), \quad i = 2, \dots, \vartheta, \quad \text{and} \quad h_1 = h(x). \quad (4.8)$$

Then, if for the ϑ -th output derivative

$$y^{(\vartheta)} = \frac{\partial h_\vartheta}{\partial x} f(x) + \frac{\partial h_\vartheta}{\partial x} g(x)u \quad (4.9)$$

the following conditions are fulfilled

$$\frac{\partial h_1}{\partial x} g(x) = \frac{\partial h_2}{\partial x} g(x) = \dots = \frac{\partial h_{\vartheta-1}}{\partial x} g(x) = 0, \quad (4.10)$$

$$\frac{\partial h_\vartheta}{\partial x} g(x) \neq 0, \quad (4.11)$$

the system has the relative degree ϑ at the point x_0 and its neighborhood. If the relative degree is equal to the system order, i.e., $\vartheta = n$, the system has a full relative degree.

In order to represent sequential differentiation, the notion of Lie derivative is commonly used. Here, (4.8) can be rewritten as

$$h_i(x) = \mathcal{L}_f^{i-1} h(x) = \mathcal{L}_f h_{i-1}(x), \quad i = 2, \dots, \vartheta \quad (4.12)$$

and

$$\frac{\partial h_i}{\partial x} g(x) = \mathcal{L}_g \mathcal{L}_f^{i-1} h(x). \quad (4.13)$$

Thus, in this notation, the system is said to have the relative degree ϑ if for the ϑ -th derivative

$$y^{(\vartheta)} = \mathcal{L}_f^\vartheta f(x) + \mathcal{L}_f \mathcal{L}_f^{\vartheta-1} h(x) u \quad (4.14)$$

the following conditions hold

$$\mathcal{L}_g h(x) = \mathcal{L}_g \mathcal{L}_f h(x) = \dots = \mathcal{L}_f \mathcal{L}_f^{\vartheta-2} h(x) = 0, \quad (4.15)$$

$$\mathcal{L}_f \mathcal{L}_f^{\vartheta-1} h(x) \neq 0. \quad (4.16)$$

In order to present the model described by (4.14) in matrix form consider the new state vector $\xi \in \mathbb{R}^n$ defined as follows:

$$\xi = \begin{pmatrix} \xi_1 \\ \xi_2 \\ \vdots \\ \xi_\vartheta \end{pmatrix} = \begin{pmatrix} y \\ \dot{y} \\ \vdots \\ y^{(\vartheta-1)} \end{pmatrix} = \begin{pmatrix} h(x) \\ \mathcal{L}_f h(x) \\ \vdots \\ \mathcal{L}_f^{\vartheta-1} h(x) \end{pmatrix}. \quad (4.17)$$

Then,

$$\begin{pmatrix} \dot{\xi}_1 \\ \dot{\xi}_2 \\ \vdots \\ \dot{\xi}_\vartheta \\ \dot{\xi}_{\vartheta+1} \\ \vdots \\ \dot{\xi}_n \end{pmatrix} = \begin{pmatrix} \xi_2 \\ \xi_3 \\ \vdots \\ \mathcal{L}_f^\vartheta f(x) + \mathcal{L}_g \mathcal{L}_f^{\vartheta-1} h(x) u \\ \kappa_1(\xi, u) \\ \vdots \\ \kappa_{n-\vartheta}(\xi, u) \end{pmatrix}, \quad (4.18)$$

$$y = \xi_1. \quad (4.19)$$

where $\kappa(\xi, u)$ are nonlinear functions.

Separating the vector ξ into two parts $\xi_d = [\xi_1, \xi_2, \dots, \xi_\vartheta]^T$ and $\xi_z = [\xi_{\vartheta+1}, \xi_{\vartheta+2}, \dots, \xi_n]^T$ the following model is obtained

$$\dot{\xi}_d = A_n \xi_d + B_n (\mathcal{L}_f^\vartheta f(x) + \mathcal{L}_g \mathcal{L}_f^{\vartheta-1} h(x) u), \quad (4.20)$$

$$\dot{\xi}_z = \kappa(\xi_d, \xi_z, u), \quad (4.21)$$

$$y = C_n \xi_d, \quad (4.22)$$

where

$$A_n = \begin{pmatrix} 0 & 1 & 0 & \dots & 0 \\ 0 & 0 & 1 & \dots & 0 \\ \vdots & \vdots & \vdots & \ddots & \vdots \\ 0 & 0 & 0 & \dots & 1 \\ 0 & 0 & 0 & \dots & 0 \end{pmatrix}, \quad B_n = \begin{pmatrix} 0 \\ 0 \\ \vdots \\ 0 \\ 1 \end{pmatrix}, \quad C_n^T = \begin{pmatrix} 1 \\ 0 \\ \vdots \\ 0 \\ 0 \end{pmatrix}. \quad (4.23)$$

Then, applying a linearizing control law with desired choice of dynamics $d(\xi_d)$ as

$$u = -\frac{1}{\mathcal{L}_g \mathcal{L}_f^{\vartheta-1} h(x)} \left(\mathcal{L}_f^{\vartheta} f(x) + d(\xi_d) \right), \quad (4.24)$$

yields

$$\dot{\xi}_d = A_n \xi_d + B_n d(\xi_d), \quad (4.25)$$

$$\dot{\xi}_z = \kappa(\xi_d, \xi_z, u), \quad (4.26)$$

$$y = C_n \xi_d. \quad (4.27)$$

Here, it can be seen that the control law (4.24) stabilizes the output variable y . However, for the input-output configuration when $\vartheta < n$, not the whole system dynamics is stabilized. In this case, the state variables ξ_z are influenced by the nonlinear internal dynamics $\kappa(\xi_d, \xi_z, u)$, which is unobservable from the output y applying the proposed linearizing control law. This internal dynamics associated with the state variables ξ_z is also called zero dynamics.

In general, it should be stated that the system described by (4.25), (4.26) and (4.27) with control law (4.24) is internally asymptotically stable at the point x_0 and its neighborhood if the zero dynamics is asymptotically stable, i.e.,

$$\dot{\xi}_z = \kappa(\xi_d, \xi_z, u), \quad (4.28)$$

is asymptotically stable.

For the SISO linear time-invariant (LTI) system

$$\dot{x} = Ax + Bu, \quad (4.29)$$

$$y = Cx, \quad (4.30)$$

the relative degree can be calculated as the difference between the orders of the denominator and numerator polynomials $\vartheta = n - m$ of the associated transfer function

$$P(s) = C(sI - A)^{-1}B = \frac{a_m s^m + a_{m-1} s^{m-1} + \dots + a_0}{s^n + b_{n-1} s^{n-1} + \dots + b_0} \quad (4.31)$$

or as the smallest positive number which satisfies

$$CA^{\vartheta-1}B \neq 0. \quad (4.32)$$

In the linear case, the zero dynamics notion is equivalent to the zeros of the associate transfer function $P(s)$. The location of the system zeros determines the stability of the zero dynamics. The system is called (strictly) minimum-phase if the zeros z_i of $P(s)$ are in the left-half plane (LHP) $\text{Re}[z_i] \leq 0$ ($\text{Re}[z_i] < 0$).

Example 4.1 Consider a velocity control that should be provided to a oil-well drill string plant [75]. The system dynamics is reflected by an electromechanical second order system with an elastic coupling and a friction load on the second mass, as presented

in Fig. 4.1. Here, the first inertia J_a is driven by the DC motor operating in torque control mode (control input - τ_m), whereas the friction torque τ_f produces an effect on the second inertia J_b . The equations of motion of this system can be written as

$$J_a \ddot{\varphi}_a + k_s \tanh k_g (\varphi_a - \varphi_b) = \tau_m, \quad (4.33)$$

$$J_b \ddot{\varphi}_b - k_s \tanh k_g (\varphi_a - \varphi_b) = -\tau_f(\dot{\varphi}_b), \quad (4.34)$$

where φ_a and φ_b are the angles of the first and second masses respectively, k_s and k_g are parameters of the nonlinear spring.

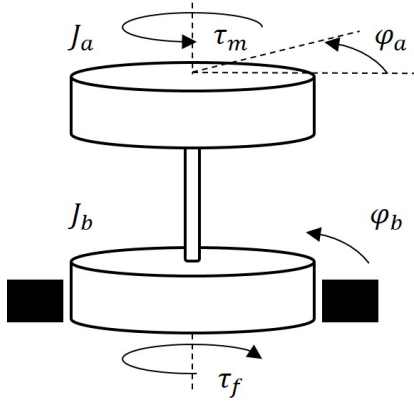


Figure 4.1.: Scheme of electromechanical system

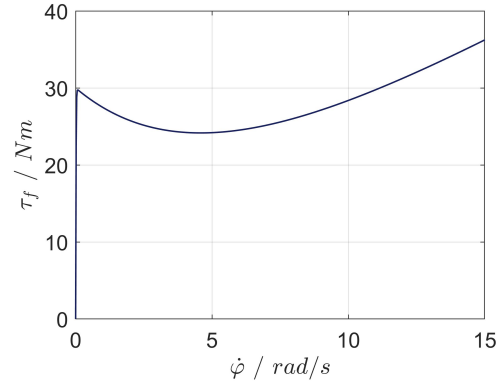


Figure 4.2.: Friction curve

Introducing the vector of states $x = [\varphi_a, \dot{\varphi}_a, \varphi_b, \dot{\varphi}_b]^T$ and control input $u = \tau_m$, the state-space representation follows

$$\dot{x}_1 = x_2, \quad (4.35)$$

$$\dot{x}_2 = -\frac{k_s}{J_a} \tanh k_g (x_1 - x_3) + \frac{1}{J_a} u, \quad (4.36)$$

$$\dot{x}_3 = x_4, \quad (4.37)$$

$$\dot{x}_4 = \frac{k_s}{J_b} \tanh k_g (x_1 - x_3) - \frac{1}{J_b} \tau_f(x_4). \quad (4.38)$$

The velocity measurements are only provided by an incremental encoder on the shaft of the motor resulting in the output equation

$$y = x_2. \quad (4.39)$$

Here, the nonlinearities are represented by the nonlinear spring and the friction effects that depend on the velocity of the second mass, as depicted in Fig. 4.2. In order to show the significance of the zero dynamics, two operating cases are considered. In the first case, the system is assumed to be operated in the region of the positive slope of the friction curve, e.g., the velocity $\dot{\varphi}_b = 10 \text{ rad/s}$ (Fig. 4.2). In the second case, an operating point of velocity $\dot{\varphi}_b = 1.5 \text{ rad/s}$ is assumed, i.e., in the negative slope region of the friction curve.

Applying the aforementioned idea of the input-output linearization the output derivative can be simply represented as

$$\dot{y} = -\frac{k_s}{J_a} \tanh k_g(x_1 - x_3) + \frac{1}{J_a} u. \quad (4.40)$$

The direct dependency of \dot{y} on the input u can be seen, which states that the system has the relative degree $\vartheta = 1$. The feedback control law, which compensates the nonlinearity of the spring and provides the desired first-order dynamics for the output velocity, can be designed as follows:

$$u = J_a \left(\frac{k_s}{J_a} \tanh k_g(x_1 - x_3) + d_0(\dot{\varphi}_{ref} - x_2) \right), \quad (4.41)$$

where d_0 is a design parameter.

Substituting the control law (4.41) in (4.40) results in the linear input-output relation

$$\dot{y} = \dot{x}_2 = d_0(\dot{\varphi}_{ref} - x_2). \quad (4.42)$$

However, it can be seen that not the whole system is linearized, and the system states x_3 and x_4 associated with the second mass dynamics are still affected by the nonlinear dynamics. The time responses of the controlled system for the described cases are presented in Fig. 4.3 and Fig. 4.4. Here, the velocity reference signal $\dot{\varphi}_{ref}$ is applied step-wise. In Fig. 4.3 the controlled system is asymptotically stable as the associated zero dynamics in the region of the positive slope of the friction curve is stable (Fig. 4.2). From a physical point of view, a positive slope of the curve provides the system energy dissipation, and, therefore, oscillating dynamics induced by the nonlinear spring is damped. From Fig. 4.4 the occurrence of a limit cycle due to operation in the negative slope region of the friction curve can be seen. Although the velocity of the first mass is stabilized by the control law, the corresponding zero dynamics leads to nonlinear stick-slip oscillations of the second mass.

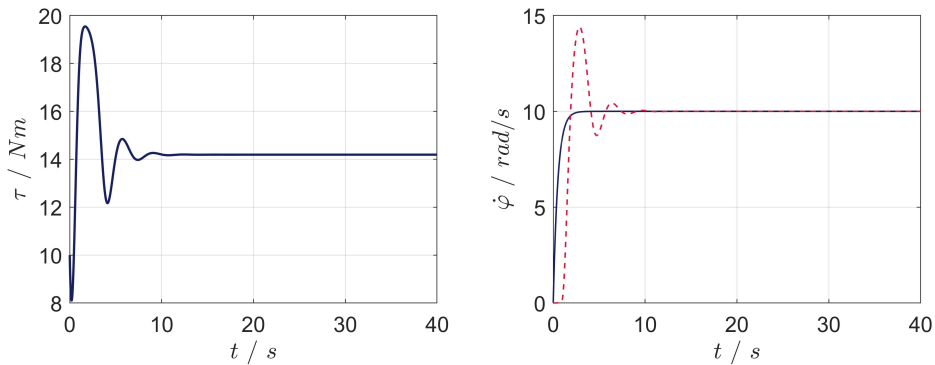


Figure 4.3.: Time responses of controlled system with friction load at operating point with positive slope: control input u (**left**), velocity of the first mass $\dot{\varphi}_a$ (blue, **right**) and the second $\dot{\varphi}_b$ (red, **right**)

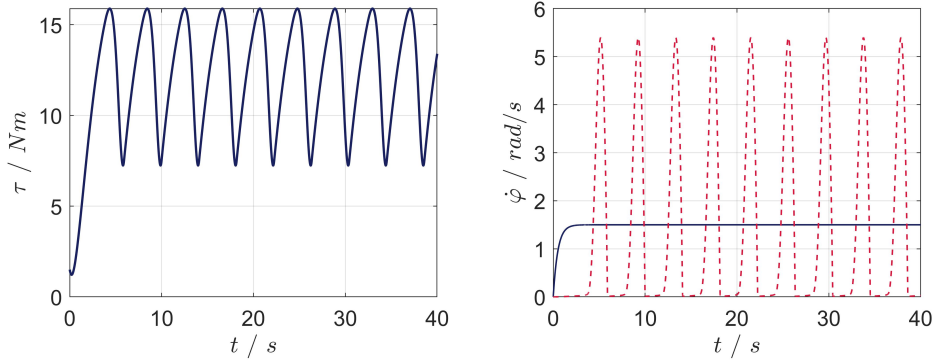


Figure 4.4.: Time responses of controlled system with friction load at operating point with negative slope: control input u (**left**), velocity of the first mass $\dot{\varphi}_a$ (blue, **right**) and the second $\dot{\varphi}_b$ (red, **right**)

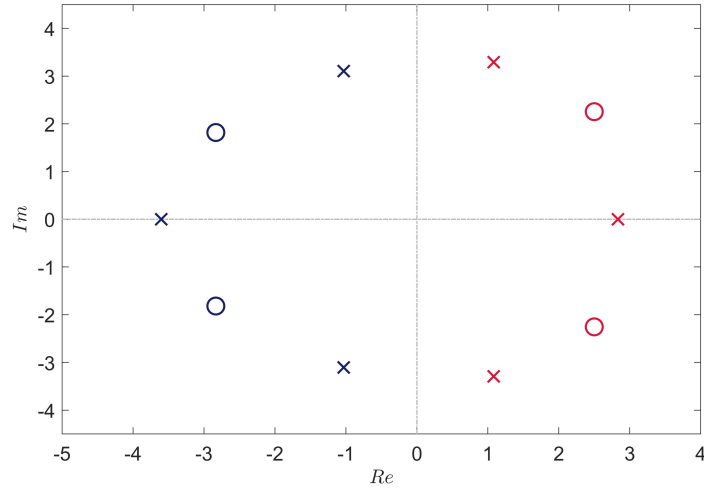


Figure 4.5.: Poles and zeros location: $P(s)$ at operating point with positive slope of the friction curve (blue) and with negative slope of the friction curve (red)

The system model (4.35), (4.36), (4.37), (4.38), and (4.39) can be linearized and represented as a transfer function with the motor torque as input and the velocity of the second mass as output

$$P(s) = \frac{J_b s^2 + k_f s + k_{ab}}{J_a J_b s^3 + J_a k_f s^2 + (J_a + J_b) k_{ab} s + k_f k_{ab}}, \quad (4.43)$$

where k_{ab} represents the linear spring coefficient between masses and k_f represents the slope of the friction curve for some operating point of interest.

The poles and zeros of two transfer functions are depicted in Fig. 4.5. Here, in the case of a positive slope of the friction curve, i.e., $k_f > 0$, the resulting transfer function is asymptotically stable and strictly minimum-phase. In the second case, i.e., $k_f < 0$, the transfer function is unstable and non-minimum-phase.

4.2. Condition of almost strictly positive realness

The concept of passivity in control theory appeared from the theory of electrical circuits. From a control point of view, passive systems with possible stable and strictly passive uncertainties are well known to be internally stable, applying negative feedback. For LTI systems, the passivity notion is equivalent to the positive realness [41]. In the following, the conditions for positive real (PR), strictly positive real (SPR), and almost strictly positive real (ASPR) systems are presented [9, 6, 118, 102, 46].

Consider the following n -th order linear system transfer function

$$P(s) = C(sI - A)^{-1}B. \quad (4.44)$$

The rational transfer function $P(s)$ is known to be PR (SPR) if the following conditions hold [9]:

- $P(s)$ is (asymptotically) stable: $\text{Re} [\lambda_i\{A\}] \leq 0$ ($\text{Re} [\lambda_i\{A\}] < 0$) for $i = 1, 2, \dots, n$,
- the Nyquist plot is in the (closed) right half of the complex plane: $\text{Re} [P(i\omega)] \geq 0$ ($\text{Re} [P(i\omega)] > 0$) for all $\omega \geq 0$,
- the relative degree of the system is 0 or 1,
- $P(s)$ is (strictly) minimum-phase, i.e., zeros z_i of $P(s)$ are in the LHP $\text{Re} [z_i] \leq 0$ ($\text{Re} [z_i] < 0$).

The notion of SPR plant is very helpful for adaptive and robust control design methods [102, 22, 8]. From a theoretical point of view, applying a static output feedback with an arbitrarily large coefficient to SPR plant always yields an asymptotically stable closed loop system. However, it should be mentioned that this property is very strong and not fulfilled for most real plants. In [6, 86] this property has been relaxed, and the notion of almost SPR plant has been introduced.

The system is known to be ASPR if there exists an output feedback gain such that the closed loop system is SPR. Here, the following conditions for the transfer function $P(s)$ should hold [6, 46]:

- the relative degree of the system is 0 or 1,
- $P(s)$ is strictly minimum-phase, i.e., zeros z_i of $P(s)$ are in the LHP $\text{Re} [z_i] < 0$.

It can be seen that ASPR property imposes less restrictions on the system plant $P(s)$. It may not be necessarily stable, but applying a static output feedback with a sufficiently large gain, the system dynamics will be stabilized. This concept is useful for guaranteeing asymptotic stability for different control applications, e.g., simple adaptive control, sliding-mode control, self-tuning PID-control, discrepancy-based control, etc. It should be mentioned that the ASPR property is also not fulfilled for most real plants. However, due to fewer restrictions, the plant may be rendered ASPR for control purpose, which will be discussed in the next Section.

4.3. Parallel feed-forward compensation

4.3.1. Control based on the parallel feed-forward compensation

One of the possibilities to introduce a correction into the open-loop plant transfer function for a feedback control design is applying a parallel feed-forward compensator (PFC), as depicted in Fig. 4.6. Here, the idea is to extend the plant with a PFC and to render the new plant $P + F$ desired properties, e.g., passivity, ASPR, full relative degree, etc. It yields a redefined output $\tilde{y} = y + y_F$, which is considered for the further feedback control design. Since the controller C is obtained for the new plant $P + F$, the overall control scheme can be alternatively represented as depicted in Fig. 4.7. In contrast to the classical cascade interconnected compensator, the PFC has not been widely utilized. However, in a number of works, it has been shown that parallel feed-forward interconnected dynamic elements can be effectively applied for certain control purposes, e.g.:

- shaping the augmented open-loop system transfer function in the frequency domain for a robust feedback control [45, 16, 20, 21];
- control of plants with delay [30, 97];
- internal model control [23, 63, 117];
- compensation of system dynamics of the augmented plant [20];
- compensation and stabilization of system zeros of the augmented plant [6, 7, 46, 93, 28, 42, 50].

The design of feedback control for non-minimum phase plants or plants that contain the undesired zero dynamics is always a challenging task. It is well known that the zero dynamics is invariant with respect to any feedback control and can be changed only by redefining the input-output plant configuration. Consequently, many of the contributions are dedicated to applying PFC for different control approaches that suffer from undesired zero dynamics, e.g., simple adaptive control, sliding-mode control, exact feedback linearization, discrepancy-based control, etc. In [6, 7] the author pioneered the application of PFC for simple adaptive control [8]. In order to apply this control approach, the plant should fulfill at least ASPR conditions. As this condition is not valid for most real plants, it has been considered that it can be fulfilled for a virtual plant $P + F$ (Fig. 4.6). Following this idea in [44, 46, 16] the authors presented a constructive design procedure of PFC for stable plants with stable zero dynamics and known leading coefficient. On the one hand, the design requires only little information about the plant, but, on the other hand, according to the restrictions, this approach is not applicable for non-minimum phase systems, and adjustment of the specific PFC parameters is not evident, which makes its practical implementation without an additional simulation study difficult.

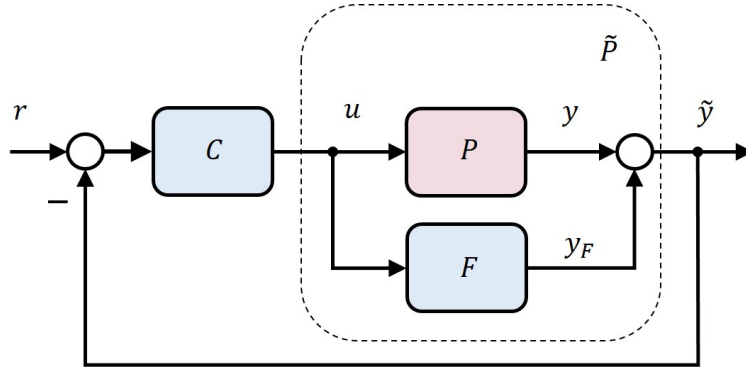


Figure 4.6.: PFC with feedback control scheme

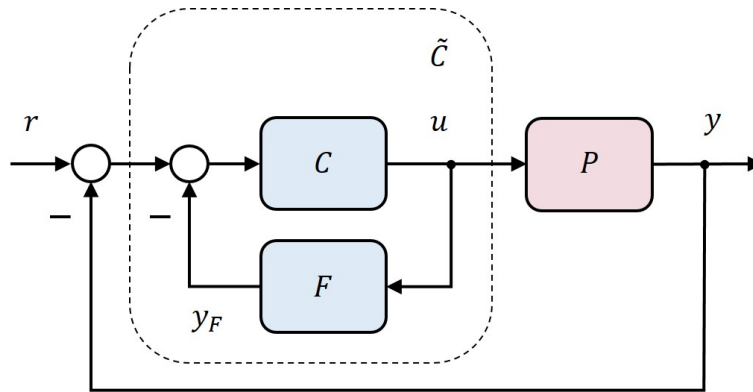


Figure 4.7.: Equivalent feedback control scheme

In [93, 28, 29, 56, 26, 50] model-based PFC were applied for stable non-minimum phase plants in order to compensate unstable zeros. In [62] PFC-based output adaptive predictive control was proposed. Another interesting PFC application can be found in sliding-mode control [31, 66]. A constructive design approach for unstable non-minimum phase plants was introduced and applied for the corresponding discrepancy-based control in [72].

4.3.2. Design of parallel feed-forward compensator for unstable systems

In the following, a general linear approach for zero dynamics stabilization of the augmented system $\tilde{P} = P + F$ is presented. Consider the following SISO LTI plant, which may be non-minimum phase and unstable, i.e., may contain poles and zeros in the left-half plane (LHP) as well as in the right-half plane (RHP)

$$P(s) = \frac{N^+(s)N^-(s)}{M^+(s)M^-(s)}, \quad (4.45)$$

where $N^+(s)$ and $M^+(s)$ are the corresponding fractions of the polynomial with roots in the LHP that are associated with the stable poles and zeros of $P(s)$, $N^-(s)$ and

$M^-(s)$ fractions with roots in the RHP that are associated with unstable poles and zeros of $P(s)$.

For changing the stability properties of the zero dynamics for the augmented system with the new output \tilde{y} , an appropriate PFC $F(s)$, as illustrated in Fig. 4.8, has to be designed.

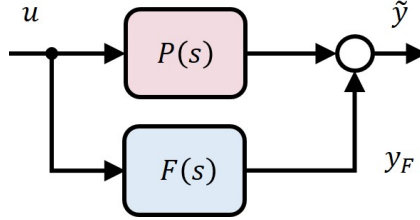


Figure 4.8.: Parallel feed-forward interconnection

According to the design procedure, which is proposed in [72], consider the PFC, which comprises the polynomial fractions with roots in LHP, i.e., $N^+(s)$ and $M^+(s)$, and two additional elements $N_c(s)$ and $M_c(s)$ that can be chosen,

$$F(s) = \frac{N^+(s)N_c(s)}{M^+(s)M_c(s)}. \quad (4.46)$$

Thus, a parallel feed-forward interconnection of the plant and PFC yields

$$\begin{aligned} \tilde{P}(s) &= P(s) + F(s) \\ &= \frac{N^+(s)[N^-(s)M_c(s) + M^-(s)N_c(s)]}{M^+(s)M^-(s)M_c(s)}. \end{aligned} \quad (4.47)$$

Here, the stability condition of the zero dynamics for the extended system $\tilde{P}(s)$ is obtained if and only if the numerator polynomial $N^-(s)M_c(s) + M^-(s)N_c(s)$ has roots only in LHP. It can be shown that the problem of PFC design for zero dynamics is equivalent to designing a controller, which stabilizes the system plant consisting of the unstable poles and zeros [72]. Also, this problem can be directly solved by placing the roots of the polynomial

$$L_d(s) = N^-(s)M_c(s) + M^-(s)N_c(s), \quad (4.48)$$

where $L_d(s)$ is an arbitrary polynomial of suitable degree, and finding the corresponding $N_c(s)$ and $M_c(s)$. In order to solve the linear Diophantine equation (4.48), a method based on Sylvester's matrix can be utilized [39].

Consider that the plant polynomials $M^-(s)$ and $N^-(s)$ of same degree m , PFC polynomials $N_c(s)$ and $M_c(s)$ of degree $n = m - 1$, and the desired polynomial $L_d(s)$ of degree $k = m + n$ are represented as follows:

$$N^-(s) = a_m s^m + a_{m-1} s^{m-1} + \cdots + a_0, \quad (4.49)$$

$$M^-(s) = b_m s^m + b_{m-1} s^{m-1} + \cdots + b_0, \quad (4.50)$$

$$N_c(s) = c_n s^n + c_{n-1} s^{n-1} + \cdots + c_0, \quad (4.51)$$

$$M_c(s) = d_n s^n + d_{n-1} s^{n-1} + \cdots + d_0, \quad (4.52)$$

$$L_d(s) = l_k s^k + l_{k-1} s^{k-1} + \cdots + l_0. \quad (4.53)$$

Thus, the placement problem (4.48) is leading to the solution of the respective matrix equation

$$R v = x, \quad (4.54)$$

where

$$R = \begin{bmatrix} a_m & 0 & \cdots & 0 & b_m & 0 & \cdots & 0 \\ a_{m-1} & a_m & \cdots & 0 & b_{m-1} & b_m & \cdots & 0 \\ \vdots & \vdots & \ddots & \vdots & \vdots & \vdots & \ddots & \vdots \\ a_0 & a_1 & \cdots & a_m & b_0 & b_1 & \cdots & b_m \\ 0 & a_0 & \cdots & a_{m-1} & 0 & b_0 & \cdots & b_{m-1} \\ \vdots & \vdots & \ddots & \vdots & \vdots & \vdots & \ddots & \vdots \\ 0 & 0 & \cdots & a_0 & 0 & 0 & \cdots & b_0 \end{bmatrix},$$

$$v = \begin{bmatrix} d_n \\ \vdots \\ d_0 \\ c_n \\ \vdots \\ c_0 \end{bmatrix}, x = \begin{bmatrix} l_k \\ l_{k-1} \\ \vdots \\ l_0 \end{bmatrix}.$$

Here, the vector v comprises the sought parameters of $N_c(s)$ and $M_c(s)$ that are included in the PFC. According to Sylvester's theorem, the parameter matrix R is non-singular if and only if $N^-(s)$ and $M^-(s)$ are coprime [39]. It should be also mentioned that the determinant of the matrix R is the resultant of two polynomials $N^-(s)$ and $M^-(s)$ [12].

Example 4.2 Consider the oil-well drill string system in Example 4.1 operated in the negative slope region of the friction curve Fig. 4.2 with velocity $\dot{\varphi}_b = 1.5 \text{ rad/s}$. Linearizing the system at this point results in an unstable linear system. For the motor reference torque $\tau_{m,ref}$ as input and the motor velocity $\dot{\varphi}_a$ as output the transfer function is obtained

$$P(s) = \frac{200 (s^2 - 5s + 26.67)}{(s + 100)(s - 2.19)(s^2 - 2.81s + 36.51)}. \quad (4.55)$$

Here, according to (4.45), the unstable non-minimum phase plant can be separated into the following fractions

$$N^-(s) = (s^2 - 5s + 26.67), \quad (4.56)$$

$$M^-(s) = (s - 2.19)(s^2 - 2.81s + 36.51), \quad (4.57)$$

$$N^+(s) = 200, \quad (4.58)$$

$$M^+(s) = (s + 100). \quad (4.59)$$

Then, the PFC elements $N_c(s)$ and $M_c(s)$ are chosen as follows:

$$N_c(s) = c_2 s^2 + c_1 s + c_0, \quad (4.60)$$

$$M_c(s) = d_2 s^2 + d_1 s + d_0. \quad (4.61)$$

In order to obtain stable zero dynamics for the augmented system (4.47), the above-presented placement approach is applied. It implies choosing the polynomial with desired roots location. Here, e.g., the desired roots location are assigned according to the reverse Bessel polynomial [40] as follows:

$$L_d(s) = s^5 + 15.24s^4 + 108.4s^3 + 440.7s^2 + 1008s + 1024. \quad (4.62)$$

Finding the vector of controller coefficients v from the matrix equation (4.54) results in PFC

$$F(s) = \frac{9.5566 (s + 40.19)(s + 0.99)}{(s + 100)(s - 7.14)(s + 1.05)}. \quad (4.63)$$

Applying the designed compensator $F(s)$ in parallel feed-forward connection with the plant $P(s)$ results in the extended system $\tilde{P}(s)$ with locally asymptotically stable zero dynamics. It should be noticed that this design approach does not provide the relative degree assignment for the augmented system. However, in this specific example, the extended plant is ASPR.

It should be also noticed that the designed PFC introduces a static error to the physical output. In addition, since the extended plant $\tilde{P}(s)$ is ASPR, high gain adjustment of the feedback controller can be used, which results in fast convergence of the output \tilde{y} to the reference value. However, since the transfer function with respect to the physical output $P(s)$ contains zeros in RHP, transients with large overshoots may occur for this controller adjustment. In order to compensate the static error and to reduce the overshoot of the physical output, an additional pre-filter W_p as depicted in Fig. 4.11 is used. Here, a simple first order system W_p is chosen as follows:

$$W_p(s) = \frac{\lim_{s \rightarrow 0} \tilde{P}(s)}{\lim_{s \rightarrow 0} P(s)} \cdot \frac{1}{T_W s + 1} = k_W \cdot \frac{1}{T_W s + 1}, \quad (4.64)$$

where the gain $k_W = 0.25$ is calculated directly from the static error introduced by the PFC and the time constant $T_W = 0.8$ is tuned iteratively to reduce the overshoot of the velocity $\dot{\varphi}_a$.

In order to analyze the stability properties of $\tilde{P}(s)$ under output feedback, the root locus for varying gain k_P is illustrated in Fig. 4.9. Here, two closed loop systems with controller gain $k_P = 16$ (green) and $k_P = 1000$ (red) are shown. It can be seen that the augmented output is stabilized for gains $k_P \geq 16$. In Fig. 4.10 the step responses of both masses applying the designed PFC $F(s)$, controller gain $k_P = 1000$ and pre-filter $W_p(s)$ are depicted.

4.3.3. Design of parallel feed-forward compensator for stable systems

In the following, a simplified design of PFC, which is limited to the application for stable systems, is presented. This design procedure provides an assignment of the desired zero dynamics of the augmented plant and desired relative degree. In addition, the bias effects appearing in the corresponding augmented output \tilde{y} can be reduced.

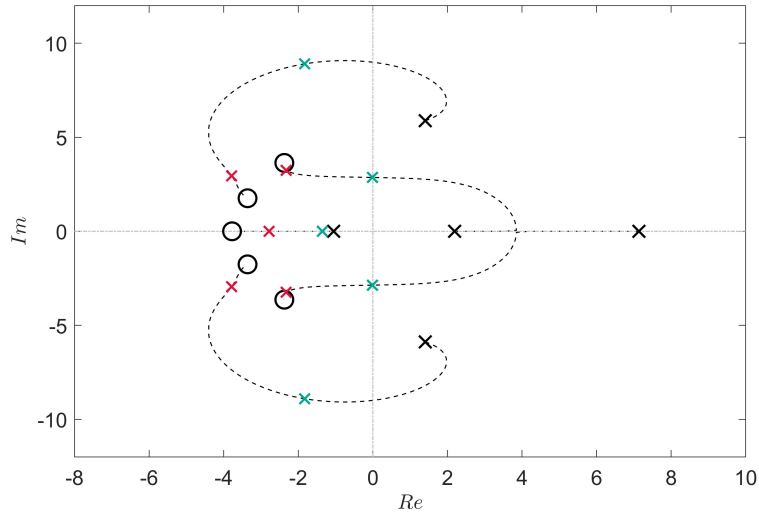


Figure 4.9.: Root locus of $\tilde{P}(s)$: poles of the open-loop system (black), poles of the closed loop system with $k_P = 16$ (green), poles of the closed loop system with $k_P = 1000$ (red)

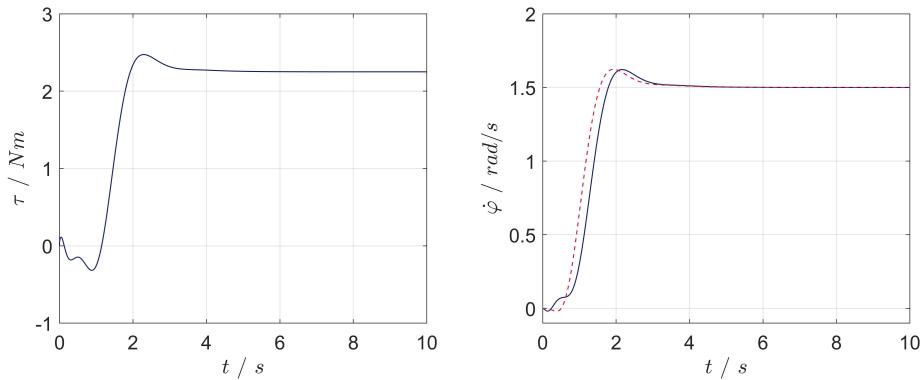


Figure 4.10.: Step responses (**right**) and control input (**left**) of the closed loop system with PFC and $k_P = 1000$: time responses of the first mass (blue), time responses of the second mass (red)

Consider the following SISO LTI plant

$$P(s) = \frac{y_p(s)}{u(s)} = k_n \frac{N(s)}{M(s)}, \quad (4.65)$$

where $M(s)$ is a polynomial of degree m , which may contain roots in LHP as well as on the imaginary axis, $N(s)$ is a normalized polynomial of degree n , which may contain roots in LHP as well as in RHP, the relative degree of the plant $\vartheta = m - n \geq 2$, and k_n is the normalization coefficient. The numerator polynomial $N(s)$ is normalized using k_n in such a manner that the coefficient of the constant term is one.

Consider the PFC consists of the plant poles and normalization coefficient, i.e., $M(s)$

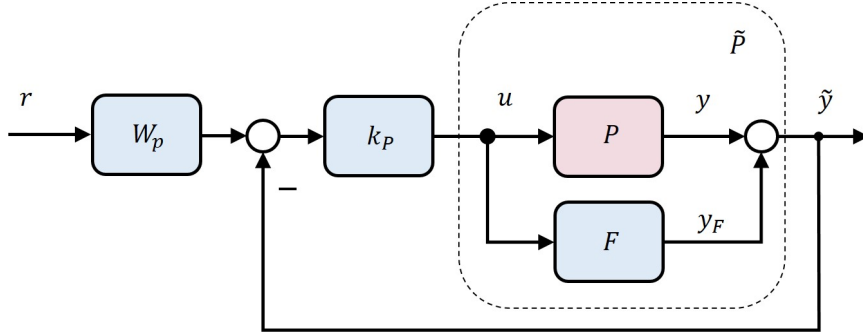


Figure 4.11.: PFC with feedback control scheme and pre-filter

and k_n , and a supplementary polynomial $A(s)$ of degree η

$$F(s) = \frac{y_f(s)}{u(s)} = k_n \frac{A(s)}{M(s)}. \quad (4.66)$$

The parallel interconnection $P(s) + F(s)$ yields an augmented plant with a new virtual output \tilde{y}

$$\tilde{P}(s) = \frac{\tilde{y}(s)}{u(s)} = k_n \frac{N(s) + A(s)}{M(s)}. \quad (4.67)$$

In order to fulfill the ASPR conditions for the augmented plant $\tilde{P}(s)$, the polynomial $A(s)$ should possess the degree $\eta = m - 1$ or $\eta = m$. For providing a desired location of zeros, the polynomial $A(s)$ can be chosen as follows:

$$A(s) = L_d(s) - N(s), \quad (4.68)$$

where $L_d(s)$ is a normalized polynomial of degree η with desired zeros

$$L_d(s) = T_d^\eta s^\eta + \lambda_{\eta-1} T_d^{\eta-1} s^{\eta-1} + \dots + \lambda_2 T_d^2 s^2 + \lambda_1 T_d s + 1. \quad (4.69)$$

Here, T_d is the time constant and λ_j are polynomial coefficients that determine the roots location.

Generally, the polynomial $L_d(s)$ can be chosen arbitrarily. However, for guaranteeing internal closed loop stability, the selected $L_d(s)$ should give a polynomial $A(s)$ without roots in RHP. Besides, applying the polynomial $L_d(s)$ in the normalized form, as mentioned above, will result in the PFC numerator $A(s)$, which includes a derivative and hence reduces the bias effects of the parallel feed-forward correction.

4.4. Control design based on parallel feed-forward compensator

In this work, the PFC design for stable systems is applied for control of the gantry crane. From a practical point of view, this approach does not require additional load

measurements nor states estimation. Moreover, it is an output feedback control approach that does not require a redesign of the drive control system. The stability and performance of the closed loop system are achieved by defining a new augmented output as a combination of the actual measured output, in this case, the trolley position, and the output of an appropriate PFC. The PFC provides the ASPR condition for the augmented plant, i.e., relative degree one and desired zeros location in LHP. After that, high gain output feedback control becomes applicable for such an augmented plant.

In Fig. 4.12 the overall control system for gantry crane positioning is presented. To provide operation of the system in the linear region, an additional friction compensator is applied [3]. For stabilization of the ASPR augmented plant $\tilde{P}(s)$ the following proportional output feedback control can be utilized

$$u(t) = k_p (r(t) - \tilde{y}(t)), \quad (4.70)$$

where k_p is a proportional controller gain.

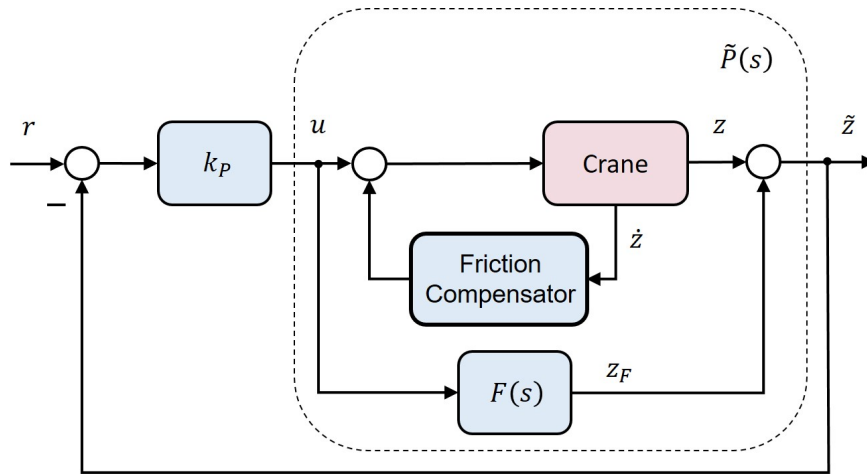


Figure 4.12.: Overall control scheme

4.5. Simulation study

In the following, the problem of undesired zeros for the gantry crane is presented. After that, the proposed PFC is applied to the gantry crane, and simulation results are presented.

4.5.1. Gantry crane plant with undesired zeros

The transfer function of the *full* crane configuration with the motor force as input F_t and the trolley position as output z is

$$P(s) = \frac{36.571 (s^2 + 13.8) (s^2 + 0.017s + 98.97)}{s^2 (s^2 + 32.94) (s^2 + 0.02s + 113.5)}. \quad (4.71)$$

Here, the system has the relative degree $\vartheta = 2$. Dynamics of the crane system is characterized by two poles at the origin, two pairs of complex conjugated poles

$$p_{1,2} = 0, \quad (4.72)$$

$$p_{5,6} = 0 \pm 5.74 i, \quad (4.73)$$

$$p_{3,4} = -9.8 \cdot 10^{-3} \pm 10.66 i, \quad (4.74)$$

and two pairs of complex conjugated zeros

$$z_{1,2} = 0 \pm 3.72 i, \quad (4.75)$$

$$z_{3,4} = -8.6 \cdot 10^{-3} \pm 9.95 i. \quad (4.76)$$

It can be seen that the transfer function contains one complex pair of poles and zeros on the imaginary axis, which is related to the undamped load swinging dynamics, and one complex pair of poles and zeros near the imaginary axis, which is related to the lightly damped structural dynamics. From a theoretical point of view, it means that applying high-gain or fast switching relay output feedback control the system poles converge to the system zeros, which cancels out part of the system dynamics and makes this part unobservable from the output. For problems with lightly damped system dynamics, this yields oscillatory internal dynamics of the closed loop system [36, 31].

Example 4.5 Consider the conventional position control of the gantry crane system with a PD controller. The open-loop plant with cascade interconnected PD controller can be represented as follows:

$$P_o(s) = k_P \cdot \left(1 + \frac{T_D s}{T_f s + 1}\right) \cdot \frac{36.571 (s^2 + 13.8) (s^2 + 0.017s + 98.97)}{s^2 (s^2 + 32.94) (s^2 + 0.02s + 113.5)}, \quad (4.77)$$

where k_P , T_D , and T_f are the PD controller parameters.

The open-loop transfer function $P_o(s)$ has the relative degree $\vartheta = 2$. In Fig. 4.13 the root locus of the gantry crane system for the fixed derivative time constant $T_D = 1 s$, the filter time constant $T_f = 1 ms$, and varying gain k_P is depicted. Here, it can be seen that the position output and internal system dynamics can be asymptotically stabilized, e.g., applying low gain $k_P = 0.25$ (green poles). However, this gain adjustment typically results in poor closed loop dynamics, as depicted in Fig. 4.14 (green lines). For higher gains, e.g., $k_P = 2$, the system poles are more attracted to the system zeros (Fig. 4.13, red poles) resulting in weakly damped oscillating dynamics of position output (Fig. 4.14, red lines). Application of much higher gains k_P will result in a stabilized position output, on the one hand, and large undamped oscillations of load and structural dynamics, on the other. In order to overcome this problem without additional sensors, control system redesign is needed.

4.5.2. PFC-based feedback control

In this Chapter, to solve zero dynamics problem without a motion control system redesign, the extension of the plant with PFC is utilized. The transfer function of

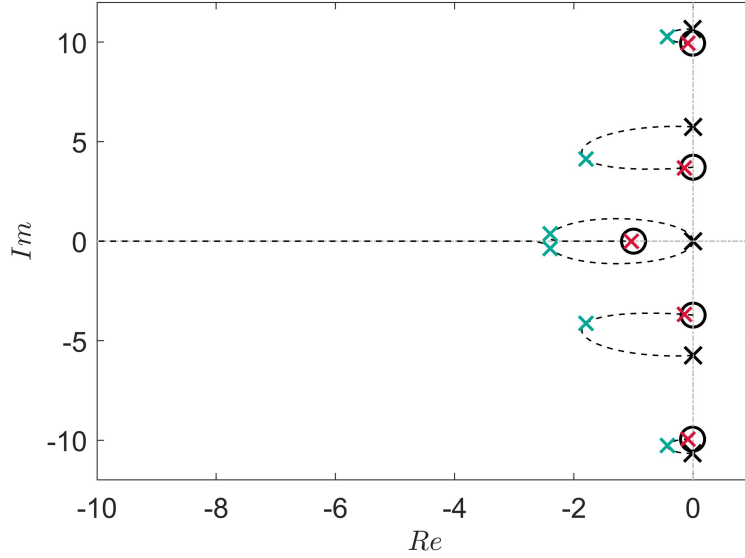


Figure 4.13.: Root locus for the crane plant $P_o(s)$: poles of the open-loop system (black), poles of the closed loop system with $k_P = 0.25$ (green), poles of the closed loop system with $k_P = 2$ (red)

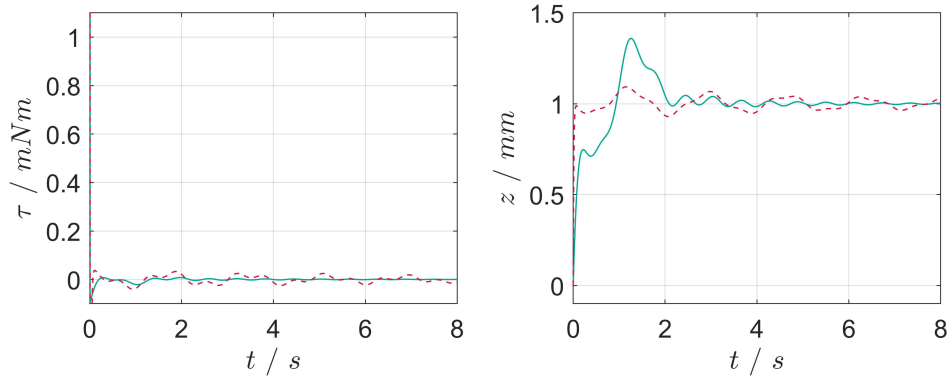


Figure 4.14.: Step responses (**right**) and control input (**left**) of the closed loop crane plant $P_o(s)$: time responses of the closed loop system with $k_P = 0.25$ (green), time responses of the closed loop system with $k_P = 2$ (red)

interest is computed according to (4.66) as follows:

$$P(s) = k_n \cdot \frac{7.32 \cdot 10^{-4} s^4 + 1.26 \cdot 10^{-5} s^3 + 8.26 \cdot 10^{-2} s^2 + 1.73 \cdot 10^{-4} s + 1}{s^6 + 1.97 \cdot 10^{-2} s^5 + 146.5 s^4 + 0.6481 s^3 + 3741 s^2}, \quad (4.78)$$

with normalization factor $k_n = 4.99 \cdot 10^4$.

In order to design an appropriate PFC, the polynomial $L_d(s)$ with the desired roots location should be defined according to (4.69). To achieve transients without large overshoots in the trolley position a Bessel polynomial of order 5 with time constant

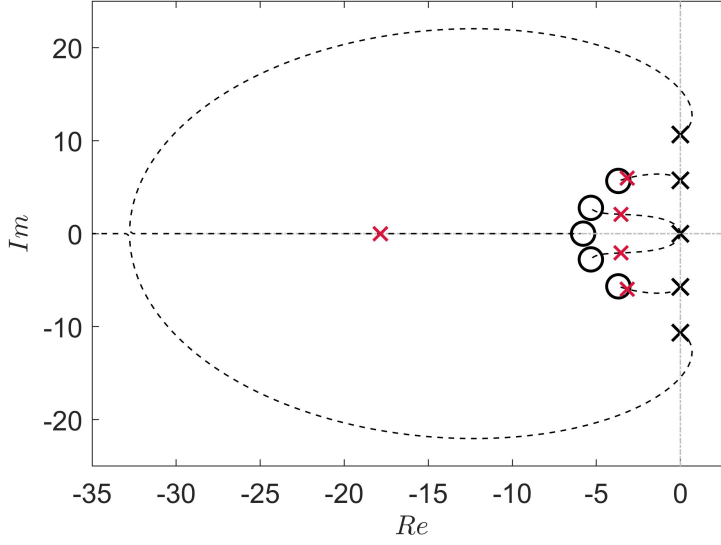


Figure 4.15.: Root locus for the augmented gantry crane plant $\tilde{P}(s)$: poles of the open-loop system (black), poles of the closed loop system with position controller gain $k_P = 20$ (red)

guaranteeing internal stability $T_d = 0.16$ is utilized [40]. The chosen polynomial can be computed as follows:

$$L_d(s) = 10^{-4} s^5 + 2.5 \cdot 10^{-3} s^4 + 2.78 \cdot 10^{-2} s^3 + 0.18 s^2 + 0.63 s + 1. \quad (4.79)$$

Therefore, according to (4.66) and (4.68) the PFC is obtained as follows:

$$F(s) = k_n \cdot \frac{10^{-4} s^5 + 1.8 \cdot 10^{-3} s^4 + 2.77 \cdot 10^{-2} s^3 + 0.1 s^2 + 0.63 s}{s^6 + 1.97 \cdot 10^{-2} s^5 + 146.5 s^4 + 0.6481 s^3 + 3741 s^2}. \quad (4.80)$$

The extended ASPR plant $\tilde{P}(s) = P(s) + F(s)$ with the desired zeros location is

$$\tilde{P}(s) = k_n \cdot \frac{10^{-4} s^5 + 2.5 \cdot 10^{-3} s^4 + 2.78 \cdot 10^{-2} s^3 + 0.18 s^2 + 0.63 s + 1}{s^6 + 1.97 \cdot 10^{-2} s^5 + 146.5 s^4 + 0.6481 s^3 + 3741 s^2}. \quad (4.81)$$

In order to analyze the linear system properties $\tilde{P}(s)$, the root locus procedure for varying gains k_P is applied as depicted in Fig. 4.15. It can be seen that, e.g., applying the gain $k_P = 20$, yields the closed loop poles that are near the desired zeros location. Hence, the performance of the closed loop augmented system under high gain feedback control or switching relay output feedback control is predefined by the PFC design.

In Fig. 4.16 the closed loop nonlinear system responses with the designed PFC and the gain $k_P = 20$ are presented. Here, it can be seen that the trolley position, as well as the internal structural and payload dynamics, settle in $t_{set} = 1.5 \text{ sec}$ without oscillations. The output of the PFC (Fig. 4.16, red line) is unbiased according to the design and therefore does not contribute a steady-state error to the output of interest, i.e., the trolley position.

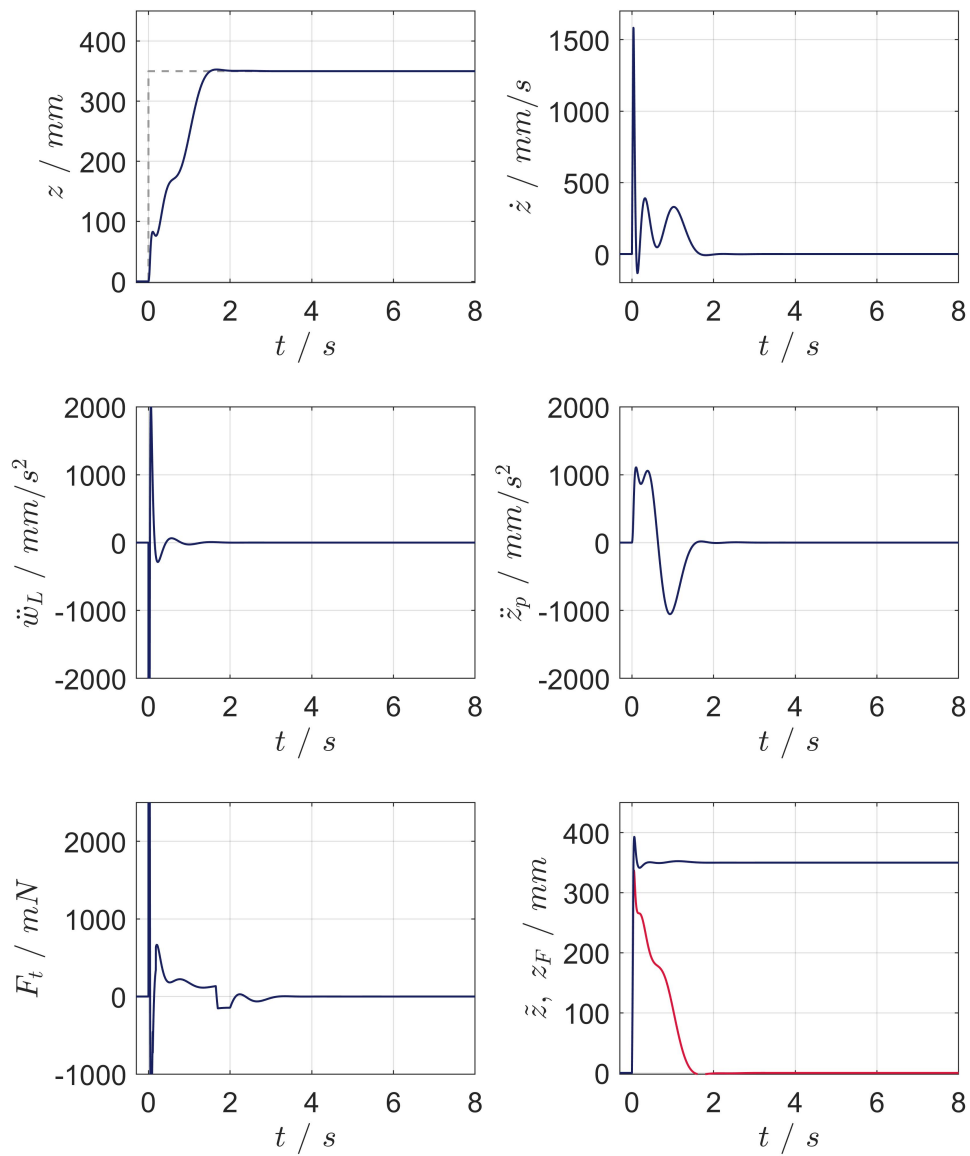


Figure 4.16.: Step responses of the closed loop system with PFC

4.6. Experimental evaluation

In this Section, the proposed PFC-based approach for gantry crane control without additional sensors is validated on the *full* configuration of the laboratory gantry crane. This approach is compared with two conventional methods. In the first case, a cascade control scheme providing position control without additional damping purposes is utilized. In the second case, an observer-based LQR controller is applied. Both methods are presented in detail in Appendix D. In order to validate the above-mentioned approaches, tracking of the trolley position with a step change of the reference signal to $z_r = 350 \text{ mm}$ is studied.

Simulation and experimental results of the closed loop system dynamics are presented in Fig. 4.17. As can be seen the trolley reaches the desired position in $t_{set} = 1.35 \text{ s}$ with an overshoot 2.8 %, a steady-state error 2.7 %, and a small residual oscillating dynamics of crane structure and payload. These mismatches are a result of the model uncertainties and, hence, non-ideal compensation of the friction forces.

In Fig. 4.18 the PFC-based control approach is compared with the above-mentioned methods in the same experimental study. For evaluation of the transients, the following properties are taking into consideration: rise time (95 % of the reference value), settling time and overshoot of the trolley position z , residual oscillations of the crane acceleration \ddot{w}_L and the load acceleration \ddot{z}_p . The obtained values are summarized in Tab. 4.1. Here, conventional cascade position control does not provide additional damping purposes and shows fast rise time due to the corresponding gains adjustment. It should be mentioned that the oscillatory behavior of the closed loop system is a result of the undesired system zero dynamics. The closed loop behavior of the system with LQR has slower transients with overshoot, notable damping of the payload dynamics and a reduction of the crane structural vibrations. The application of the proposed PFC approach results in a faster settling time, larger payload damping, and reduction of the structural vibrations.

Table 4.1.: Properties of the time responses

Control Approach	PFC	Cascade	LQR
Rise time [s]	1.35	0.65	1.1
Settling time [s]	1.35	-	2.08
Overshoot [%]	2.8	11.2	-
Residual oscillations \ddot{w}_L [mm/s ²]	145	239.33	228
Residual oscillations \ddot{z}_p [mm/s ²]	105	4028	637

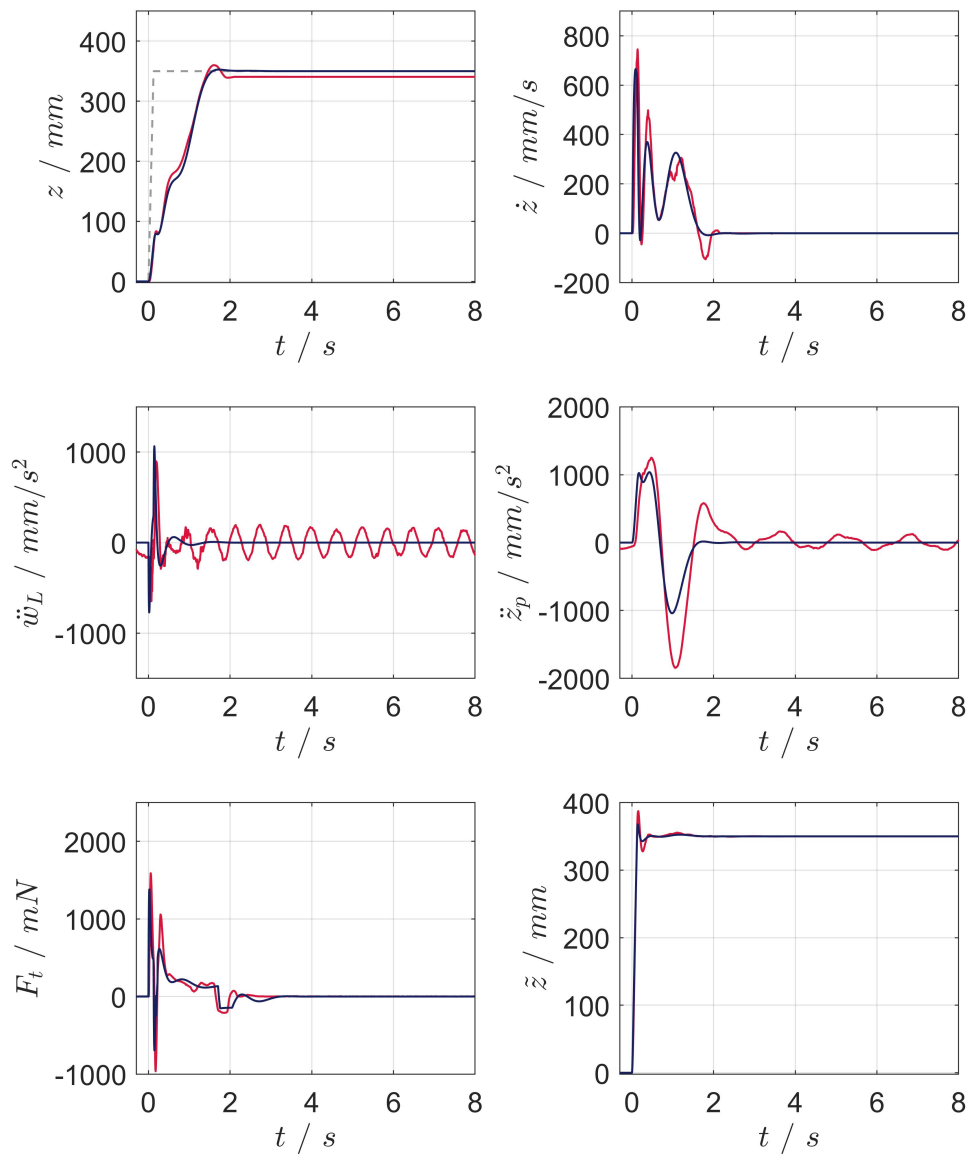


Figure 4.17.: Simulated (blue) and experimental (red) time responses of elastic gantry crane with PFC-based feedback control

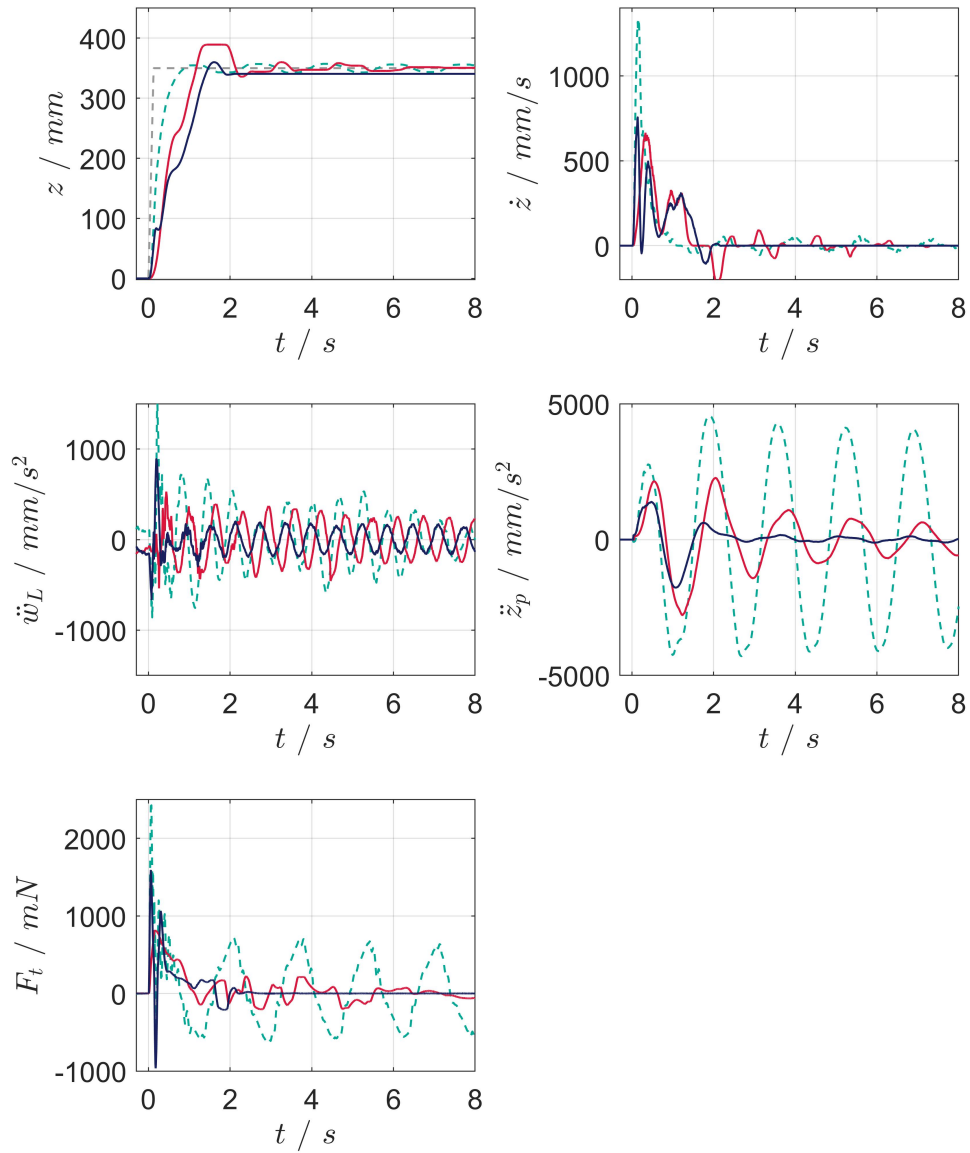


Figure 4.18.: Experimental time responses of elastic gantry crane: high gain with PFC (blue), cascade PID-control (green) and LQR control (red)

5. Discrepancy-based control

In this Chapter, the nonlinear control design for the *full* configuration of laboratory crane is presented [38]. This approach allows deriving a control law directly, i.e., without model simplifications. Here, for stabilization of the gantry crane, a generalized error measure, called discrepancy, is taken into consideration. Applying the associated stability theory, i.e., stability with respect to two discrepancies, a nonlinear control law for the underactuated gantry crane based on Lyapunov direct design approach can be derived. The presented approach is validated in the corresponding simulation study and on the *full* configuration of the laboratory gantry crane.

5.1. Direct control of underactuated gantry cranes

In previous Chapters, linear control approaches have been proposed that are essentially based on approximated models. The approximation of an infinite-dimensional model is always an additional step in the control design, which introduces uncertainties due to the assumption that an infinite number of system modes can be neglected by corresponding discretization and order reduction. Direct control design methods eliminate this step and are, hence, preferable. However, applicability is in general limited due to a number of restrictions, e.g., simple geometries [14, 76].

One of the most common direct control approaches for electromechanical systems, that provides dissipation, is based on the total system energy [17, 53, 103, 111]. The derivation of the energy-based control law for the underactuated gantry crane is presented in detail in Appendix E. Here, since the system energy $E = T + U$ is a positive definite function, it is suitable as a Lyapunov functional candidate. Taking its time derivative along the system trajectory and substituting the equations of motion yields

$$\dot{E} = - \int_0^L c\dot{w}^2 dx + (F_t - F_{fr})\dot{z}. \quad (5.1)$$

Here, the first term characterizes the natural damping of the mechanical structure, which is always negative. It can be seen that choosing $F_t = -k\dot{z} + F_{fr}$ as the system input and the trolley velocity \dot{z} as the output yields the well-known energy dissipation. However, being a result of the underactuated nature of the system, the control law does not comprise terms related to payload or crane structural dynamics. One way to solve this problem is to increase the coupling in the control law. It can be done by introducing an additional term that depends on the velocity of interest, e.g., the payload velocity in (5.1), and to find reversely an appropriately shaped energy functional [103, 123].

Another way to solve the problem is to combine the energy-based control with another damping control [111]. In this work, another approach based on a generalized error measure, called discrepancy, is proposed.

5.2. Stability with respect to two discrepancies

In this Section, the most important definitions, properties, and remarks about stability with respect to two discrepancies are introduced according to the contributions [64, 94, 95, 71, 72]. Consider the process $\phi(\cdot, t)$ is a solution of a DPS and $\phi_0 = 0$ its equilibrium.

Definition 1. *Discrepancy [71, 72]*

A discrepancy is a real valued functional $\rho = \rho[\phi(\cdot, t), t]$ with the following properties

- $\rho(\phi, t) \geq 0$
- $\rho(0, t) = 0$
- for an arbitrary process $\phi(\cdot, t)$ the real valued functional $\rho[\phi(\cdot, t), t]$ is continuous with respect to t
- presenting the second discrepancy $\rho_0(\phi)$ with $\rho_0(\phi) \geq 0$ and $\rho_0(0) = 0$. Then the discrepancy $\rho[\phi(\cdot, t), t]$ is continuous at time $t = t_0$ with respect to ρ_0 at $\rho_0 = 0$, if for every $\epsilon > 0$ and $t_0 > 0$ there exists a $\beta(\epsilon, t_0) > 0$, such that from $\rho_0 \leq \beta(\epsilon, t_0)$ follows $\rho < \epsilon$

It should be mentioned that the discrepancy ρ does not satisfy all properties of a metric, e.g., triangular inequality $d(x, y) = d(y, z) + d(z, y)$ or symmetry $d(x, y) = d(y, x)$. And more importantly, it has not to satisfy the definiteness property, i.e., if the discrepancy vanishes $\rho(\phi, t) = 0$ it does not naturally mean that $\phi = 0$. Therefore, the discrepancy is an extension of the distance measures normally used in stability theory of DPS like L_p and L_∞ -norms [71, 72].

Definition 2. *Stability with respect to two discrepancies ρ and ρ_0 [71, 72]*

The equilibrium $\phi_0 = 0$ is stable in terms of Lyapunov with respect to the two discrepancies ρ and ρ_0 for all $t \geq t_0$ if for every $\epsilon > 0$ and $t_0 \geq 0$ there exists a $\beta = \beta(\epsilon, t_0)$ such that for every process $\phi(\cdot, t)$ with $\rho_0 < \beta(\epsilon, t_0)$ it follows that $\rho < \epsilon$ for all $t \geq t_0$. If in addition $\lim_{t \rightarrow \infty} \rho = 0$, then the equilibrium ϕ_0 is called asymptotically stable in terms of Lyapunov with respect to the two discrepancies ρ and ρ_0 .

Lyapunov stability theory is a base for many nonlinear control methods. In order to determine a relationship between stability with respect to two discrepancies and the existence of a Lyapunov functional V , the definitions of positivity and positive definiteness of a functional with respect to a discrepancy can be presented.

Definition 3. *Positivity with respect to a discrepancy ρ [71, 72]*

The functional $V = V[\phi, t]$ is called positive with respect to the discrepancy ρ , if $V \geq 0$ and $V[0, t] = 0$ for all ϕ with $\rho(\phi, t) < \infty$.

Definition 4. *Positive definiteness with respect to a discrepancy ρ [71, 72]*

The functional $V = V[\phi, t]$ is positive definite with respect to the discrepancy ρ , if $V \geq 0$ and $V[0, t] = 0$ for all ϕ with $\rho(\phi, t) < \infty$, and for every $\epsilon > 0$ exists a $\beta = \beta(\epsilon) > 0$, such that $V \geq \beta(\epsilon)$ for all ϕ with $\rho[\phi, t] \geq \epsilon$.

Thereafter, two theorems that determine the conditions for a function V to guarantee (asymptotic) stability with respect to two discrepancies [95, 71, 72].

Theorem 1. *The process ϕ with equilibrium $\phi_0 = 0$ is stable with respect to the two discrepancies ρ and ρ_0 if and only if there exists a functional $V = V[\phi, t]$ positive definite with respect to the discrepancy ρ , continuous at time $t = t_0$ with respect to ρ_0 at $\rho_0 = 0$ and not increasing along the process ϕ , i.e., $\dot{V} \leq 0$.*

Theorem 2. *The process ϕ with equilibrium $\phi_0 = 0$ is asymptotically stable with respect to the two discrepancies ρ and ρ_0 if and only if there exists a functional $V = V[\phi, t]$ positive definite with respect to the discrepancy ρ , continuous at time $t = t_0$ with respect to ρ_0 at $\rho_0 = 0$ and not increasing along the process ϕ , i.e., $\dot{V} \leq 0$, with $\lim_{t \rightarrow \infty} V = 0$.*

In general, it should be also stated that stability with respect to two discrepancies is necessary but in general not sufficient for stability with respect to a L_p or L_∞ norms.

5.3. Design of discrepancy-based control for gantry crane

In the following, the discrepancy-based control design for the underactuated gantry crane is presented. As mentioned above, the idea of the approach is a stabilization of the generalized error e in the sense of two discrepancies. Here, in the first step, the error should be defined to fulfill the control objectives. This error should be chosen such that the relative degree of the input-output system of interest is equal to one, and the corresponding zero dynamics is stable. The stability of zero dynamics for DPS is complicated to analyze. One possible approximate solution is to examine the location of the zeros of the linear discretized system. It should also be noted that this error may not have a distinct physical meaning. Moreover, to provide an additional degree of freedom for the control law, each particular component of the generalized error may be weighted.

The aim of the gantry crane control system is to locate the trolley in the desired position and to reduce the unwanted oscillations of the payload and the crane structure. Here, the generalized error e is chosen such that it comprises the deviation of the trolley position from its reference value $\varepsilon(t) = z(t) - z_{ref}(t)$, the trolley velocity \dot{z} , velocity of the crane girder $\dot{w}(L, t)$, angular velocity of the payload $\dot{\varphi}$, and can be represented as follows:

$$e = k_1 \varepsilon + k_2 \dot{z} + k_3 \dot{w}(L) + k_4 \dot{\varphi}, \quad (5.2)$$

where k_1 to k_4 are shaping weights that increase the coupling of the associated states.

Thereafter, the established error e yields the following discrepancy ρ

$$\rho = \frac{1}{2} (k_1\varepsilon + k_2\dot{z} + k_3\dot{w}(L) + k_4\dot{\varphi})^2. \quad (5.3)$$

The second discrepancy ρ_0 is selected to be equal to ρ at time $t = t_0 = 0$. Assuming that at time t_0 the gantry crane is in its equilibrium state, the second discrepancy is

$$\rho_0 = \rho(t_0) = 0. \quad (5.4)$$

As was stated in *Theorem 2* existence of a suitable positive definite functional V is sufficient to guarantee asymptotic stability with respect to the two discrepancies ρ and ρ_0 . Then, the corresponding Lyapunov functional can be represented as follows:

$$V = \frac{1}{2} (k_1\varepsilon + k_2\dot{z} + k_3\dot{w}(L) + k_4\dot{\varphi})^2. \quad (5.5)$$

In accordance with stability in terms of two discrepancies, the control input has to be chosen such that the time derivative of the functional \dot{V} along the state trajectories is always negative definite and vanishes only for $V = 0$. Calculating the time derivative of the corresponding Lyapunov functional results in

$$\dot{V} = e\dot{e} = e[k_1\dot{\varepsilon} + k_2\dot{z} + k_3\ddot{w}(L) + k_4\ddot{\varphi}]. \quad (5.6)$$

Here, it can be seen that by substituting the equation of motion (2.22), a direct dependency on the control input $k_m u(t)$ appears and that the relative degree of the associated input-output system is one. Assuming that $\ddot{w}(L)$ can be directly measured and eliminating the angular acceleration $\ddot{\varphi}$, (5.6) can be rewritten as follows:

$$\begin{aligned} \dot{V} = e & \left(k_1\dot{\varepsilon} + \frac{k_3 l f_1(\varphi) - m_s f_2(\varphi)}{l f_1(\varphi)} \ddot{w}(L) - \frac{f_2(\varphi)}{l f_1(\varphi)} F_{fr} \right. \\ & \left. - \frac{k_4 g m_s - k_2 g m_p \cos \varphi + m_p l \dot{\varphi}^2 f_2(\varphi)}{l f_1(\varphi)} \sin \varphi + \frac{k_m f_2(\varphi)}{l f_1(\varphi)} u \right), \end{aligned} \quad (5.7)$$

where

$$f_1(\varphi) = m_s - m_p \cos \varphi^2, \quad (5.8)$$

$$f_2(\varphi) = k_2 l - k_4 \cos \varphi. \quad (5.9)$$

In order to achieve the required negative definiteness of the time derivative along the state trajectory of the Lyapunov functional \dot{V} and exponential convergence of V , the control law has to be chosen as follows:

$$\begin{aligned} u = & \frac{l f_1(\varphi)}{k_m f_2(\varphi)} \left(- \frac{k_3 l f_1(\varphi) - m_s f_2(\varphi)}{l f_1(\varphi)} \ddot{w}(L) - \frac{f_2(\varphi)}{l f_1(\varphi)} F_{fr} - k_1 \dot{\varepsilon} \right. \\ & \left. + \frac{k_4 g m_s - k_2 g m_p \cos \varphi + m_p l \dot{\varphi}^2 f_2(\varphi)}{l f_1(\varphi)} \sin \varphi - a e \right) \end{aligned} \quad (5.10)$$

where $a > 0$ is a design parameter influencing the control performance.

Thereafter, substituting the designed control law (5.10) in \dot{V} (5.7) yields the aforementioned exponential convergence

$$\dot{V} = -a e^2 = -2aV. \quad (5.11)$$

The control scheme of the designed control system is depicted in Fig. 5.1.

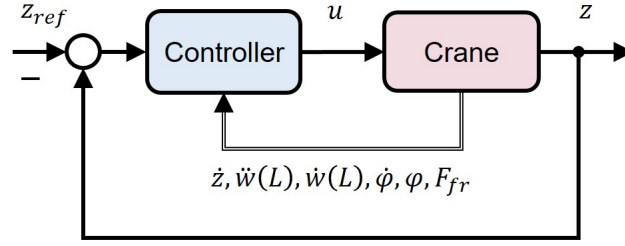


Figure 5.1.: Discrepancy-based control scheme

5.3.1. Extension of the control system

The installed crane sensors of the laboratory gantry crane provide measurements of the motor states τ, \dot{z}, z and accelerations of the crane girder $\ddot{w}(L)$ and payload \ddot{z}_p . For practical implementation of the control law (5.10) additional system states are required, in particular, the velocity of the crane girder $\dot{w}(L)$, angular velocity and angle of the payload $\dot{\phi}, \phi$, and the friction force $F_{fr}(\dot{z})$. As these can not be measured directly, the control system should be extended, as depicted in Fig. 5.2.

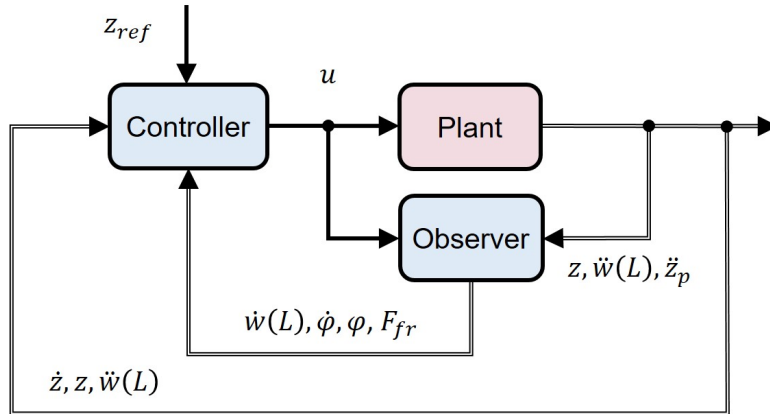


Figure 5.2.: Extended control scheme of discrepancy-based control

In this work, for the estimation of the lacking states an additional observer is used. In order to design the observer, the reduced order gantry crane plant model with linearized trigonometrical dynamics in the operating point $x = x_0$ and a nonlinear frictional model is utilized. Consider the fully observable linear reduced order crane model in its physical coordinates with the state vector $x = [z, \dot{z}, w(L), \dot{w}(L), \phi, \dot{\phi}]^T$, the measured output vector $y = [z, \ddot{w}(L), \ddot{z}_p]^T$, and two inputs - the control input u and the additional nonlinear friction force input $F_{fr}(x_2)$, which depends on the trolley velocity the crane. This model can be written as follows:

$$\dot{x} = Ax + B_1u + B_2F_{fr}(x_2), \quad (5.12)$$

$$y = Cx + D_1u + D_2F_{fr}(x_2), \quad (5.13)$$

where $A \in \mathbb{R}^{6 \times 6}$, $B_1 \in \mathbb{R}^{6 \times 1}$, $B_2 \in \mathbb{R}^{6 \times 1}$, $C \in \mathbb{R}^{3 \times 6}$, $D_1 \in \mathbb{R}^{3 \times 1}$, and $D_2 \in \mathbb{R}^{3 \times 1}$ are the associated system matrices.

The observer consisting of the plant model and the correction term based on the gained measurements error can be represented as follows:

$$\dot{\hat{x}} = A\hat{x} + B_1u + B_2F_{fr}(\hat{x}_2) + L(y - \hat{y}), \quad (5.14)$$

$$\hat{y} = C\hat{x} + D_1u + D_2F_{fr}(\hat{x}_2), \quad (5.15)$$

where $L \in \mathbb{R}^{6 \times 3}$ is the gain matrix of the observer.

Thus, taking into consideration the error between the system trajectories and observer states $\chi = x - \hat{x}$, the equation of the error dynamics can be derived as follows:

$$\begin{aligned} \dot{\chi} &= \dot{x} - \dot{\hat{x}} \\ &= Ax + B_1u + B_2F_{fr}(x_2) - A\hat{x} - B_1u - B_2F_{fr}(\hat{x}_2) - L(y - \hat{y}) \\ &= (A - LC)\chi + (B_2 - LD_2)\Delta_{fr} \end{aligned} \quad (5.16)$$

where $\Delta_{fr} = F_{fr}(x_2) - F_{fr}(\hat{x}_2)$ is the residual of the friction force.

Here, according to the dual principle in control systems, the gain matrix L can be found from the solution of the pole placement problem or LQ optimal control problem. From (5.16) it can be seen that the nonlinear term Δ_{fr} vanishes for $x_2 = \hat{x}_2$. However, from a practical point of view, the effects of friction are difficult to model accurately, and, therefore, nonlinear residuals Δ_{fr} may remain. In general, the convergence of the error χ in the presence of Lipschitz continuous nonlinearities can be guaranteed if the gains of the observer matrix L are sufficiently high such that the linear term $A - LC$ in (5.16) dominates the system dynamics [84]. However, this condition is difficult to fulfill in the presence of nonlinear discontinuous functions. It should also be mentioned that as the motion of the payload is linearized in the operating point $x = x_0$, only local convergence can be guaranteed for the real plant.

5.4. Simulation study

In the following, evaluation of the designed discrepancy-based control is presented. As the designed control system requires more information about the system states, an additional observer has been designed and verified. For contrast, this approach has been compared to another direct approach, which is based on the total system energy.

5.4.1. Evaluation of the state observer

In the following, the designed observer is presented and verified in a simulation study. The numerical system matrices of the associated gantry crane model (5.12) and (5.13) with the state vector $x = [z, \dot{z}, w(L), \dot{w}(L), \varphi, \dot{\varphi}]^T$, the measured output vector $y = [z, \ddot{w}(L), \ddot{z}_p]^T$, and two inputs - the control input u and the additional nonlinear friction

force input $F_{fr}(x_2)$ can be computed as follows:

$$A = \begin{bmatrix} 0 & 1 & 0 & 0 & 0 & 0 \\ 0 & 0 & 251.5 & 4.16 \cdot 10^{-2} & 1.15 \cdot 10^4 & 0 \\ 0 & 0 & 0 & 1 & 0 & 0 \\ 0 & 0 & -115.9 & -1.92 \cdot 10^{-2} & 0 & 0 \\ 0 & 0 & 0 & 0 & 0 & 1 \\ 0 & 0 & -0.38 & -6.21 \cdot 10^{-5} & -31.74 & 0 \end{bmatrix}, C = \begin{bmatrix} 1 & 0 & 0 \\ 0 & 0 & 0 \\ 0 & -115.9 & 0 \\ 0 & -1.92 \cdot 10^{-2} & 0 \\ 0 & 0 & -9.8 \cdot 10^3 \\ 0 & 0 & 0 \end{bmatrix}^T,$$

$$B_1 = \begin{bmatrix} 0 \\ 40.13 \\ 0 \\ -1.97 \\ 0 \\ -5.99 \cdot 10^{-2} \end{bmatrix}, B_2 = \begin{bmatrix} 0 \\ -13.99 \\ 0 \\ 0.69 \\ 0 \\ 2.09 \cdot 10^{-2} \end{bmatrix}, D_1 = \begin{bmatrix} 0 \\ -1.97 \\ 0 \end{bmatrix}, D_2 = \begin{bmatrix} 0 \\ 0.69 \\ 0 \end{bmatrix}.$$

In this work, the deterministic Kalman filter has been used as the observer [110]. Here, as the system is in the physical coordinates, the assignment of the weighting matrices Q and R is a trade-off between the model and the measured output contribution in the observed physical states. Choosing the weights as follows: $q_{i,i} = [1, 1, 0.5, 0.5, 0.5, 0.5]$, $r_{i,i} = [10^{-3}, 5, 25]$, and $q_{i,j} = r_{i,j} = 0$, the observer gain matrix L can be calculated as follows:

$$L = \begin{bmatrix} 38.37 & -9.3 \cdot 10^{-3} & -6.87 \cdot 10^{-4} \\ 236.2 & -1.4 & -1.17 \\ 0.41 & -0.31 & 3.49 \cdot 10^{-5} \\ -30.31 & 4.28 \cdot 10^{-2} & -6.9 \cdot 10^{-5} \\ 1.75 \cdot 10^{-3} & 2.06 \cdot 10^{-6} & -0.14 \\ -0.48 & 2.92 \cdot 10^{-3} & -0.14 \end{bmatrix}.$$

In order to verify the designed observer, the following open-loop simulation scenario is studied on the high-order nonlinear gantry crane model. Here, the initial value of the payload angle is chosen as $\varphi_0 = 0.05 \text{ rad}$. After 4 s a uniform random input with sample time 0.5 s appears. The obtained simulation results are depicted in the Fig. 5.3 and Fig. 5.4. Fig. 5.3 shows the time responses of the input force of the trolley F_t as well as the plant and observer outputs. In Fig. 5.4 the system states x (blue curves) and observed states (red curves) are presented. From the results, a relatively accurate matching between the estimated and plant states can be seen.

5.4.2. Evaluation of the discrepancy-based control

In order to perform the evaluations based on simulation, a plant model and the above-presented control law have been implemented in MATLAB. For this reason, the nonlinear lumped high-order model of the *full* gantry crane has been utilized. Here, the method of lines has been applied. The spatial coordinate of PDE (2.19) was discretized applying the FDM with $N = 20$ points. The resulting system of ODEs has been solved using the Dormand-Prince algorithm with a variable time step.

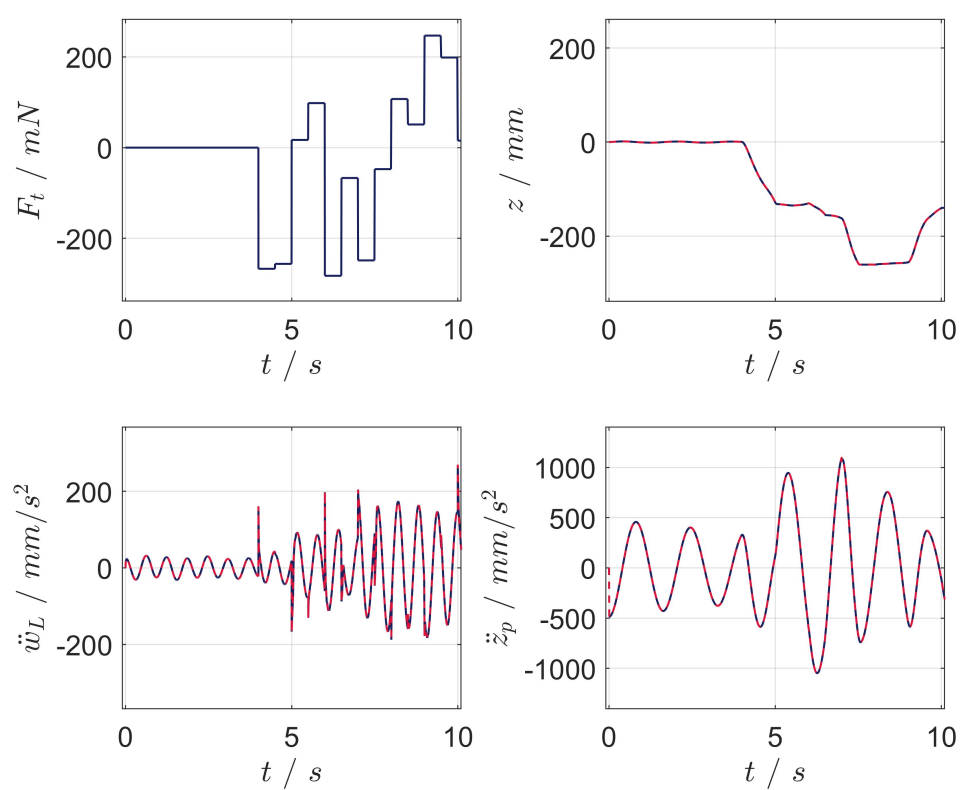


Figure 5.3.: Time responses of output measurements (blue) and observer output (red)

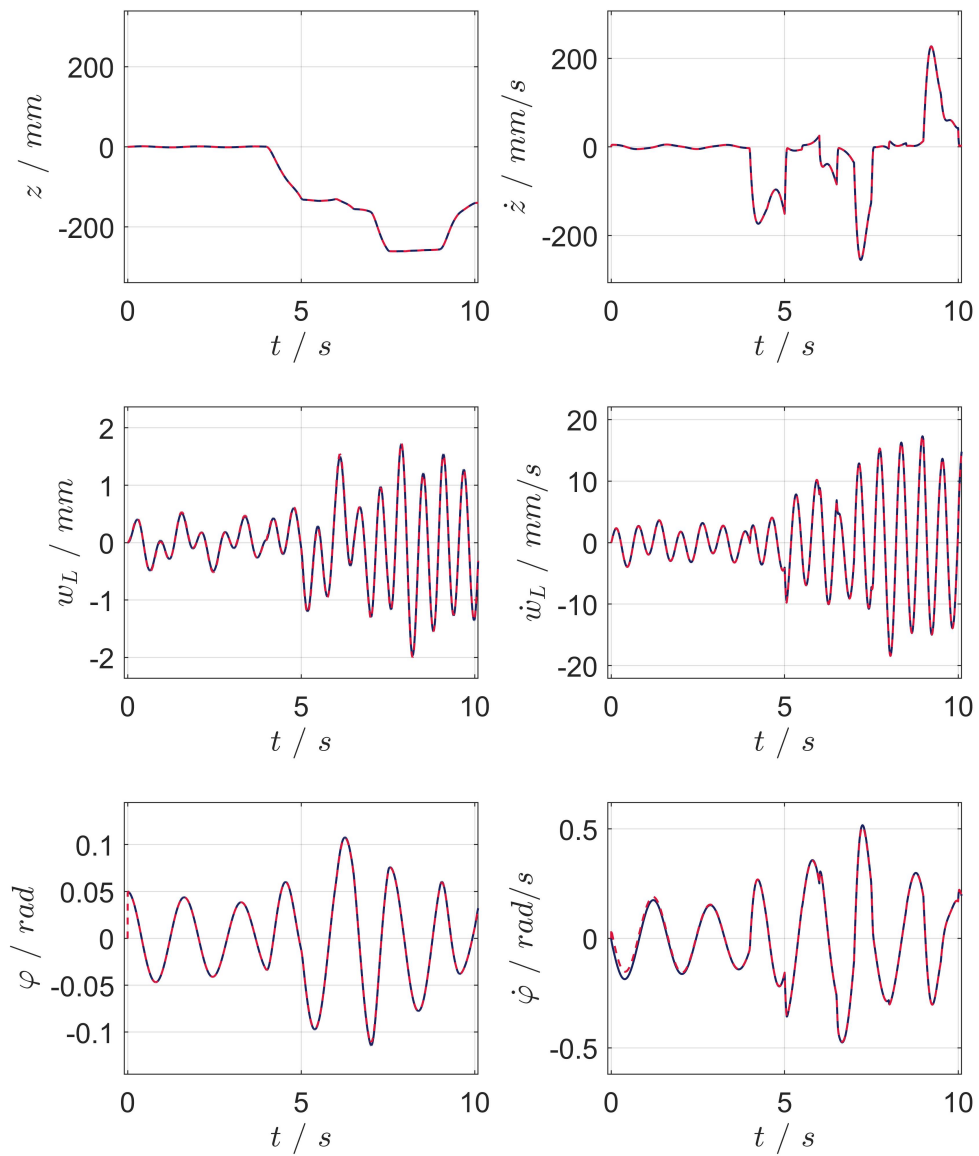


Figure 5.4.: Time responses of the plant (blue) and observed states (red)

As aforementioned, the generalized error (5.2) as well as the derived control law (5.10) contain additional tuning parameters $k_1 - k_4$ to influence the coupling. These parameters have a strong impact on the system zero dynamics. The assigning of their values is an ad hoc problem that requires an iterative tuning procedure. Here, trade-offs between the contribution of the different components according to appropriate design objectives should be taken into account. An optimal parameter adjustment has not been part of the work and should be investigated in future contributions.

Here, to provide a relatively fast reference tracking and reasonable damping of both oscillatory components, the parameters values $k_1 - k_4$ and the control performance parameter a have been chosen as follows:

$$k_1 = 11, \quad k_2 = 2.5, \quad k_3 = 11.8, \quad k_4 = 980, \quad a = 3. \quad (5.17)$$

As has been aforementioned, the stability of zero dynamics associated with the discrepancy can be examined for a linear discretized system. The zeros of the linear system of a reduced order 6 with the input u and output (5.2) are

$$z_{1,2} = -2.65 \pm 10.6 i, \quad (5.18)$$

$$z_{3,4} = -1.13 \pm 4.15 i, \quad (5.19)$$

$$z_5 = -16.46. \quad (5.20)$$

Here, it can be seen that the zeros are in the LHP and, therefore, the zero dynamics is locally stable.

For comparison the energy-based control derived in Appendix E has been applied to the same gantry crane model. This simple control law can be rewritten as follows:

$$u = \frac{1}{k_m} \left(-d_c \dot{z} + F_{fr} - k_p \varepsilon \right) \quad (5.21)$$

where d_c and k_p are corresponding positive tuning parameters of the controller. Parameters of the energy-based control law are adjusted to reach a relatively fast reference performance and acceptable damping as follows: $k_p = 11$ and $d_c = 2.5$.

In order to verify the proposed control law (5.10) and compare it with energy-based control law (5.21), the time responses of the positioning process have been studied. The obtained simulation results are depicted in Fig. 5.5, 5.6, and 5.7. From Fig. 5.5 it can be seen that applying the presented energy-based control, the trolley rises to the desired position after approximately 0.9 s. However, the application of this control law yields oscillatory behavior of the internal dynamics with relatively small energy dissipation. Moreover, after rising to the desired position, the magnitudes of the payload oscillations and crane vibrations are still relatively large, which does not meet the practical specifications. Applying the proposed discrepancy-based control results in notable damping of payload and structural motion. Here, the trolley rises to the desired position after 1.3 s and settles after approximately 1.8 s. It can also be seen that the corresponding Lyapunov functional V converges exponentially to zero after 3.5 s.

From Fig. 5.6 and 5.7 it can be seen that not only the oscillations of the girder point $w(L, t)$ but also the distributed state $w(x, t)$ itself and its L_2 - and L_∞ -norms are stabilized. This is remarkable, as this has not been part of the design. However, it can be

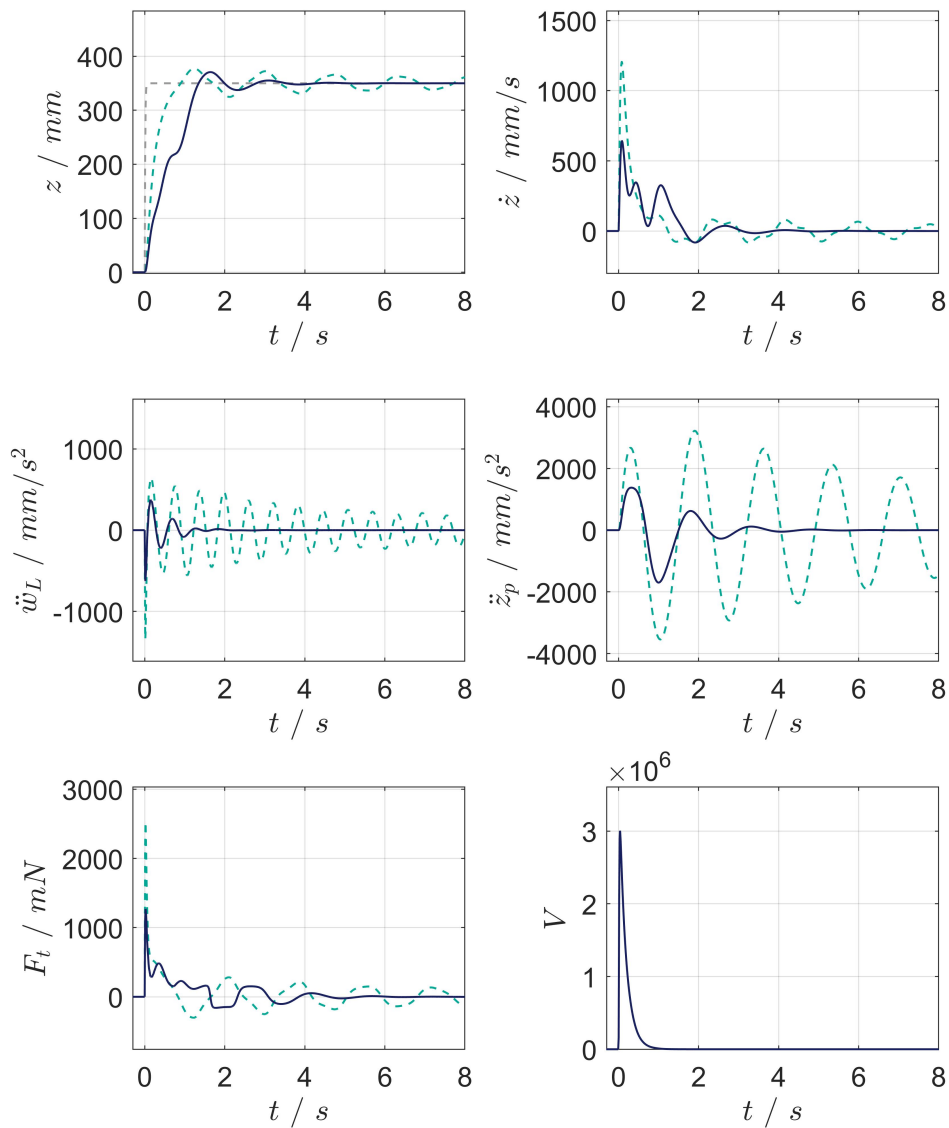


Figure 5.5.: Time responses of gantry crane applying discrepancy-based control (blue) and energy-based control (green), reference position (gray)

shown that stability in the sense of Lyapunov with respect to two discrepancies yields stability with respect to the L_p - or the L_∞ -norm if the zero dynamics associated with the discrepancy ρ is stable in the sense of the L_p - or L_∞ -norm [71, 72].

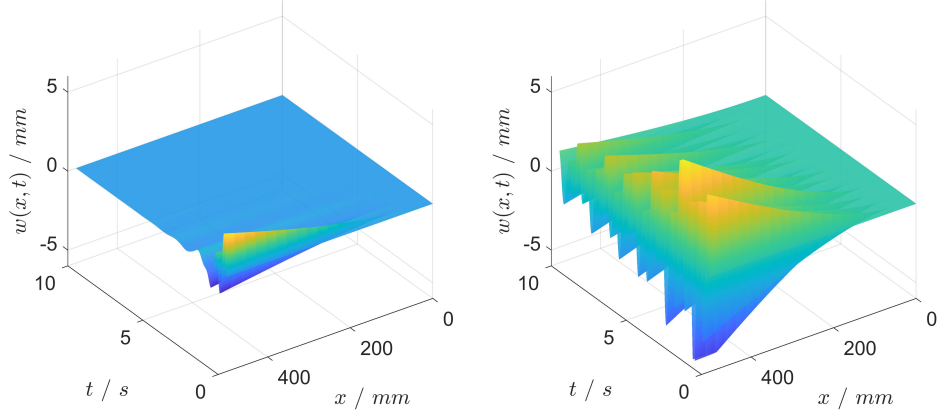


Figure 5.6.: Time responses of the distributed state applying energy-based control (**right**) and discrepancy-based control (**left**)

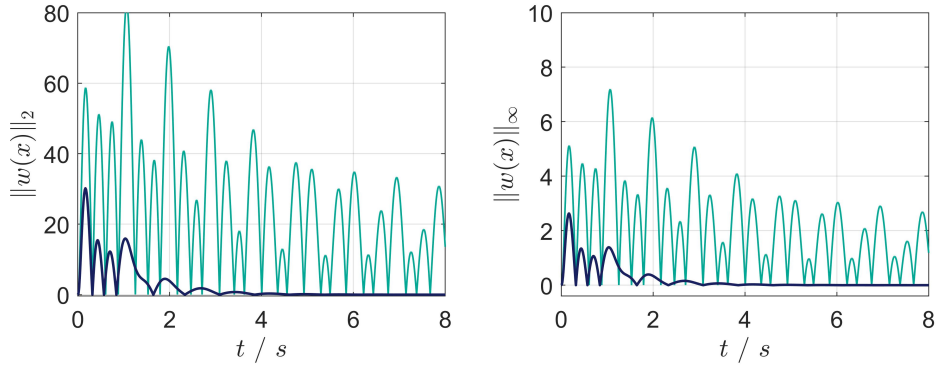


Figure 5.7.: L_2 -norm (**top**) and L_∞ -norm (**bottom**) with respect to x of the displacement $w(x, t)$ applying energy-based control (green) and discrepancy-based control (blue)

5.5. Experimental evaluation

In this Section, the proposed discrepancy-based control approach is evaluated on the *full* configuration of the laboratory gantry crane. As this approach requires more information about the system states, the designed observer has been validated in the first instance. This approach is compared with the energy-based control presented in Appendix E. In order to validate the above-mentioned approaches, tracking of the trolley position with a step change of the reference signal to $z_r = 350 \text{ mm}$ is studied.

The obtained results are presented in Fig. 5.8, 5.9, 5.10, and 5.11. Here, Fig. 5.8 shows the comparison of the simulation and experimental results. From the simulated curves it can be seen that the trolley rises to the desired position after 1.3 s and settles after approximately 1.8 s with an overshoot 6 %. The vibrations of the structure are notably damped after 1.5 s, and the payload swaying after approximately 3 s. The experimental

results show that the trolley position settles at the set-point after 1.3 s without large overshoots. The structural vibrations are notably damped after 2.5 s with small residual oscillations of the acceleration $\ddot{w}(L) \approx 50 \text{ mm/s}^2$. The payload swaying is damped after approximately 3 s with residual oscillations of the acceleration $\ddot{z}_p \approx 110 \text{ mm/s}^2$. These mismatches are a result of the model uncertainties and non-ideal compensation of the friction forces.

In Fig. 5.9 the discrepancy-based control approach is compared with the mentioned energy-based control in the same experimental study. It can be seen that application of the discrepancy-based control leads to better closed loop performance.

In Fig. 5.10 and 5.11 experimental results of disturbance rejection for the discrepancy-based control are shown. In the first case, an impulse disturbance is applied to the mechanical structure at time 12.5 s, as depicted in Fig. 5.10. It can be seen that the vibrations are notably damped after approximately 1 s with relatively small residual oscillations of acceleration $\ddot{w}(L) \approx 60 \text{ mm/s}^2$. In the second case, an impulse disturbance is applied to the payload at time 19.7 s, as presented in Fig. 5.11. The control system rejected the disturbance after 2 s with residual oscillations of the acceleration $\ddot{z}_p \approx 300 \text{ mm/s}^2$.

Fig. 5.12 and 5.13 show a robust performance evaluation of the discrepancy-based control. In this study the following cases from Tab. 5.1 are taken into consideration. The payload mass m_p and the rope length l are assumed to be variable parameters, while the the control law parameters remain the same as in the nominal case Tab. 5.1. From Fig. 5.12 and 5.13 it can be seen that for all cases the gantry crane is stable and the oscillations are notably suppressed.

Table 5.1.: Cases for robust performance evaluation

Cases	Payload mass m_p	Rope length l
Case 1 (nominal)	0.1 [kg]	670 [mm]
Case 2	0.03 [kg]	670 [mm]
Case 3	0.16 [kg]	670 [mm]
Case 4	0.1 [kg]	860 [mm]
Case 5	0.03 [kg]	860 [mm]
Case 6	0.16 [kg]	860 [mm]

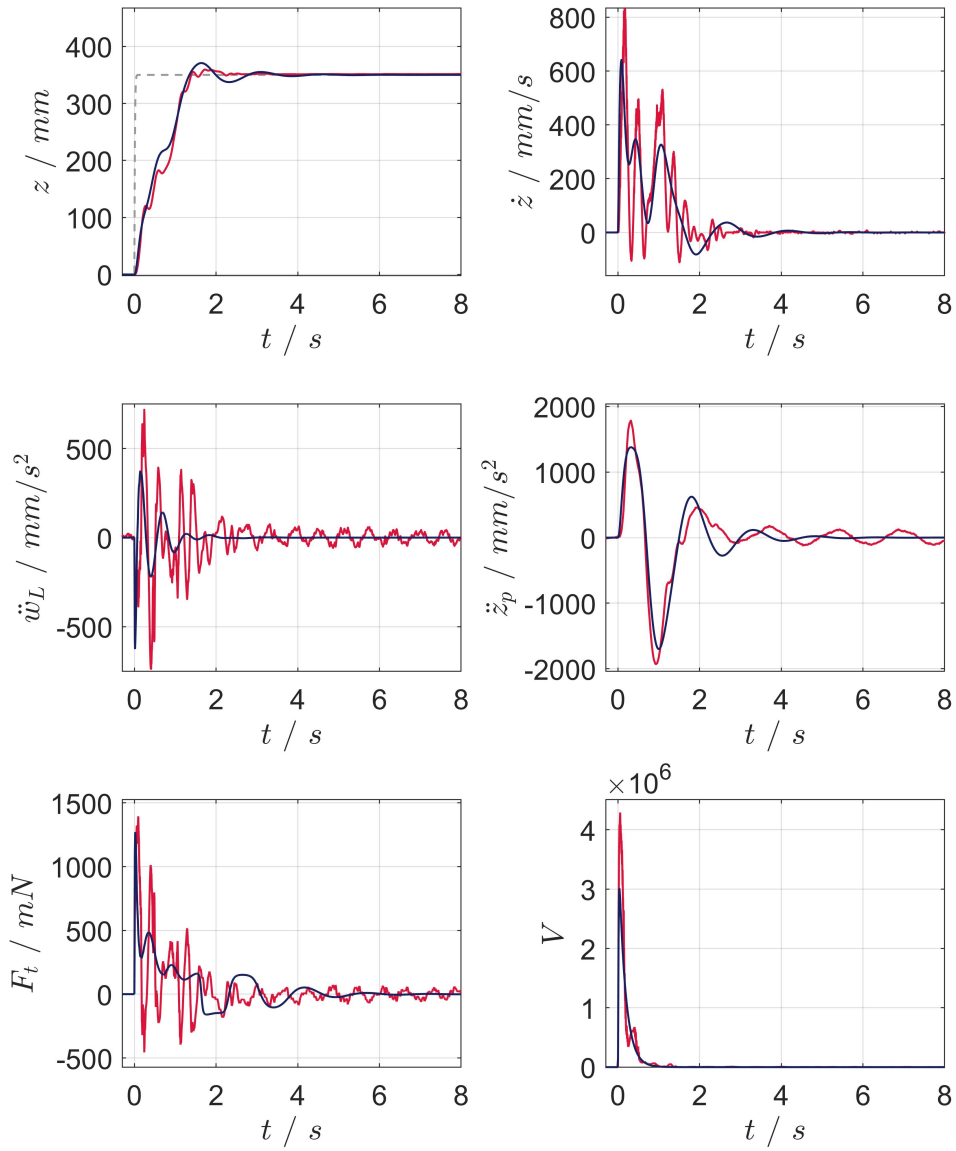


Figure 5.8.: Simulated (blue) and experimental (red) time responses of elastic gantry crane with discrepancy-based control by reference tracking

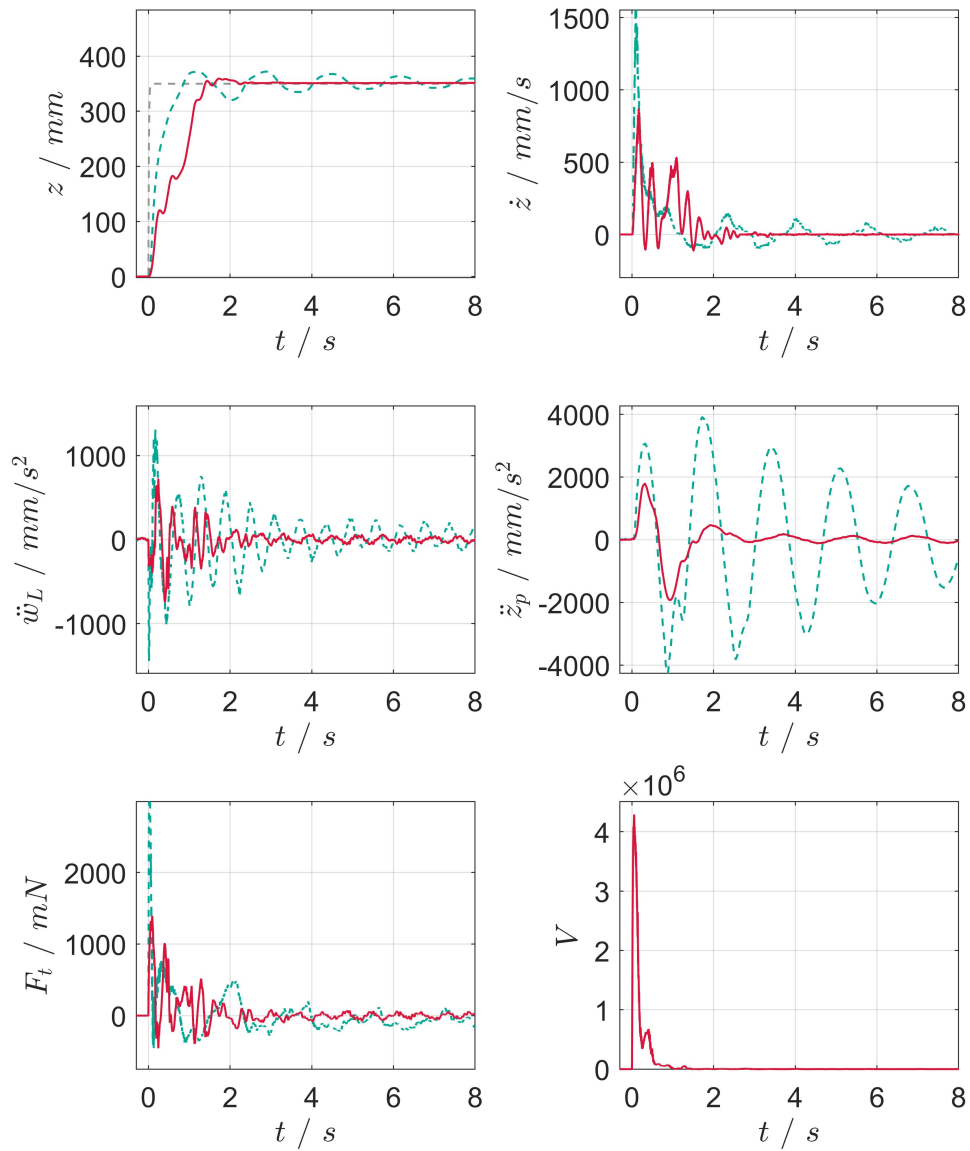


Figure 5.9.: Experimental time responses of elastic gantry crane with discrepancy-based control (red) and energy-based control (green)

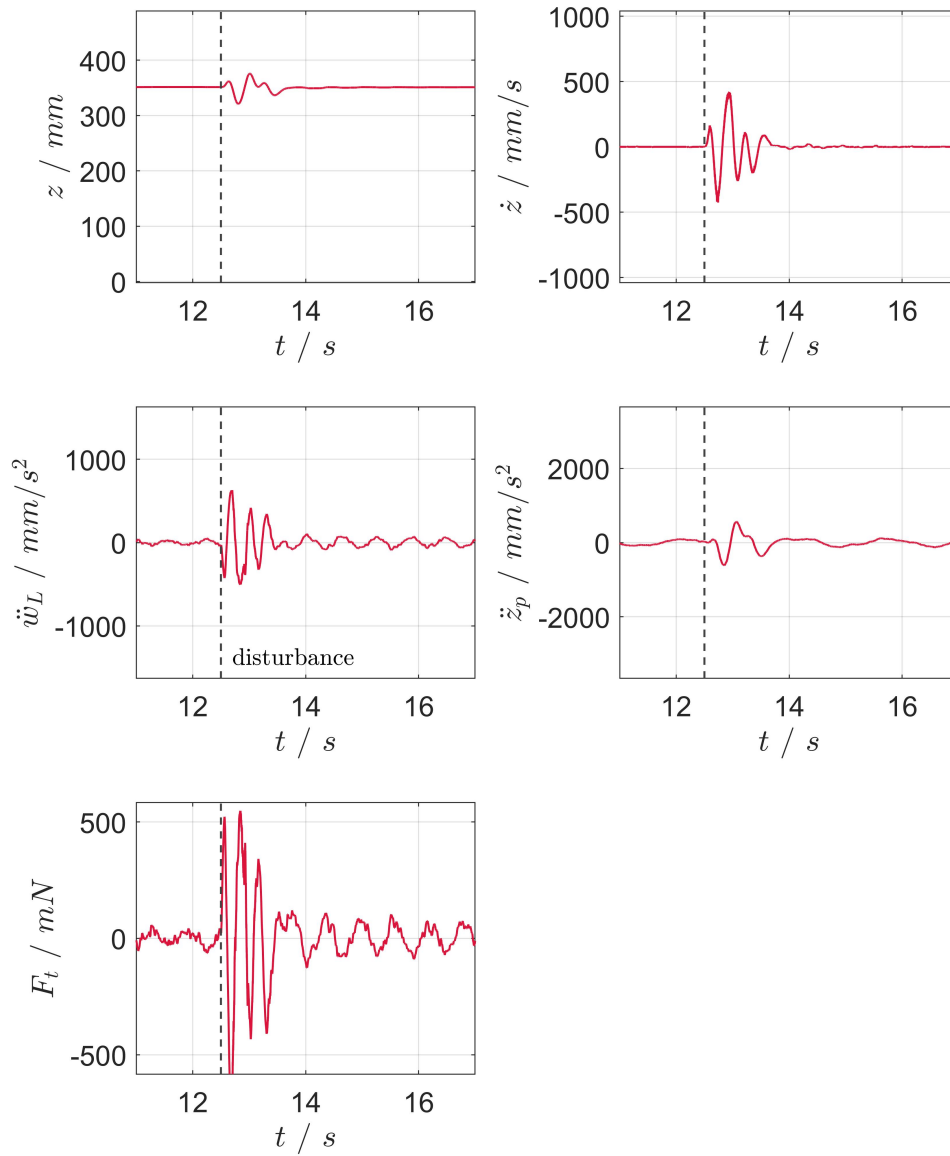


Figure 5.10.: Experimental time responses of elastic gantry crane with discrepancy-based control after applying a disturbance on the mechanical structure at time 12.5 s

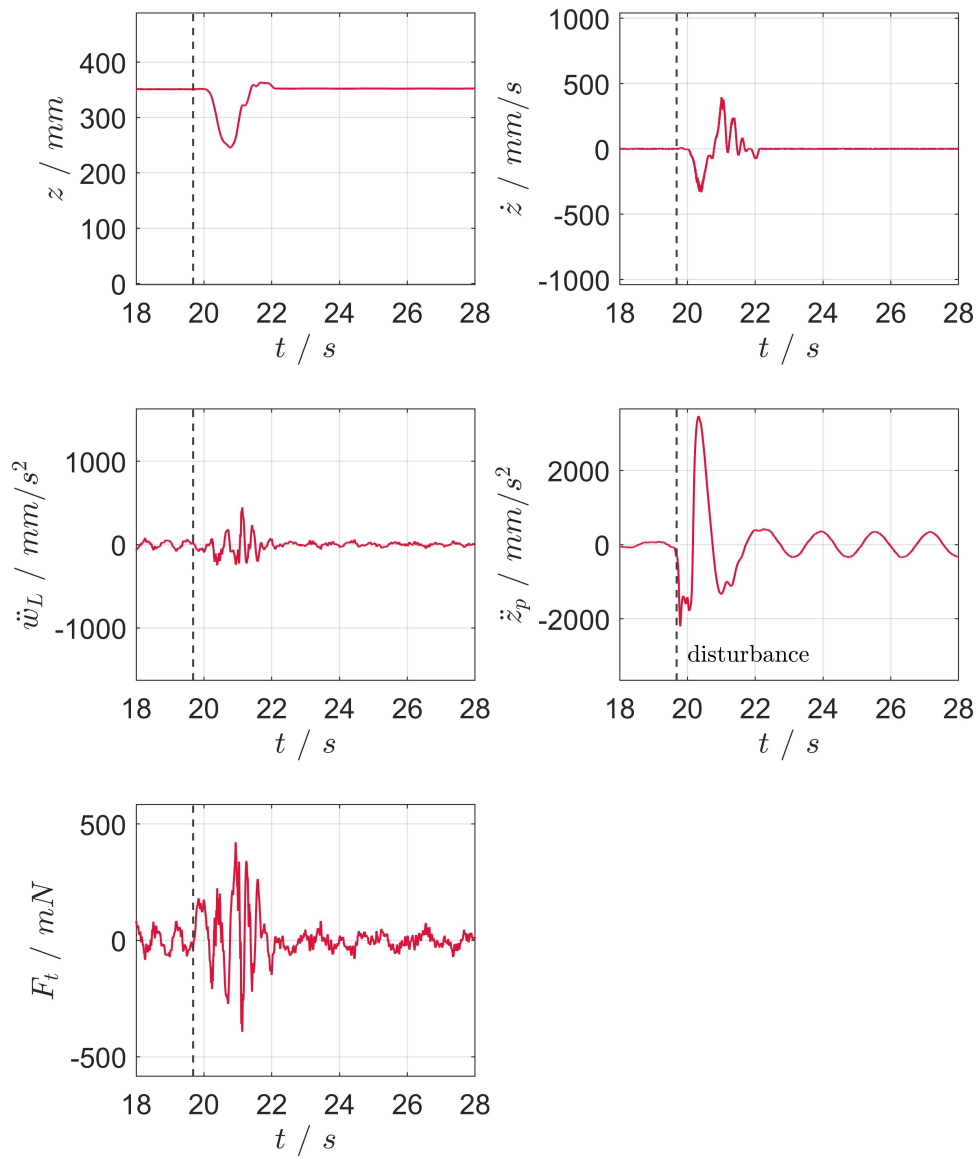


Figure 5.11.: Experimental time responses of elastic gantry crane with discrepancy-based control applying a disturbance on payload at time 19.7 s

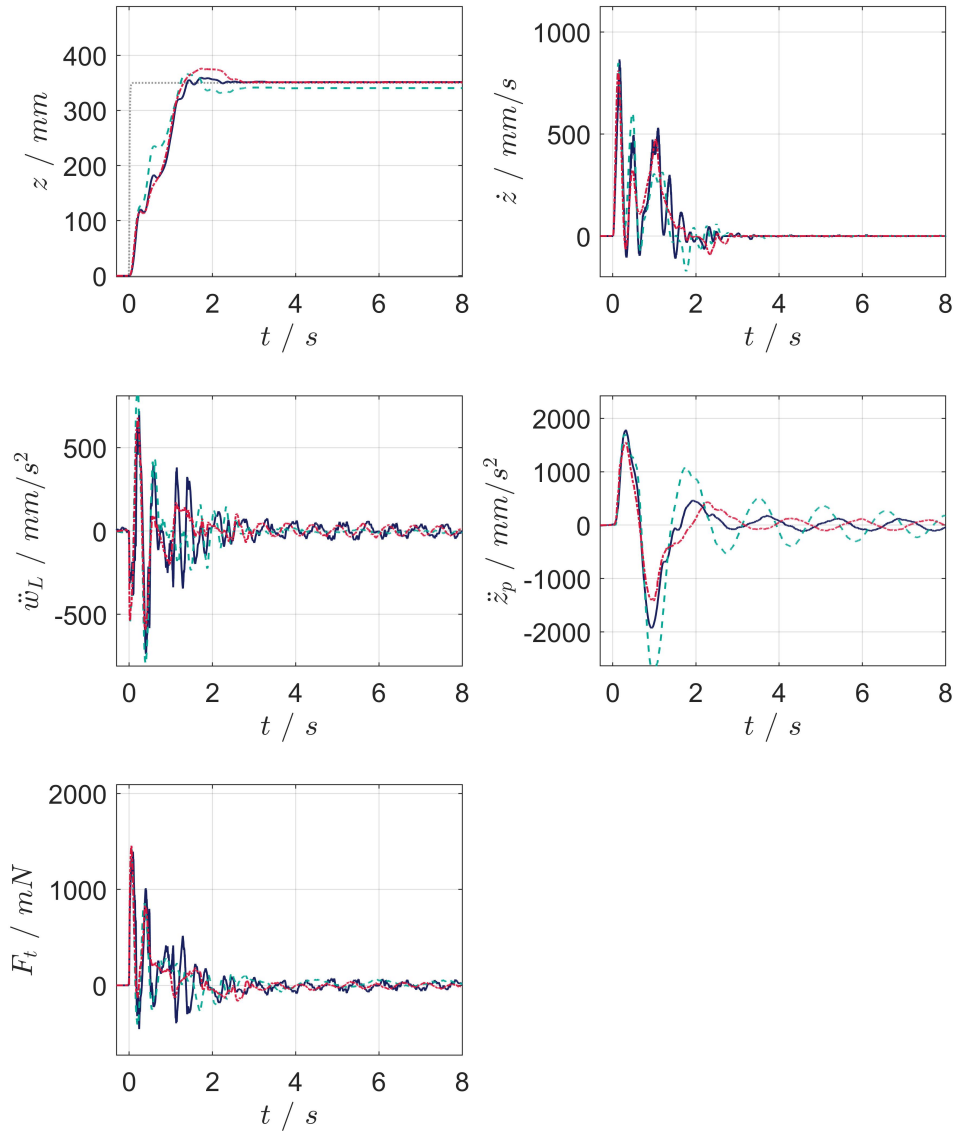


Figure 5.12.: Experimental time responses of elastic gantry crane with discrepancy-based control. Cases of robust performance evaluation: case 1 (solid blue), case 2 (dashed green), case 3 (dash dotted red)

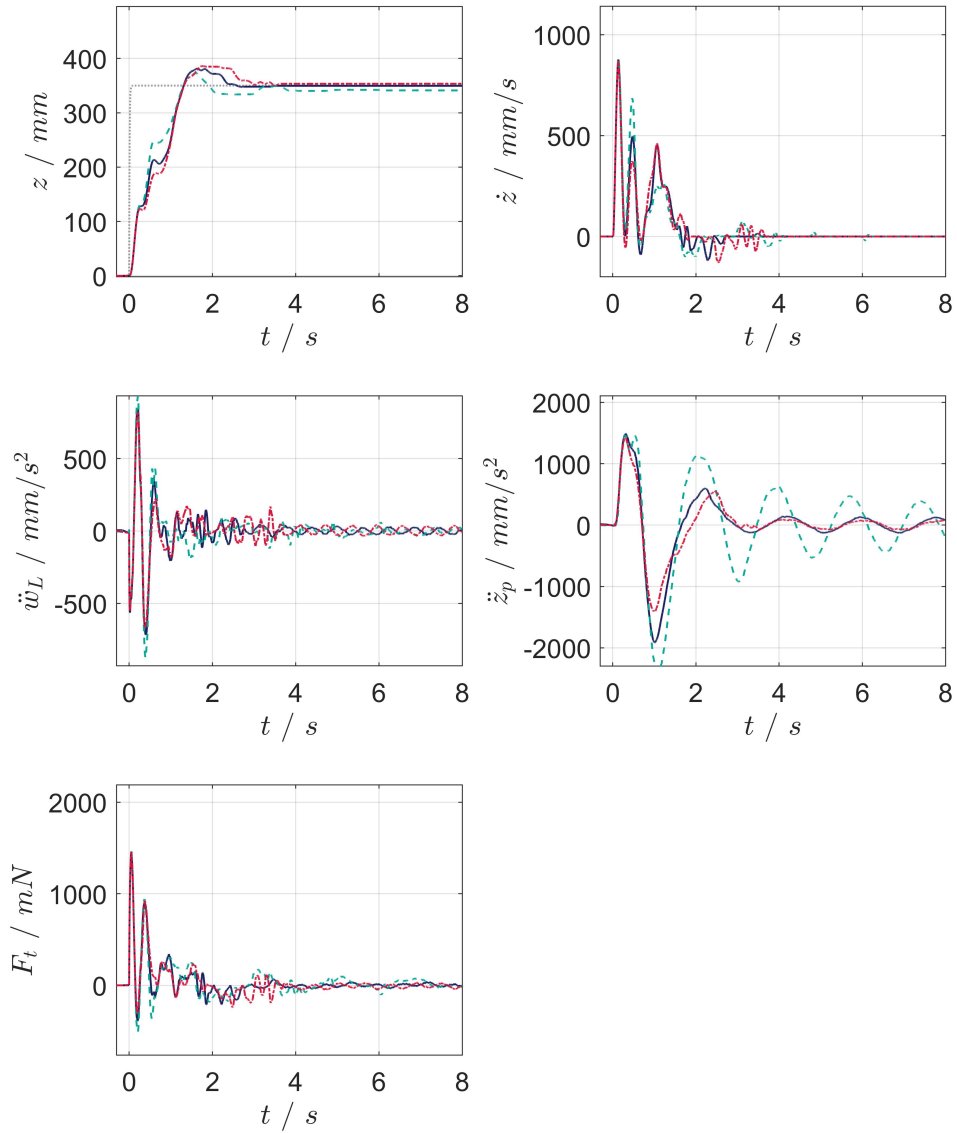


Figure 5.13.: Experimental time responses of elastic gantry crane with discrepancy-based control. Cases of robust performance evaluation: case 4 (solid blue), case 5 (dashed green), case 6 (dash dotted red)

6. Summary

6.1. Conclusion

Gantry cranes are a broad class of cranes that can be found in different industrial locations. Large gantry cranes are often utilized for handling containers at port terminals. During the last decades, a common trend in crane construction design was the application of lightweight structure elements. On the one hand, this led to resource conservation, but, on the other hand, this increased the influence of flexible structural vibrations. These weakly damped vibrations yield faster wear of construction and deteriorate the overall performance of crane operation. Furthermore, neglecting the structural dynamics for feedback control may result in excitation of the natural frequencies and even in unstable closed loop dynamics. The focus of this thesis was to reduce the undesired low-frequency vibrations in trolley travel direction using the trolley actuator. For this reason, three model-based control approaches for different crane configurations and control assumptions have been proposed.

In Chapter 1 introduction and general motivation on this topic have been discussed. Chapter 2 starts with the mathematical modeling of the gantry crane with flexible structural dynamics. Here, the distributed parameter model applying Hamilton's principle has been derived. It has also been shown that for more complex models, the FEM-approach is well suited. After this, the laboratory gantry crane has been introduced. In this thesis, two different practical configurations are considered:

- *simplified* crane configuration without the payload;
- *full* crane configuration.

Each configuration has its own drive and corresponding motion control system. Finally, the mathematical models of these configurations have been validated with the laboratory setups.

In Chapter 3 linear robust feedback control design for gantry cranes has been proposed. Here, the trolley drive system is considered to be in the position control mode such that the trolley position is the new control input. In order to design a control law that fulfills the performance specifications and guarantees the robust stability for a crane with not exactly known parameters, the H_∞ -loop-shaping synthesis has been applied. To introduce parametric uncertainties, the normalized coprime factor description with the associated gap metric has been used and applied for the generation of a set of the gantry crane models. The designed robust controller has been successfully evaluated in

simulations and on the *simplified* configuration of the laboratory gantry crane.

In Chapter 4 linear control design that does not require measurement of oscillations has been presented. This PFC-based output feedback approach has been applied to the *full* configuration of the gantry crane. It has been shown that this approach can be applied as an extension to the standard cascade motion control. Here, the PFC has been designed to compensate the system zero dynamics and to render the resulting plant ASPR. Thereafter, the closed loop system is stabilized applying high-gain output feedback. At the beginning of the chapter, a theoretical background on the relative degree and the zero dynamics is given. After this, several design procedures for PFC have been shown, and one of them has been applied for the gantry crane. The proposed feedback control approach has been successfully validated in simulations and experiments.

In Chapter 5 direct nonlinear control design for gantry cranes has been proposed. Here, the trolley drive system is in torque control mode, and a full redesign of the motion control system is considered. For stabilization, a generalized error measure, called discrepancy, has been taken into consideration. Applying the associated stability theory, i.e., stability with respect to two discrepancies, the nonlinear control law for the gantry crane based on Lyapunov direct design approach has been derived. As the control law requires unmeasured system states, an additional observer has been designed. The designed discrepancy-based control has been successfully tested in simulations and on the *full* configuration of the laboratory gantry crane.

In the present thesis, it has been shown and experimentally verified that the flexible structural vibrations in the trolley travel direction can be suppressed using only one actuator, i.e., the trolley drive system. It has been also demonstrated that all of the proposed approaches can be easily implemented in practice, e.g., as an extension to a conventional motion control system (methods from Chapter 3, Chapter 4) or as a full redesign (method from Chapter 5).

6.2. Future perspectives

For future practical applications of the PFC-based control presented in Chapter 4, a detailed robustness analysis has to be performed. It should be mentioned that the proposed design procedure of the PFC for the gantry crane is, on the one hand, simple in application and provides ASPR properties as well as zero placement for the extended plant but, on the other hand, this design can be sensitive to uncertainties, in particular, for weakly damped systems. In the presence of uncertainties, an additional weakly damped complex conjugate pair of poles and zeros appear in the extended plant \tilde{P} resulting in weakly damped residual oscillations. The amplitude of such oscillations depends on how considerable the uncertainty is and is often insignificant for small uncertainties. However, for more complex systems, where the dynamics can change and be unstable, this method is not suitable, and the design approach from Section 4.3.2 should be preferred.

In addition, robustness analysis with respect to the friction effects has to be performed for PFC-based control from Chapter 4 and discrepancy-based control from Chapter 5. In both cases, the friction compensation has been part of the control system design. In this work, a standard friction model with static parameters has been used. Since the mass of payload varies during the real crane operation affecting the friction, the corresponding parameter variations should be taken into account in the friction model. Here, it should be noted that an overcompensation of the friction force leads to the system energy increase and may result in unstable closed loop dynamics. In order to solve this problem, a friction compensator with parameter adaptation can be used.

The concept of active damping and the methods proposed in this work can be further used to generalize and solve other structural dynamics problems in different types of cranes. For example, an actuator of a load-lifting mechanism can be used for active damping of vertical vibrations, which are often found in STS-cranes. Furthermore, to control such a system, the methods presented in this work can be applied.

Furthermore, the presented approaches have to be evaluated on a full-scale real crane. In human-operated gantry cranes, weakly damped structural vibrations of high amplitudes disturb the crane operator. However, a massive actuation on the trolley motion due to the additional damping strategy can also be unpleasant for the crane operator. Therefore, for such cases, this fact has to be also taken into consideration as a control objective.

A. Detailed derivation of gantry crane model

In this Appendix, the general crane model derivation based on Hamilton's variational principle is presented. For clarity, let the kinetic energy of the system (2.15) and the potential energy of the system (2.16) be divided into the following terms

$$\begin{aligned}
T &= \frac{1}{2}m_c \dot{r}_c^T \dot{r}_c + \frac{1}{2}m_t \dot{r}_t^T \dot{r}_t + \frac{1}{2}m_p \dot{r}_p^T \dot{r}_p + \frac{1}{2} \int_0^L \rho \dot{w}^2 dx, \\
&= \underbrace{\frac{1}{2}m_p [(\dot{w}(L) + \dot{z} + \dot{\varphi}l \cos \varphi)^2 + (\dot{\varphi}l \sin(\varphi))^2]}_{T_1} \\
&\quad + \underbrace{\frac{1}{2}m_t (\dot{w}(L) + \dot{z})^2 + \frac{1}{2}m_c \dot{w}^2(L)}_{T_2} + \underbrace{\frac{1}{2} \int_0^L \rho \dot{w}^2 dx}_{T_3}. \tag{A.1}
\end{aligned}$$

$$U = \underbrace{m_p g l (1 - \cos \varphi)}_{U_1} + \underbrace{\frac{1}{2} \int_0^L EI (w'')^2 dx}_{U_2}. \tag{A.2}$$

Taking into account the energy (A.1), (A.2) and the work (2.17), extended Hamilton's principle (2.1) can be written as

$$\int_{t_1}^{t_2} (\delta T_1 + \delta T_2 + \delta T_3 - (\delta U_1 + \delta U_2) + \delta W) dt = 0. \tag{A.3}$$

In following calculation of the variations for each energy term is presented. For the term T_1 it follows

$$\begin{aligned}
\int_{t_1}^{t_2} \delta T_1 dt &= \int_{t_1}^{t_2} \delta \left\{ \frac{1}{2}m_p [(\dot{w}(L) + \dot{z} + \dot{\varphi}l \cos \varphi)^2 + (\dot{\varphi}l \sin \varphi)^2] \right\} dt \\
&= \int_{t_1}^{t_2} \delta \left\{ \frac{1}{2}m_p l^2 \dot{\varphi}^2 \left((\sin \varphi)^2 + (\cos \varphi)^2 \right) + \frac{1}{2}m_p \dot{w}(L)^2 + \frac{1}{2}m_p \dot{z}^2 \right. \\
&\quad \left. + m_p \dot{w}(L) \dot{z} + m_p l \dot{w}(L) \dot{\varphi} \cos \varphi + m_p l \dot{z} \dot{\varphi} \cos \varphi \right\} dt \\
&= \int_{t_1}^{t_2} \left\{ m_p l^2 \dot{\varphi} \delta \dot{\varphi} + m_p (\dot{w}(L) + \dot{z}) \delta \dot{w}(L) + m_p (\dot{w}(L) + \dot{z}) \delta \dot{z} \right. \\
&\quad - m_p l \dot{w}(L) \dot{\varphi} \sin \varphi \delta \varphi + m_p l \dot{w}(L) \cos \varphi \delta \dot{\varphi} + m_p l \dot{\varphi} \cos \varphi \delta \dot{w}(L) \\
&\quad \left. - m_p l \dot{z} \dot{\varphi} \sin \varphi \delta \varphi + m_p l \dot{z} \cos \varphi \delta \dot{\varphi} + m_p l \dot{\varphi} \cos \varphi \delta \dot{z} \right\} dt. \tag{A.4}
\end{aligned}$$

In order to avoid time derivatives of variations $\delta\varphi$, δz and $\delta w(L)$ in (A.4) integration by parts can be applied

$$\begin{aligned}
\int_{t_1}^{t_2} \delta T_1 dt &\stackrel{P.I.}{=} [m_p l^2 \dot{\varphi} \delta\varphi] \Big|_{t_1}^{t_2} - \int_{t_1}^{t_2} \left\{ m_p l^2 \ddot{\varphi} \right\} \delta\varphi dt \\
&+ [m_p (\dot{w}(L) + \dot{z}) \delta w(L)] \Big|_{t_1}^{t_2} - \int_{t_1}^{t_2} \left\{ m_p (\ddot{w}(L) + \ddot{z}) \right\} \delta w(L) dt \\
&+ [m_p (\dot{w}(L) + \dot{z}) \delta z] \Big|_{t_1}^{t_2} - \int_{t_1}^{t_2} \left\{ m_p (\ddot{w}(L) + \ddot{z}) \right\} \delta z dt \\
&+ [m_p l \dot{w}(L) \cos \varphi \delta\varphi] \Big|_{t_1}^{t_2} - \int_{t_1}^{t_2} \left\{ m_p l (\ddot{w}(L) \cos \varphi - \dot{w}(L) \sin \varphi \dot{\varphi}) \right\} \delta\varphi dt \\
&+ [m_p l \dot{\varphi} \cos \varphi \delta w(L)] \Big|_{t_1}^{t_2} - \int_{t_1}^{t_2} \left\{ m_p l (\ddot{\varphi} \cos \varphi - \dot{\varphi}^2 \sin \varphi) \right\} \delta w(L) dt \\
&+ [m_p l \dot{z} \cos \varphi \delta\varphi] \Big|_{t_1}^{t_2} - \int_{t_1}^{t_2} \left\{ m_p l (\ddot{z} \cos \varphi - \dot{z} \sin \varphi \dot{\varphi}) \right\} \delta\varphi dt \\
&+ [m_p l \dot{\varphi} \cos \varphi \delta z] \Big|_{t_1}^{t_2} - \int_{t_1}^{t_2} \left\{ m_p l (\ddot{\varphi} \cos \varphi - \dot{\varphi}^2 \sin \varphi) \right\} \delta z dt \\
&- \int_{t_1}^{t_2} \left\{ m_p l (\dot{w}(L) \dot{\varphi} \sin \varphi + \dot{z} \dot{\varphi} \sin \varphi) \right\} \delta\varphi dt. \tag{A.5}
\end{aligned}$$

Taking into account that variations vanish at time moments t_1 and t_2 , collecting integral terms with same variations $\delta\varphi$, δz and $\delta w(L)$ and making corresponding simplifications (A.5) can be rewritten

$$\begin{aligned}
\int_{t_1}^{t_2} \delta T_1 dt &= - \int_{t_1}^{t_2} \left\{ m_p l^2 \ddot{\varphi} + m_p l \ddot{w}(L) \cos \varphi + m_p l \ddot{z} \cos \varphi \right\} \delta\varphi dt \\
&- \int_{t_1}^{t_2} \left\{ m_p (\dot{w}(L) + \dot{z}) + m_p l \ddot{\varphi} \cos \varphi - m_p l \dot{\varphi}^2 \sin \varphi \right\} \delta w(L) dt \\
&- \int_{t_1}^{t_2} \left\{ m_p (\dot{w}(L) + \dot{z}) + m_p l \ddot{\varphi} \cos \varphi - m_p l \dot{\varphi}^2 \sin \varphi \right\} \delta z dt. \tag{A.6}
\end{aligned}$$

Taking variations for the term T_2 yields

$$\begin{aligned}
\int_{t_1}^{t_2} \delta T_2 dt &= \int_{t_1}^{t_2} \delta \left\{ \frac{1}{2} m_c \dot{w}(L)^2 + \frac{1}{2} m_t (\dot{w}(L) + \dot{z})^2 \right\} dt \\
&= \int_{t_1}^{t_2} \left\{ ((m_c + m_t) \dot{w}(L) + m_t \dot{z}) \delta \dot{w}(L) + m_t (\dot{z} + \dot{w}(L)) \delta \dot{z} \right\} dt \tag{A.7}
\end{aligned}$$

To eliminate time derivatives of variations δz and $\delta w(L)$ in (A.7) integration by parts can be applied

$$\begin{aligned} \int_{t_1}^{t_2} \delta T_2 dt &\stackrel{P.I.}{=} \left[((m_c + m_t)\dot{w}(L) + m_t\dot{z})\delta w(L) \right] \Big|_{t_1}^{t_2} \\ &\quad - \int_{t_1}^{t_2} \left\{ ((m_c + m_t)\ddot{w}(L) + m_t\ddot{z}) \right\} \delta w(L) dt \\ &\quad + \left[(m_t(\dot{z} + \dot{w}(L))\delta z) \right] \Big|_{t_1}^{t_2} - \int_{t_1}^{t_2} \left\{ m_t(\ddot{z} + \ddot{w}(L)) \right\} \delta z dt. \end{aligned} \quad (A.8)$$

Taking into account that variations vanish at time moments t_1 and t_2 (A.8) can be rewritten

$$\begin{aligned} \int_{t_1}^{t_2} \delta T_2 dt &= - \int_{t_1}^{t_2} \left\{ ((m_c + m_t)\ddot{w}(L) + m_t\ddot{z}) \right\} \delta w(L) dt \\ &\quad - \int_{t_1}^{t_2} \left\{ m_t(\ddot{z} + \ddot{w}(L)) \right\} \delta z dt. \end{aligned} \quad (A.9)$$

Applying the same procedure for the distributed term T_3 results in

$$\begin{aligned} \int_{t_1}^{t_2} \delta T_3 dt &= \int_{t_1}^{t_2} \int_0^L \varrho \dot{w} \delta \dot{w} dx dt \\ &\stackrel{P.I.}{=} \left[\varrho \dot{w} \delta w \right] \Big|_{t_1}^{t_2} - \int_{t_1}^{t_2} \int_0^L \varrho \ddot{w} \delta w dx dt \\ &= - \int_{t_1}^{t_2} \int_0^L \varrho \ddot{w} \delta w dx dt. \end{aligned} \quad (A.10)$$

For the term of potential energy U_1 it follows

$$\begin{aligned} \int_{t_1}^{t_2} \delta U_1 dt &= \int_{t_1}^{t_2} \delta \left\{ m_p g l (1 - \cos \varphi) \right\} dt \\ &= - \int_{t_1}^{t_2} \left\{ m_p g l \sin \varphi \right\} \delta \varphi dt. \end{aligned} \quad (A.11)$$

Applying variation to the distributed elasticity term U_2 and eliminating spatial derivatives in variation δw using integration by parts the second term of the potential energy can be obtained as

$$\begin{aligned} \int_{t_1}^{t_2} \delta U_2 dt &= \int_{t_1}^{t_2} \int_0^L E \mathcal{I} w'' \delta w'' dx dt \\ &\stackrel{P.I.}{=} \int_{t_1}^{t_2} \left\{ \left[E \mathcal{I} w'' \delta w' \right] \Big|_0^L - \int_0^L E \mathcal{I} w''' \delta w' dx \right\} dt \\ &\stackrel{P.I.}{=} \int_{t_1}^{t_2} \left\{ \left[E \mathcal{I} w'' \delta w' \right] \Big|_0^L - \left[E \mathcal{I} w''' \delta w \right] \Big|_0^L \right. \\ &\quad \left. + \int_0^L E \mathcal{I} w'''' \delta w dx \right\} dt. \end{aligned} \quad (A.12)$$

Substituting (A.6), (A.9), (A.10), (A.11), (A.12), and the virtual work (2.17) into Hamilton's principle (A.3), collecting terms with the same variations, and taking into consideration the geometrical boundary conditions $w(0) = w'(0) = 0$, the following sum is obtained

$$\begin{aligned}
0 = & - \int_{t_1}^{t_2} \int_0^L \left[\rho \ddot{w} + EI w'''' + c \dot{w} \right] \delta w \, dx \, dt - \int_{t_1}^{t_2} \left[EI w''(L) \right] \delta w'(L) \, dt \\
& - \int_{t_1}^{t_2} \left[m_\Sigma \ddot{w}(L) + m_s \ddot{z} + m_p l \ddot{\varphi} \cos \varphi - m_p l \dot{\varphi}^2 \sin \varphi - EI w'''(L) \right] \delta w(L) \, dt \\
& - \int_{t_1}^{t_2} \left[m_s \ddot{w}(L) + m_s \ddot{z} + m_p l \ddot{\varphi} \cos \varphi - m_p l \dot{\varphi}^2 \sin \varphi - F_t + F_{fr} \right] \delta z \, dt \\
& - m_p l \int_{t_1}^{t_2} \left[l \ddot{\varphi} + \ddot{w}(L) \cos \varphi + \ddot{z} \cos \varphi + g \sin \varphi \right] \delta \varphi \, dt, \tag{A.13}
\end{aligned}$$

where $m_\Sigma = m_p + m_t + m_c$ and $m_s = m_p + m_t$.

From (A.13) it can be seen that for any arbitrary variations the equation holds only if integrands vanish independently. Hence, the equations of motion of the gantry crane follow

$$\rho \ddot{w} + EI w'''' + c \dot{w} = 0, \tag{A.14}$$

$$w(0) = w'(0) = w''(L) = 0, \tag{A.15}$$

$$m_\Sigma \ddot{w}(L) + m_s \ddot{z} + m_p l \ddot{\varphi} \cos \varphi - m_p l \dot{\varphi}^2 \sin \varphi - EI w'''(L) = 0, \tag{A.16}$$

$$m_s \ddot{w}(L) + m_s \ddot{z} + m_p l \ddot{\varphi} \cos \varphi - m_p l \dot{\varphi}^2 \sin \varphi - F_t + F_{fr} = 0, \tag{A.17}$$

$$l \ddot{\varphi} + \ddot{w}(L) \cos \varphi + \ddot{z} \cos \varphi + g \sin \varphi = 0. \tag{A.18}$$

The above equations of motion describe the flexible gantry crane dynamics under the made assumptions. As can be seen, the application of Hamilton's principle for such an one-dimensional problems is straightforward. However, the corresponding algebraic operations are often bulky, making applications of this method unreasonable for more complicated problems.

B. Numerical-based model

Modeling of flexible structures is a complex task because of their infinite-dimensional nature. The utilization of analytical methods is restricted to problems with simple geometries and boundary conditions. For more complex problems, e.g., 3D geometry of real gantry crane, application of numerical modeling methods is preferred [126, 81, 54]. For modeling and analysis of various infinite-dimensional physical problems, the FEM can be used. Nowadays, there are many commercial FEM packages that provide possibilities for importing CAD model geometries and exporting dynamic models. Having reliable models at the stage of crane production enables early analysis, control system design, and virtual commissioning.

For a derivation of the dynamic model of flexible crane structure, including the displacements and its derivatives, the Solid Mechanics interface of the commercial software COMSOL Multiphysics is well suited. Here, the geometry of the gantry crane can be imported from a CAD model. After defining material properties, boundary and loading conditions, outputs, and meshes, a linear lumped model of n DOF can be derived automatically as

$$M\ddot{Y} + P\dot{Y} + QY = F, \quad (\text{B.1})$$

where Q , P , and M are derived global stiffness, damping, and mass matrices, Y , \dot{Y} , and \ddot{Y} are displacement, velocity, and acceleration vectors at all domain nodes of the structure as well as F is the nodal forces vector.

Taking into consideration the input and output of interest, the structural model can be represented as a linear state-space model of $2n$ -th order and coupled with the other model subsystems, e.g., as depicted in Fig. B.1.

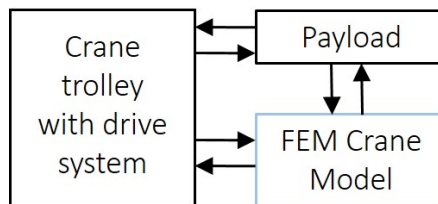


Figure B.1.: Possible model interaction scheme

C. Model parameters

In this Appendix the parameters of the gantry cranes configurations are presented.

Simplified crane configuration

Table C.1.: System parameters

ϱ	6124	$[kg/m^3]$	EI	$4.34 \cdot 10^3$	$[Nm^2]$
L	0.548	$[m]$			
α	0.116	$[-]$	β	0.002	$[-]$
m_t	5.37	$[kg]$	m_p	$0.3 - 0.6$	$[kg]$
m_c	1.46	$[kg]$	T_z	0.4	$[s]$
T_{d1}	0.005	$[s]$			

Full crane configuration

Table C.2.: System parameters

ϱ	6124	$[kg/m^3]$	EI	$4.34 \cdot 10^3$	$[Nm^2]$
L	0.5	$[m]$			
α	0.116	$[-]$	β	0.002	$[-]$
m_t	0.1	$[kg]$	m_p	0.1	$[kg]$
m_c	1.46	$[kg]$	l	0.67	$[m]$
F_{vi}	0.5	$[Ns/m]$	F_{st}	310	$[N]$
F_{co}	145	$[N]$	b_{sb}	1.67	$[-]$
k_{fr}	0.5	$[-]$			

D. Linear control approaches

In this Appendix, two classical linear control approaches for evaluating and comparing the gantry crane control from Chapter 4 are presented. Here, it is assumed that the crane configuration is back-drivable, i.e., the coupling between trolley with the drive, flexible structure, and payload subsystems exist, and no additional sensors for the oscillations measurements are needed.

The first approach is a classical cascade control for drive position control (Fig. 2.7) where no additional damping goals are considered. Such simple control law can be written as follows:

$$\tau = [k_r(z_{ref} - z) - sz] \left(k_v + \frac{1}{T_v s} \right), \quad (\text{D.1})$$

where k_r is the coefficient of position controller, k_v and T_v are parameters of the velocity PI controller.

Parameters of the controller can be adjusted for reaching a fast reference performance as follows $k_v = 2$, $T_v = 0.14$, and $k_r = 10$. In Fig. D.1 simulation and experimental results applying the control law (D.1) for the *full* crane configuration from Section 2.4.3 are depicted. As has been discussed in Section 4.5.1, applying high gain output feedback control to plants with zeros near the imaginary axis results in oscillatory closed loop dynamics.

The second approach is an observer-based state feedback control, as depicted in Fig. D.2. Here, the state feedback control law with additional integral part

$$u(t) = -K [\hat{x}^T, \hat{x}_i^T]^T \quad (\text{D.2})$$

acts on all internal system states providing positioning and damping for the oscillatory plant subsystems. The controller vector K can be calculated by minimizing the following linear quadratic value function

$$J = \int_0^{\infty} (x^T(t)Qx(t) + u^T(t)Ru(t)) dt, \quad (\text{D.3})$$

where Q and R are corresponding weighting matrices.

Recalling the linear reduced order model of gantry crane from Section 2.4.3 with the state vector $x = [x_{s1}, x_{s2}, z, \dot{z}, \varphi, \dot{\varphi}]$, the trolley position as output $y = z$, and nonlinear

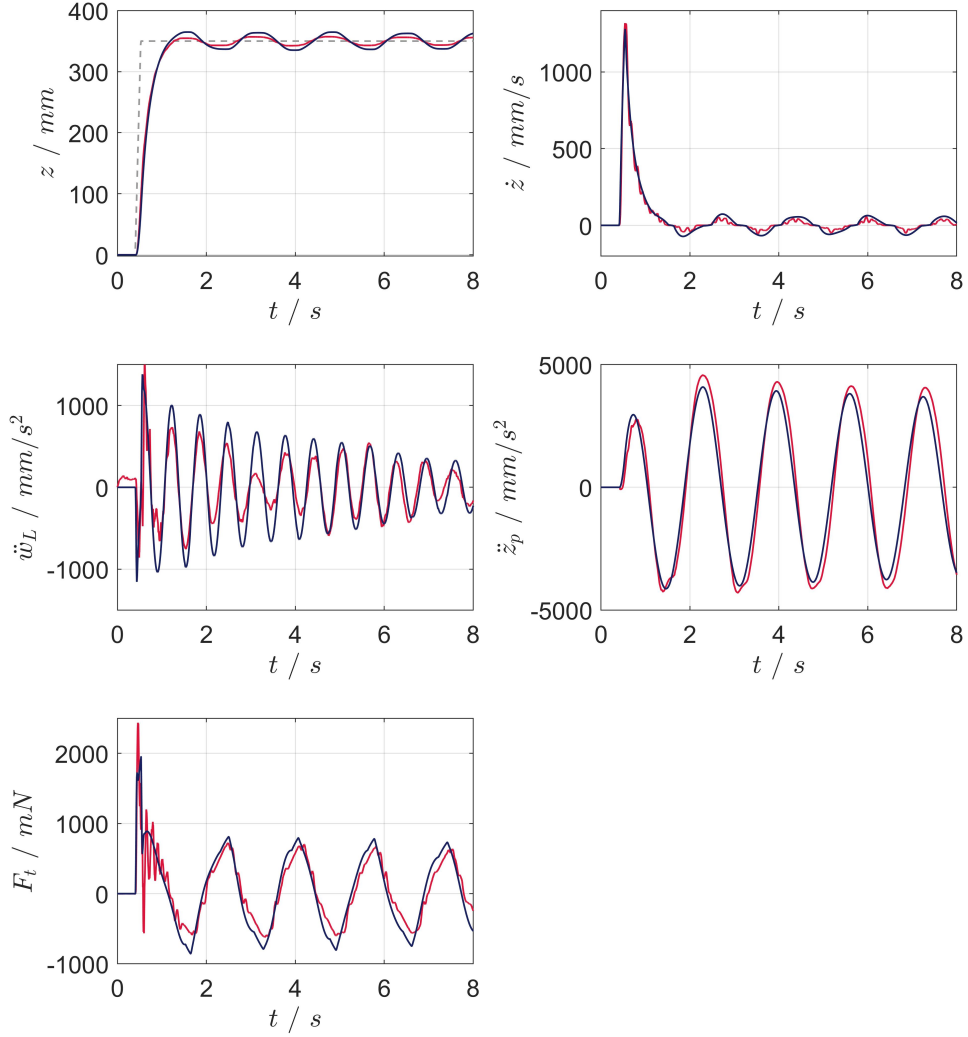


Figure D.1.: Simulated (blue) and experimental (red) time responses of elastic gantry crane with cascade feedback control

friction force as additional input $F_f(\dot{z})$, the model matrices can be computed as

$$A_c = \begin{bmatrix} -8.56 \cdot 10^{-3} & 10.45 & 0 & 0 & 0 & 0 \\ -10.45 & -8.56 \cdot 10^{-3} & 0 & 0 & 0 & 0 \\ 0 & 0 & 0 & 1 & 0 & 0 \\ 8.94 \cdot 10^{-2} & 1.97 & 0 & 0 & 1.36 \cdot 10^4 & 0 \\ 0 & 0 & 0 & 0 & 0 & 1 \\ 0 & 0 & 0 & 0 & -32.94 & 0 \end{bmatrix},$$

$$B_c = \begin{bmatrix} 3.66 & 3.66 \\ -0.17 & -0.17 \\ 0 & 0 \\ 11.8 & 11.8 \\ 0 & 0 \\ -1.57 \cdot 10^{-2} & -1.57 \cdot 10^{-2} \end{bmatrix}, \quad C_c = \begin{bmatrix} 0 \\ 0 \\ 1 \\ 0 \\ 0 \\ 0 \end{bmatrix}^T, \quad D_c = \begin{bmatrix} 0 \\ 0 \end{bmatrix}^T.$$

In order to design an appropriate feedback control the weighting matrices Q and R that represent states and input penalties have been chosen such that a reasonable trade-off between the oscillations damping and positioning for this setup has been found. Here, the elements of diagonal matrix Q are chosen as follows: $q_{i,i} = [1 \cdot 10^4, 1 \cdot 10^4, 50, 80, 6 \cdot 10^8, 6 \cdot 10^8, 1 \cdot 10^6]$ and $R = 1$. The observer gain L_c can be calculated by solving the pole placement problem

$$L_c = [42.72 \quad 646.45 \quad 26.59 \quad -292.08 \quad -0.05 \quad -1.2]^T. \quad (\text{D.4})$$

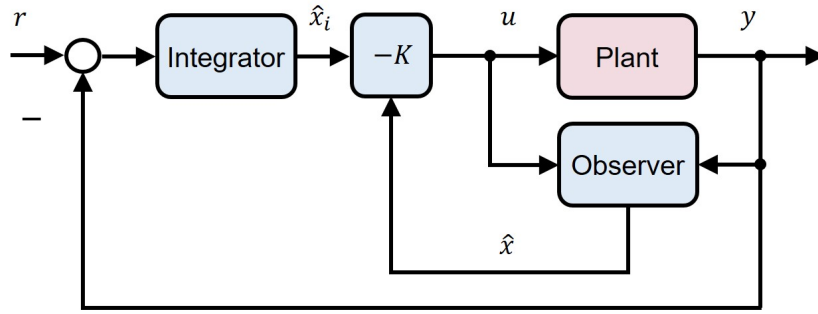


Figure D.2.: LQR control scheme

In Fig. D.3 simulation and experimental results by applying the observer-based state feedback control law (D.2) to the *full* crane configuration are depicted. Here, a fast reference tracking with notable damping of the load oscillations and reduction of crane vibrations can be seen.

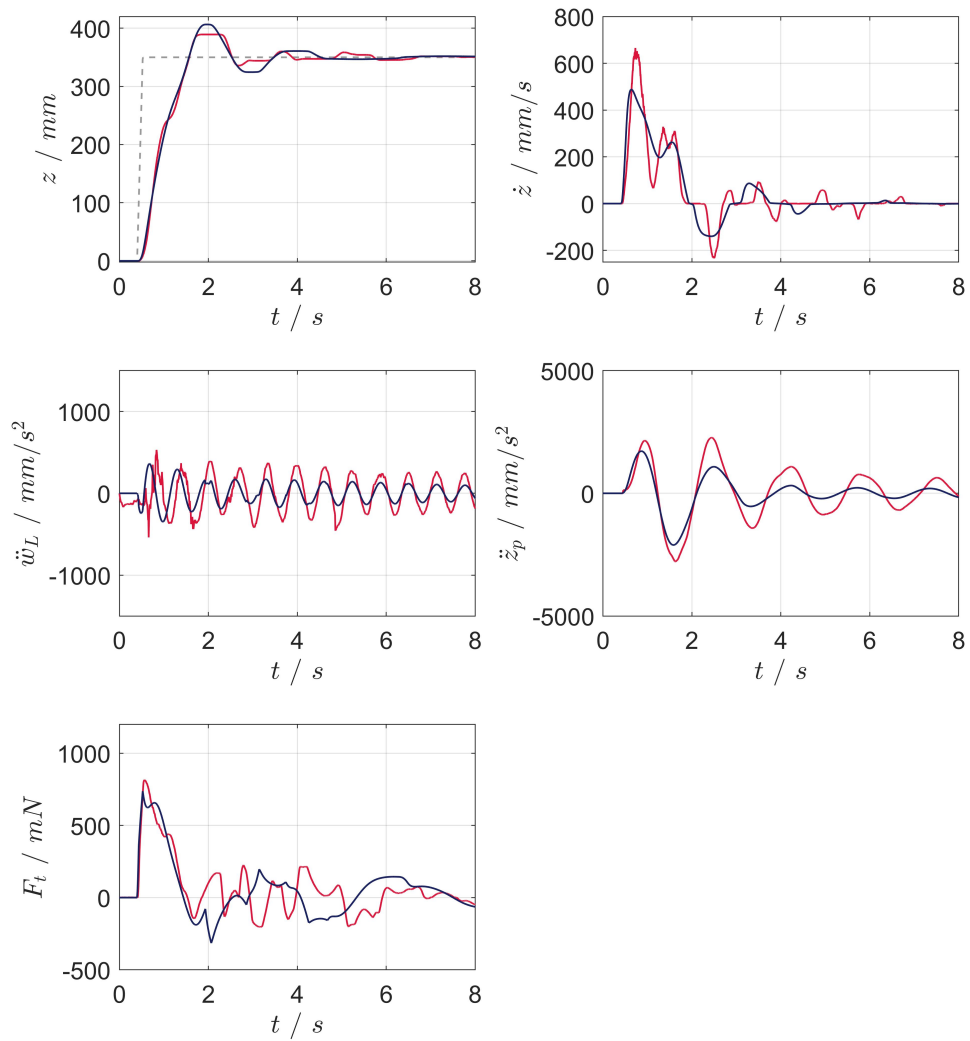


Figure D.3.: Simulated (blue) and experimental (red) time responses of elastic gantry crane with LQR

E. Energy-based control

One of the most common control approaches for mechanical systems that provide dissipation is based on the total system energy [17, 103, 111]. Since the system energy is a positive definite function, it is well suited for as a Lyapunov functional candidate. The control objective of the gantry crane is the positioning of the trolley and simultaneous damping of the payload swinging and structural vibrations. Therefore, the Lyapunov functional candidate can be chosen as follows:

$$V = E + \frac{1}{2}k_p\varepsilon^2, \quad (\text{E.1})$$

where $E = T + U$ is the total system energy, $\varepsilon = z - z_{ref}$ is the trolley position error, and k_p is a positive constant. Here, according to (2.15) and (2.16) the total system energy can be divided into three terms

$$\begin{aligned} E &= \frac{1}{2}m_p [(\dot{w}(L) + \dot{z} + \dot{\varphi}l \cos \varphi)^2 + (\dot{\varphi}l \sin(\varphi))^2] + \frac{1}{2}m_t(\dot{w}(L) + \dot{z})^2 \\ &\quad + \frac{1}{2}m_c\dot{w}^2(L) + \frac{1}{2} \int_0^L \rho \dot{w}^2 dx + m_p g l (1 - \cos \varphi) + \frac{1}{2} \int_0^L EI(w'')^2 dx \\ &= \underbrace{\frac{1}{2}m_p \left(l^2 \dot{\varphi}^2 + (\dot{w}(L) + \dot{z})^2 + 2l\dot{\varphi} \cos \varphi (\dot{w}(L) + \dot{z}) \right)}_{E_1} \\ &\quad + \underbrace{\frac{1}{2}m_t (\dot{w}(L) + \dot{z})^2 + \frac{1}{2}m_c \dot{w}^2(L) + m_p g l (1 - \cos \varphi)}_{E_2} \\ &\quad + \underbrace{\frac{1}{2} \int_0^L (\rho \dot{w}^2 + EI(w'')^2) dx}_{E_3} \geq 0. \end{aligned} \quad (\text{E.2})$$

In the following, a calculation of the time derivatives along the state trajectory for each energy term is presented

$$\begin{aligned} \dot{E}_1 &= m_p l^2 \dot{\varphi} \ddot{\varphi} + m_p (\dot{w}(L) + \dot{z}) \ddot{w}(L) + m_p (\dot{w}(L) + \dot{z}) \ddot{z} \\ &\quad - m_p l \dot{\varphi}^2 \sin \varphi (\dot{w}(L) + \dot{z}) + m_p l \ddot{\varphi} \cos \varphi (\dot{w}(L) + \dot{z}) \\ &\quad + m_p l \dot{\varphi} \cos \varphi (\ddot{w}(L) + \ddot{z}), \end{aligned} \quad (\text{E.3})$$

$$\begin{aligned} \dot{E}_2 &= m_t (\dot{w}(L) + \dot{z}) \ddot{w}(L) + m_t (\dot{w}(L) + \dot{z}) \ddot{z} \\ &\quad + m_c \dot{w}(L) \ddot{w}(L) + m_p g l \dot{\varphi} \sin \varphi, \end{aligned} \quad (\text{E.4})$$

$$\dot{E}_3 = \int_0^L (\rho \dot{w} \ddot{w} + EI w'' \dot{w}'') dx. \quad (\text{E.5})$$

Substituting PDE (2.19) in (E.5) and eliminating mixed derivatives via integration by parts, the \dot{E}_3 can be rewritten as follows:

$$\begin{aligned}
\dot{E}_3 &= \int_0^L \left(\dot{w} \left(-EIw'''' - c\dot{w} \right) + EIw''\dot{w}'' \right) dx \\
&\stackrel{P.I.}{=} \int_0^L \left(-EIw''''\dot{w} - c\dot{w}^2 \right) dx + \underbrace{[EIw''\dot{w}']}_0^L - \int_0^L EIw'''\dot{w}' dx \\
&\stackrel{P.I.}{=} \int_0^L \left(-EIw''''\dot{w} - c\dot{w}^2 \right) dx - [EIw'''\dot{w}]_0^L + \int_0^L EIw''''\dot{w} dx \\
&= -EIw(L)'''\dot{w}(L) - \int_0^L c\dot{w}^2 dx. \tag{E.6}
\end{aligned}$$

Adding the terms (E.3), (E.4), (E.6) and collecting them with the corresponding velocities, the time derivative along the state trajectory of the total energy can be derived as follows:

$$\begin{aligned}
\dot{E} &= - \int_0^L c\dot{w}^2 dx + m_p l \left[l\ddot{\varphi} + \ddot{w}(L) \cos \varphi + \ddot{z} \cos \varphi + g \sin \varphi \right] \dot{\varphi} \\
&\quad + \left[m_\Sigma \ddot{w}(L) + m_s \ddot{z} + m_p l \ddot{\varphi} \cos \varphi - m_p l \dot{\varphi}^2 \sin \varphi - EIw''''(L) \right] \dot{w}(L) \\
&\quad + \left[m_s \ddot{w}(L) + m_s \ddot{z} + m_p l \ddot{\varphi} \cos \varphi - m_p l \dot{\varphi}^2 \sin \varphi \right] \dot{z}. \tag{E.7}
\end{aligned}$$

Substituting (2.21), (2.22), and (2.23) in (E.7), the time derivative along the state trajectory of the total energy can be simplified and represented as follows:

$$\dot{E} = - \int_0^L c\dot{w}^2 dx + \left(F_t - F_{fr} \right) \dot{z}. \tag{E.8}$$

Thereafter, taking into account the trolley force $F_t(t) = k_m u(t)$, the time derivative of the Lyapunov functional along the state trajectory can be rewritten as follows:

$$\dot{V} = - \int_0^L c\dot{w}^2 dx + \left(k_m u - F_{fr} \right) \dot{z} + k_p \varepsilon \dot{z}. \tag{E.9}$$

Thus, choosing the energy-based feedback control law as

$$u = \frac{1}{k_m} \left(-d_c \dot{z} + F_{fr} - k_p \varepsilon \right) \tag{E.10}$$

yields in

$$\dot{V} = - \int_0^L c\dot{w}^2 dx - d_c \dot{z}^2 \leq 0. \tag{E.11}$$

The parameters of the energy-based control law are adjusted to achieve a relatively fast reference performance and acceptable damping: $k_p = 11$ and $d_c = 2.5$. From (E.10) it can be seen that for the control system, only measurements of the trolley position and velocity are needed. In Fig. E.1 simulation and experimental results applying the control law (E.10) to the *full* crane configuration are depicted. Here, it can be seen that the closed loop system dynamics is stable, and the crane trolley reaches the desired position relatively fast.

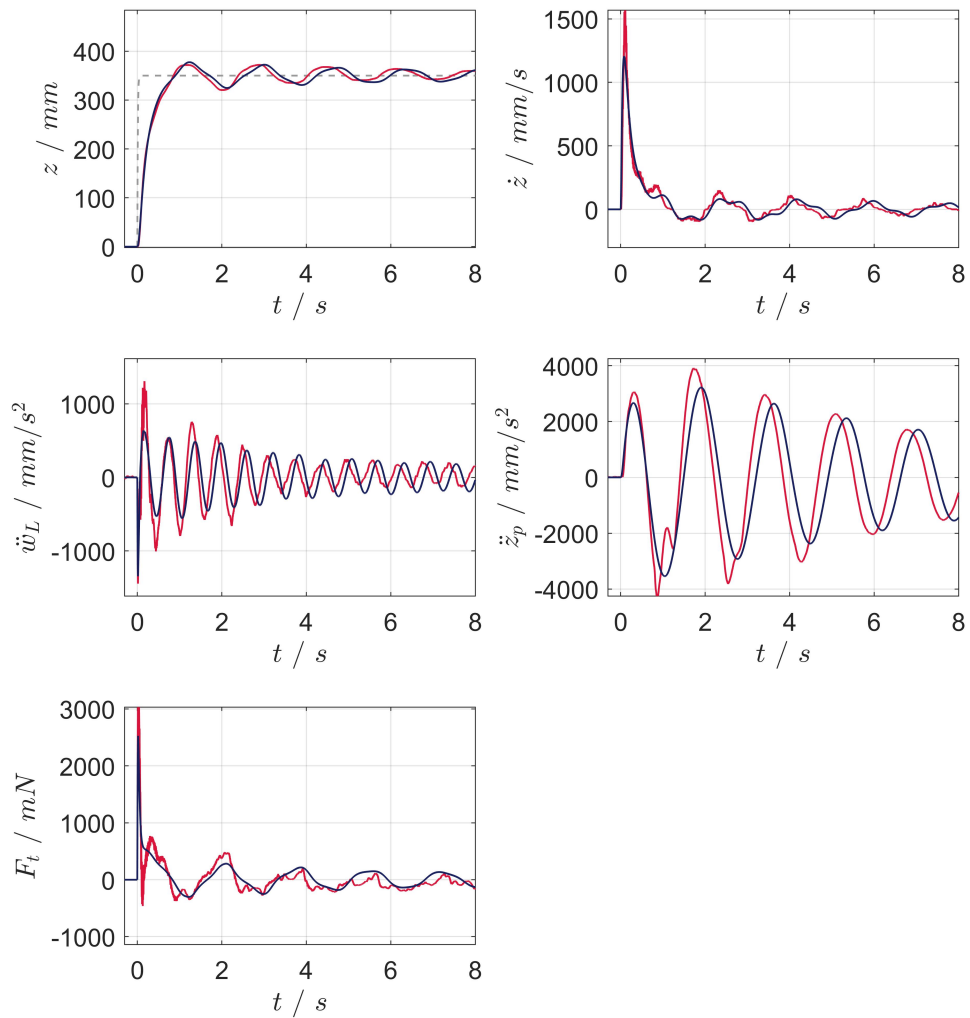


Figure E.1.: Simulated (blue) and experimental (red) time responses of elastic gantry crane with energy-based feedback control

Bibliography

- [1] ABDEL-RAHMAN, E. M., NAYFEH, A. H., AND MASOUD, Z. N. Dynamics and Control of Cranes: A Review. *Journal of Vibration and Control* 9 (2003), 863–908.
- [2] ABDULLAHI, A. M., MOHAMED, Z., SELAMAT, H., POTA, H. R., ZAINAL ABIDIN, M. S., ISMAIL, F. S., AND HARUNA, A. Adaptive output-based command shaping for sway control of a 3D overhead crane with payload hoisting and wind disturbance. *Mechanical Systems and Signal Processing* 98 (2018), 157–172.
- [3] ARMSTRONG-HELOUVRY, B., DUPONT, P., AND DE WIT, C. C. A survey of models, analysis tools and compensation methods for the control of machines with friction. *Automatica* 30, 7 (1994), 1083–1138.
- [4] ARNOLD, E., SAWODNY, O., NEUPERT, J., AND SCHNEIDER, K. Anti-sway system for boom cranes based on a model predictive control approach. In *IEEE International Conference Mechatronics and Automation, 2005* (2005), vol. 3, pp. 1533–1538.
- [5] AZELOGLU, C. O., EDINCLILER, A., AND SAGIRLI, A. Investigation of seismic behavior of container crane structures by shake table tests and mathematical modeling. *Shock and Vibration 2014* (2014), 1–9.
- [6] BARKANA, I. Positive-realness in discrete-time adaptive control systems. *International Journal of Systems Science* 17, 7 (1986), 1001–1006.
- [7] BARKANA, I. Parallel feedforward and simplified adaptive control. *International Journal of Adaptive Control and Signal Processing* 1, 2 (1987), 95–109.
- [8] BARKANA, I. Simple adaptive control - a stable direct model reference adaptive control methodology - brief survey. *IFAC Proceedings Volumes* 40, 13 (2007), 310 – 327.
- [9] BROGLIATO, B., LOZANO, R., MASCHKE, B., AND EGELAND, O. Dissipative Systems Analysis and Control. *Communications and Control Engineering* (2007).
- [10] CETON, C. *Model reduction for robust controller design*. 1992.
- [11] CHEN, H., FANG, Y., AND SUN, N. An adaptive tracking control method with swing suppression for 4-DOF tower crane systems. *Mechanical Systems and Signal Processing* 123 (2019), 426–442.
- [12] COX, D., LITTLE, J., AND O’SHEA, D. *Ideals, Varieties, and Algorithms: an introduction to computational algebraic geometry and commutative algebra*. 2013.

- [13] DAS, S., MAROO, K., DHALMAHAPATRA, P., AND MAITI, J. A self-tuning neuromorphic controller to minimize swing angle for overhead cranes. In *2018 4th International Conference on Recent Advances in Information Technology (RAIT)* (2018), pp. 1–6.
- [14] DE QUEIROZ, M., DAWSON, D., NAGARKATTI, S., ZHANG, F., AND BENTSMAN, J. Lyapunov-Based Control of Mechanical Systems. *Applied Mechanics Reviews* (2001).
- [15] DEBROUWERE, F., VUKOV, M., QUIRYNEN, R., DIEHL, M., AND SWEVERS, J. Experimental validation of combined nonlinear optimal control and estimation of an overhead crane. *IFAC Proceedings Volumes 47, 3* (2014), 9617–9622.
- [16] DENG, M., IWAI, Z., AND MIZUMOTO, I. Robust parallel compensator design for output feedback stabilization of plants with structured uncertainty. *Systems and Control Letters 36, 3* (1999), 193–198.
- [17] FANG, Y., DIXON, W. E., DAWSON, D. M., AND ZERGEROGLU, E. Nonlinear coupling control laws for an underactuated overhead crane system. *IEEE/ASME Transactions on Mechatronics 8, 3* (2003), 418–423.
- [18] FARD, M. P. *Modelling and Control of Mechanical Flexible Systems*, 2001.
- [19] FEAU, C., POLITOPOULOS, I., KAMARIS, G. S., MATHEY, C., CHAUDAT, T., AND NAHAS, G. Experimental and numerical investigation of the earthquake response of crane bridges. *Engineering Structures 84* (2015), 89–101.
- [20] FILIMONOV, A. B., AND FILIMONOV, N. B. Concerning the problem of a parallel feedforward correction of the regulation systems (in russian). *Mekhatronika, Avtomatizatsiya, Upravlenie*, 16(8) (2015), 507–514.
- [21] FILIMONOV, A. B., AND FILIMONOV, N. B. Application parallel feedforward correction of dynamic objects in the robust regulation tasks. *Journal of Advanced Research in Technical Science*, 13 (2019), 74–80.
- [22] FRADKOV, A., MIROSHNIK, I. V., AND NIKIFOROV, V. *Nonlinear and Adaptive Control of Complex Systems*. Springer Netherlands, 1999.
- [23] FRANKLIN, G., POWELL, J. D., AND EMAMI-NAEINI, A. *Feedback control of dynamic systems, 3e*. American Society of Mechanical Engineers, Dynamic Systems and Control Division (Publication) DSC, 1994.
- [24] FUJIMOTO, Y., WAKAYAMA, Y., OMORI, H., AND SMADI, I. A. On a high-backdrivable direct-drive actuator for musculoskeletal bipedal robots. *International Workshop on Advanced Motion Control, AMC* (2010), 389–395.
- [25] GAŠIĆ, V., ZRNIĆ, N., AND MILOVANCEVIC, M. Considerations of Various Moving Load Models in Structural Dynamics of Large Gantry Cranes. *FME Transactions 41* (2013), 311 – 316.

- [26] GAVINI, L., IZADIAN, A., AND LINGXI LI. A parallel compensation approach in controls of buck-boost converters. In *IECON 2011 - 37th Annual Conference of the IEEE Industrial Electronics Society* (2011), pp. 451–455.
- [27] GEORGIU, T. T., AND SMITH, M. C. Optimal Robustness in the Gap Metric. *IEEE Transactions on Automatic Control* 35, 6 (1990), 673–686.
- [28] GESSING, R. Parallel Compensator for Control Systems with Nonminimum Phase Plants. In *Proceedings of the 2004 American Control Conference* (2004), vol. 1, pp. 3351–3356.
- [29] GESSING, R. Parallel Compensator for Control of Multivariable Systems With Difficult Plants. *IFAC Proceedings Volumes* 40, 9 (2007), 218–223.
- [30] GESSING, R. Parallel compensator versus Smith predictor for control of the plants with delay. *Bulletin Of The Polish Academy Of Sciences Technical Sciences* 56, 4 (2008), 339–345.
- [31] GESSING, R. S. Sliding mode versus parallel compensator based control under measurement noise. *IFAC Proceedings Volumes (IFAC-PapersOnline)* 19 (2014), 4601–4606.
- [32] GLAD, T., AND LJUNG, L. *Control Theory: Multivariable and Nonlinear Methods*. 1989.
- [33] GLOVER, K., AND MCFARLANE, D. Robust Stabilization of Normalized Coprime Factor Plant Descriptions with H_∞ -Bounded Uncertainty. *IEEE Transactions on Automatic Control* (1989).
- [34] GOLOVIN, I., MAKSAKOV, A., AND PALIS, S. Gantry crane position control via parallel feed-forward compensator. In *2020 28th Mediterranean Conference on Control and Automation, MED 2020* (2020), pp. 1045–1050.
- [35] GOLOVIN, I., AND PALIS, S. Control-based damping of elastic gantry crane vibrations. In *2017 22nd International Conference on Methods and Models in Automation and Robotics, MMAR 2017* (2017), pp. 599–604.
- [36] GOLOVIN, I., AND PALIS, S. Design of parallel feed-forward compensator and its application to electromechanical system with friction load. *IFAC-PapersOnLine* 50, 1 (2017), 15524–15529.
- [37] GOLOVIN, I., AND PALIS, S. Robust control for active damping of elastic gantry crane vibrations. *Mechanical Systems and Signal Processing* 121 (2019), 264–278.
- [38] GOLOVIN, I., AND PALIS, S. Modeling and discrepancy based control of under-actuated large gantry cranes. In *21-st IFAC World Congress (Berlin)* (2020).
- [39] GOODWIN, G. C., GRAEBE, S. F., AND SALGADO, M. E. *Control System Design*, 1st ed. Prentice Hall PTR, USA, 2000.
- [40] GROSSWALD, E. *Lecture Notes in Mathematics: Bessel Polynomials*. Springer, Heidelberg, 1978.

- [41] HUANG, C., IOANNOU, P. A., MAROULAS, J., AND SAFONOV, M. G. Design of strictly positive real systems using constant output feedback. *IEEE Transactions on Automatic Control* 44, 3 (1999), 569–573.
- [42] ISIDORI, A., AND MARCONI, L. A note on robust output feedback stabilization of nonlinear nonminimum phase systems. *IFAC Proceedings Volumes* 41, 2 (2008), 3776–3780.
- [43] ISIDORI, A., THOMA, M., SONTAG, E. D., DICKINSON, B. W., FETTWEIS, A., MASSEY, J. L., AND MODESTINO, J. W. *Nonlinear Control Systems*, 3rd ed. Springer-Verlag, Berlin, Heidelberg, 1995.
- [44] IWAI, Z., AND MIZUMOTO, I. Robust and simple adaptive control systems. *International Journal of Control* 55, 6 (1992), 1453–1470.
- [45] IWAI, Z., MIZUMOTO, I., AND ADACHI, K. Model output following control by static output feedback and its robustness in the presence of parasitics. *Transactions of the Society of Instrument and Control Engineers* 30 (01 1994), 31–38.
- [46] IWAI, Z., MIZUMOTO, I., AND MINGCONG DENG. A parallel feedforward compensator virtually realizing almost strictly positive real plant. *Proceedings of 1994 33rd IEEE Conference on Decision and Control* 3, December (1994), 2827–2832.
- [47] JAAFAR, H. I., MOHAMED, Z., SHAMSUDIN, M. A., MOHD SUBHA, N. A., RAMLI, L., AND ABDULLAHI, A. M. Model reference command shaping for vibration control of multimode flexible systems with application to a double-pendulum overhead crane. *Mechanical Systems and Signal Processing* 115 (2019), 677–695.
- [48] JIAN, T. Y., AND MOHAMED, Z. Modelling and Sway Control of a Double-Pendulum Overhead Crane System. *Applications of Modelling and Simulation* 1, 1 (2017), 15–21.
- [49] KECK, A., ZIMMERMANN, J., AND SAWODNY, O. Friction parameter identification and compensation using the ElastoPlastic friction model. *Mechatronics* 47 (2017), 168–182.
- [50] KIM, H., KIM, S., BACK, J., SHIM, H., AND SEO, J. H. Design of stable parallel feedforward compensator and its application to synchronization problem. *Automatica* 64 (2016), 208–216.
- [51] KIM, J. L. J., AND YODAN. *Introduction to Dynamics and Control of Flexible Structures*. American Institute of Aeronautics and Astronautics, Inc., 1993.
- [52] KIMMERLE, S. J., GERDTS, M., AND HERZOG, R. An Optimal Control Problem for a Rotating Elastic Crane-Trolley-Load System. *IFAC-PapersOnLine* 51, 2 (2018), 272 – 277.
- [53] KONSTANTOPOULOS, G. C., AND ALEXANDRIDIS, A. T. Simple energy based controllers with nonlinear coupled-dissipation terms for overhead crane systems. *Proceedings of the IEEE Conference on Decision and Control* (2009), 3149–3154.

- [54] KREUZER, E., SRI NAMACHCHIVAYA, N., PICK, M.-A., AND RAPP, C. Reduced normal form approach to swing control of crane systems: theory and experiments. *Cybernetics and Physics* 1, 1 (2012), 42 – 50.
- [55] LEHNERT, M. Dämpfung von elastischen Kranschwingungen, 2014.
- [56] LIU, L., AND LIN, H. Force Control of a Distributed-Parameter Flexible Arm via Parallel Compensation. *Advanced Materials Research 201-203* (2011), 1898–1906.
- [57] LU, B., FANG, Y., AND SUN, N. Sliding mode control for underactuated overhead cranes suffering from both matched and unmatched disturbances. *Mechatronics* 47, September (2017), 116–125.
- [58] MAGHSOUDI, M. J., RAMLI, L., SUDIN, S., MOHAMED, Z., HUSAIN, A. R., AND WAHID, H. Improved unity magnitude input shaping scheme for sway control of an underactuated 3D overhead crane with hoisting. *Mechanical Systems and Signal Processing* 123 (2019), 466–482.
- [59] MILORADOVIC, N., AND VUJANAC, R. Analysis of overhead travelling crane’s motion in horizontal plane. *ANNALS of Faculty Engineering Hunedoara - International Journal of Engineering XIV* (2016), 21 – 24.
- [60] MIRANDA-COLORADO, R., AND AGUILAR, L. T. A family of anti-swing motion controllers for 2D-cranes with load hoisting/lowering. *Mechanical Systems and Signal Processing* 133 (2019), 106253.
- [61] MIROSHNIK, I. V. *Control Theory: Nonlinear and optimal systems (in Russian)*. Piter, 2016.
- [62] MIZUMOTO, I., AND TANAKA, H. Model free design of parallel feedforward compensator for adaptive output feedback control via frit with t-s fuzzy like model. *IFAC Proceedings Volumes* 43, 10 (2010), 139–144.
- [63] MORARI, M., AND ZAFIRIOU, E. *Robust process control*. Prentice Hall, 1989.
- [64] MOVCHAN, A. A. Stability of processes with respect to two metrics. *Journal of Applied Mathematics and Mechanics* 24, 6 (1960), 1506–1524.
- [65] OBINATA, G., ANDERSON, B., AND LUTZE, F. *Model Reduction for Control System Design*. Springer Verlag, 2001.
- [66] OHTSUKA, H., IWAI, Z., AND MIZUMOTO, I. Output feedback tracking sliding mode control with parallel feedforward compensator. *IFAC-PapersOnline* 16 (2005), 730–735.
- [67] OLSSON, H. *Control Systems with Friction*. Department of Automatic Control Lund Institute of Technology, 1996.
- [68] OLSSON, H., ÅSTRÖM, K. J., GAFVERT, M., LISCHINSKY, P., AND CANUDAS DE WIT, C. Friction Models and Friction Compensation. *European Journal of Control* 4, 3 (1998), 176–195.

- [69] OLSSON, M. Analysis of structures subjected to moving loads, 1986.
- [70] OUYANG, H., ZHANG, G., MEI, L., DENG, X., XI, H., AND WANG, D. Simple robust control for double-pendulum overhead cranes. In *2018 IEEE International Conference on Real-time Computing and Robotics (RCAR)* (2018), pp. 190–195.
- [71] PALIS, S. Control of fluidized bed spray granulation processes, 2012.
- [72] PALIS, S., AND KIENLE, A. Discrepancy based control of particulate processes. *Journal of Process Control* 24, 3 (2014), 33–46.
- [73] PIATKOWSKI, T. Dahl and LuGre dynamic friction models - The analysis of selected properties. *Mechanism and Machine Theory* 73 (2014), 91–100.
- [74] PIETRYGA, U. Aktuelle Trends in der Entwicklung von Ship-to-Shore (STS) Containerkrane. In *19. Internationale Kranfachtagung 2011: Der Kran und sein Umfeld in Industrie und Logistik* (2011), pp. 129 – 140.
- [75] PUEBLA, H., AND ALVAREZ-RAMIREZ, J. Suppression of stick-slip in drillstrings: A control approach based on modeling error compensation. *Journal of Sound and Vibration* 310, 4 (2008), 881–901.
- [76] RAHN, C. D. *Mechatronic Control of Distributed Noise and Vibration*. Springer-Verlag, 2001.
- [77] RAMLI, L., MOHAMED, Z., ABDULLAHI, A. M., JAAFAR, H. I., AND LAZIM, I. M. Control strategies for crane systems: A comprehensive review. *Mechanical Systems and Signal Processing* 95 (2017), 1–23.
- [78] RAMLI, L., MOHAMED, Z., EFE, M., LAZIM, I. M., AND JAAFAR, H. I. Efficient swing control of an overhead crane with simultaneous payload hoisting and external disturbances. *Mechanical Systems and Signal Processing* 135 (2020), 106326.
- [79] RAMLI, L., MOHAMED, Z., AND JAAFAR, H. I. A neural network-based input shaping for swing suppression of an overhead crane under payload hoisting and mass variations. *Mechanical Systems and Signal Processing* 107 (2018), 484–501.
- [80] RAPP, C. Aktive Dämpfung der Lastschwingungen bei Containerkranen, 2012.
- [81] RAUSCHER, F., AND SAWODNY, O. An Elastic Jib Model for the Slewing Control of Tower Cranes. *IFAC-PapersOnLine* 50, 1 (2017), 9796 – 9801.
- [82] RAUSCHER, F., AND SAWODNY, O. RLS-Based Adaptive Feedforward Control of Cranes with Double Pendulum Dynamics. In *Proceedings - 2019 IEEE International Conference on Mechatronics, ICM 2019* (2019), vol. 1, pp. 91–96.
- [83] RECKTENWALD, A. Aktiver Schwingungsdämpfer für Krane. In *19. Internationale Kranfachtagung 2011: Der Kran und sein Umfeld in Industrie und Logistik* (2011), pp. 143 – 146.

- [84] RÖBENACK, K. *Nichtlineare Regelungssysteme: Theorie und Anwendung der exakten Linearisierung*. Springer-Verlag, 2017.
- [85] RUDERMAN, M., AND BERTRAM, T. Two-state dynamic friction model with elasto-plasticity. *Mechanical Systems and Signal Processing* 39, 1-2 (2013), 316–332.
- [86] RUSNAK, I., AND BARKANA, I. Spr and aspr untangled. *IFAC Proceedings Volumes* 42, 6 (2009), 126–131.
- [87] RYU, B.-J., AND KONG, Y.-S. Dynamic Responses and Active Vibration Control of Beam Structures Under a Travelling Mass. In *Advances on Analysis and Control of Vibrations – Theory and Applications*. 2012, pp. 231 – 252.
- [88] SALDIVAR MÁRQUEZ, M. B., BOUSSAADA, I., MOUNIER, H., AND NICULESCU, S.-I. *Analysis and Control of Oilwell Drilling Vibrations*. Springer Link, 2015.
- [89] SCHIESSER, W. E., AND GRIFFITHS, G. W. *A compendium of partial differential equation models: Method of lines analysis with matlab*. Cambridge University Press, 2009.
- [90] SCHLOTT, P., RAUSCHER, F., AND SAWODNY, O. Modelling the structural dynamics of a tower crane. *IEEE/ASME International Conference on Advanced Intelligent Mechatronics, AIM* (2016), 763–768.
- [91] SCHRÖDER, D. *Elektrische Antriebe - Regelung von Antriebssystemen*. Springer-Verlag, 2015.
- [92] SCHRÖDER, D. *Elektrische Antriebe – Grundlagen*. Springer-Verlag, 2017.
- [93] SCHWARZ, H. Changing the unstable zero dynamics of nonlinear systems via parallel compensation. *IFAC International Conference on Control*, 427 (1996), 1226–1231.
- [94] SIRAZETDINOV, T. K. On the theory of stability of processes with distributed parameters. *Journal of Applied Mathematics and Mechanics* 31, 1 (1967), 36–47.
- [95] SIRAZETDINOV, T. K. *Stability of Systems with Distributed Parameters (in Russian)*. 1987.
- [96] SKOGESTAD, S., AND POSTLETHWAITE, I. *Multivariable Feedback Control - Analysis and design*. 2001.
- [97] SMITH, O. J. *Feedback control systems*. Mc Graw-Hill, New York, 1958.
- [98] SMOCZEK, J., AND SZPYTKO, J. Particle swarm optimization-based multivariable generalized predictive control for an overhead crane. *IEEE/ASME Transactions on Mechatronics* 22, 1 (2017), 258–268.
- [99] SONG, Z., AND SU, C. Computation of Rayleigh Damping Coefficients for the Seismic Analysis of a Hydro-Powerhouse. *Shock and Vibration* 2017, 2 (2017).

- [100] SORENSEN, K., SINGHOSE, W., AND DICKERSON, S. A controller enabling precise positioning and sway reduction in bridge and gantry cranes. *Control Engineering Practice* 15 (2005), 580 – 585.
- [101] SOWA, L., PIEKARSKA, W., SKRZYPCZAK, T., AND KWIATOŃ, P. The effect of the gantry crane beam cross section on the level of generated stresses. *MATEC Web of Conferences* 157 (2018), 1–9.
- [102] STEINBERG, A. A sufficient condition for output feedback stabilization of uncertain dynamical systems. *IEEE Transactions on Automatic Control* 33, 7 (1988), 676–677.
- [103] SUN, N., AND FANG, Y. New energy analytical results for the regulation of underactuated overhead cranes: An end-effector motion-based approach. *IEEE Transactions on Industrial Electronics* 59, 12 (2012), 4723–4734.
- [104] SUN, N., WU, Y., CHEN, H., AND FANG, Y. An energy-optimal solution for transportation control of cranes with double pendulum dynamics: Design and experiments. *Mechanical Systems and Signal Processing* 102 (2018), 87–101.
- [105] SUN, Y., LYU, J., FANG, J., FU, Z., AND DONG, D. Robust LQR Anti-Swing Control for Quay-Side Crane System with Variable Load. *8th Annual IEEE International Conference on Cyber Technology in Automation, Control and Intelligent Systems, CYBER 2018* (2019), 796–801.
- [106] VERSCHOOF, J. *Cranes - Design Practice and Maintenance*. Wiley, 2002.
- [107] VINNICOMBE, G. Measuring robustness of a feedback systems, 1993.
- [108] VU THI-THUY, N. LMI based antiswing adaptive controller for uncertain overhead cranes. *International Journal of Electrical and Computer Engineering* 10, 6 (2020), 5793–5801.
- [109] WANG, T., TAN, N., ZHOU, C., ZHANG, C., AND ZHI, Y. A Novel Anti-Swing Positioning Controller for Two Dimensional Bridge Crane via Dynamic Sliding Mode Variable Structure. *Procedia Computer Science* 131 (2018), 626 – 632.
- [110] WILLEMS, J. C. Deterministic least squares filtering. *Journal of Econometrics* 118 (2004), 341–373.
- [111] WON, I.-S., AND HOANG, N. Q. Comparative study of energy-based control design for overhead cranes. *International Robotics & Automation Journal Research* 4, 3 (2018), 197–203.
- [112] WU, J.-J. An analysis of the structural dynamics of a mobil gantry crane with application to automation of container management, 2000.
- [113] XIAO, R., WANG, Z., CHEN, Z., AND SHEN, J. Anti-swing design for overhead crane based on dual sliding mode control. In *Proceedings of the IEEE International Conference on Industrial Technology* (2018), pp. 81–86.

- [114] YAZICI, H., AZELOGLU, C., AND KUCUKDEMIRAL, I. Active vibration control of container cranes against earthquake by the use of delay-dependent H_∞ controller under consideration of actuator saturation. *Journal of Low Frequency Noise Vibration and Active Control* 33, 3 (2014), 289–316.
- [115] YAZID, E., PARMAN, S., AND FUAD, K. Vibration analysis of flexible gantry crane system subjected swinging motion of payload. *Journal of Applied Sciences* 11 (2011), 1707 – 1715.
- [116] YOUNESIAN, D., GHAFoori, E., AND SADEGHPOUR, M. Nonlinear vibration of a three-dimensional moving gantry crane subjected to a travelling trolley hoisting a swinging object. *Transactions of the Canadian Society for Mechanical Engineering* 34, 3 - 4 (2010), 333 – 350.
- [117] ZAFIRIOU, E., AND MORARI, M. A. Internal model control: robust digital controller synthesis for multivariable open-loop stable or unstable processes. *International Journal of Control* 54, 3 (1991), 665–704.
- [118] ZEHEB, E. A Sufficient Condition for Output Feedback Stabilization of Uncertain Systems. *IEEE Transactions on Automatic Control* 31, 11 (1986), 1055–1057.
- [119] ZHANG, M., MA, X., RONG, X., TIAN, X., AND LI, Y. Adaptive tracking control for double-pendulum overhead cranes subject to tracking error limitation, parametric uncertainties and external disturbances. *Mechanical Systems and Signal Processing* 76-77 (2016), 15–32.
- [120] ZHANG, M., MA, X., RONG, X., TIAN, X., AND LI, Y. Error tracking control for underactuated overhead cranes against arbitrary initial payload swing angles. *Mechanical Systems and Signal Processing* 84 (2017), 268–285.
- [121] ZHANG, M., ZHANG, Y., CHEN, H., AND CHENG, X. Model-independent PD-SMC method with payload swing suppression for 3D overhead crane systems. *Mechanical Systems and Signal Processing* 129 (2019), 381–393.
- [122] ZHANG, S., HE, X., AND CHEN, Q. Energy coupled–dissipation control for 3-dimensional overhead cranes. *Nonlinear Dynamics* 99 (2020), 2097–2107.
- [123] ZHANG, S., HE, X., ZHU, H., CHEN, Q., AND FENG, Y. Partially saturated coupled-dissipation control for underactuated overhead cranes. *Mechanical Systems and Signal Processing* 136 (2020), 106449.
- [124] ZHOU, K., AND DOYLE, J. C. *Essentials of Robust Control*. Prentice-Hall, 1998.
- [125] ZHOU, M., SUN, N., CHEN, H., AND FANG, Y. A Novel Sliding Mode Control Method for Underactuated Overhead Cranes. In *IEEE Proceedings of the Chinese Automation Congress (CAC)* (2017), pp. 4548 – 4552.
- [126] ZRNIĆ, N., OGUAMANAM, D., AND BOŠNJAK, S. Dynamics and modelling of mega quayside container cranes. *FME Transactions* 34 (2006), 193–198.
- [127] ZRNIĆ, N., PETKOVIĆ, Z., AND BOŠNJAK, S. Automation of ship-to-shore container cranes: A review of state-of-the-art. *FME Transactions* 33 (2005), 111–121.

Declaration of honor

I hereby declare that I produced this thesis without prohibited external assistance and that none other than the listed references and tools have been used. I did not make use of any commercial consultant concerning graduation. A third party did not receive any nonmonetary perquisites neither directly nor indirectly for activities which are connected with the contents of the presented thesis.

All sources of information are clearly marked, including my own publications.

In particular I have not consciously:

- Fabricated data or rejected undesired results
- Misused statistical methods with the aim of drawing other conclusions than those warranted by the available data
- Plagiarized data or publications
- Presented the results of other researchers in a distorted way

I do know that violations of copyright may lead to injunction and damage claims of the author and also to prosecution by the law enforcement authorities. I hereby agree that the thesis may need to be reviewed with an electronic data processing for plagiarism.

This work has not yet been submitted as a doctoral thesis in the same or a similar form in Germany or in any other country. It has not yet been published as a whole.

Magdeburg, 01.04.2021

List of contributions

- I. Golovin, S. Palis, F. Palis. Design of oscillations damping for elastic construction of container cranes. *Internationale Konferenz “Electronics, electrical engineering and power engineering” (Moscow, Russia)*, 2013.
- I. Golovin, S. Palis, V. Shamardina. Damping of elastic crane vibrations. *International conference on “Problems of Energy and Resource Saving in Electrical Systems. Science, Education and Practice” (Kremenchuk, Ukraine)*, 2015.
- I. Golovin, S. Palis. Aktive Regelung von Lastpendelungen für elastische Kransysteme. *12. Magdeburger Maschinenbau-Tage*, 2015.
- I. Golovin, S. Palis, A. Timoschenko, V. Klepikov. Damping of friction-induced vibrations applying parallel compensator. *International Summer School-Conference “Advanced Problems in Mechanics” (Saint Petersburg, Russia)*, 2016.
- I. Golovin, S. Palis. Design of parallel feedforward compensator and its application to electromechanical system with friction load. *IFAC Papers OnLine*, 50-1 (2017), pp. 15524 – 15529.
- I. Golovin, S. Palis. A parallel feedforward compensation approach in control of gantry cranes. *International Conference “Electromechanical and power systems, modelling and optimization approaches” (Kremenchuk, Ukraine)*, 2017.
- I. Golovin, S. Palis, A. Timoschenko, A. Tkachenko. Physical modelling and robust control of gantry crane. *International Conference “Problems of automated electric drive systems” (Kharkov, Ukraine)*, 2017.
- I. Golovin, S. Palis. Control-based damping of elastic gantry crane vibrations. *IEEE-Proceedings of the 22nd International Conference on Methods and Models in Automation and Robotics*, MMAR 2017 8046896, pp. 599 – 604.
- R. Hermann, I. Golovin, S. Palis. Robuste Regelung von Drehkränen mit Hakendrehwerken. *26. Kranfachtagung (Dresden)*, 2018.
- I. Golovin, G. Strenzke, R. Dürr, S. Palis, A. Bück, E. Tsotsas, A. Kienle. Parameter identification for continuous fluidized bed spray agglomeration, *Journal: Processes*, 2018.

- G. Strenzke, I. Golovin, M. Wegner, S. Palis, A. Bück, A. Kienle, E. Tsotsas. Influence of drying conditions on process properties and parameter identification for continuous fluidized bed spray agglomeration. *21st International Drying Symposium (Valencia, Spain)*, 2018.
- I. Golovin, S. Palis. Robust control for active damping of elastic gantry crane vibrations. *Journal: Mechanical Systems and Signal Processing*, 121 (2019), pp. 264 – 278.
- I. Golovin, E. Otto, R. Dürr, S. Palis, A. Kienle. Lyapunov-based online parameter estimation in continuous fluidized bed spray agglomeration processes. *IFAC Papers OnLine*, 52(1) (2019), pp. 329 - 334.
- I. Golovin, S. Palis. Modeling and discrepancy based control of underactuated large gantry cranes. *21st IFAC World Congress (Berlin)*, 2020.
- I. Golovin, S. Palis, A. Maksakov. Gantry Crane Position Control via Parallel Feed-forward Compensator. *IEEE-Proceedings to 21th Mediterranean Conference on Control and Automation*, MED 2020 9182930, pp. 1045-1050.
- Ievgen Golovin, Anton Maksakov, Myroslav Shysh, Stefan Palis. Discrepancy-based control for positioning of large gantry crane. *Mechanical Systems and Signal Processing*, 163 (2022), 108199.